

CLOSED LOOP DYNAMIC SYSTEM IDENTIFICATION OF A MANNED
CLASSICAL CONFIGURATION HELICOPTER

A THESIS PROPOSAL FOR
THE GRADUATE SCHOOL OF NATURAL AND APPLIED SCIENCES
OF
MIDDLE EAST TECHNICAL UNIVERSITY

BY

ILGAZ DOĞA OKCU

IN PARTIAL FULFILLMENT OF THE REQUIREMENTS
FOR
THE DEGREE OF DOCTOR OF PHILOSOPHY
IN
ELECTRICAL AND ELECTRONICS ENGINEERING

JANUARY 2024

Approval of the thesis:

**CLOSED LOOP DYNAMIC SYSTEM IDENTIFICATION OF A MANNED
CLASSICAL CONFIGURATION HELICOPTER**

submitted by **ILGAZ DOĞA OKCU** in partial fulfillment of the requirements for the degree of **Doctor of Philosophy in Electrical and Electronics Engineering Department, Middle East Technical University** by,

Prof. Dr. Halil Kalıpçılar
Dean, Graduate School of **Natural and Applied Sciences** _____

Prof. Dr. İlkey Ulusoy
Head of Department, **Electrical and Electronics Engineering** _____

Prof. Dr. M. Kemal Leblebicioğlu
Supervisor, **Electrical and Electronics Engineering, METU** _____

Examining Committee Members:

Prof. Dr. Ozan Tekinalp
Aerospace Engineering, METU _____

Prof. Dr. M. Kemal Leblebicioğlu
Electrical and Electronics Engineering, METU _____

Prof. Dr. Mehmet Önder Efe
Computer Engineering, Hacettepe University _____

Assoc. Prof. Dr. Mustafa Mert Ankaralı
Electrical and Electronics Engineering, METU _____

Assist. Prof. Dr. Yakup Özkazanç
Electrical and Electronics Engineering, Hacettepe University _____

Date: 23.01.2024

I hereby declare that all information in this document has been obtained and presented in accordance with academic rules and ethical conduct. I also declare that, as required by these rules and conduct, I have fully cited and referenced all material and results that are not original to this work.

Name, Surname: Ilgaz Dođa Okcu

Signature :

ABSTRACT

CLOSED LOOP DYNAMIC SYSTEM IDENTIFICATION OF A MANNED CLASSICAL CONFIGURATION HELICOPTER

Okcu, Ilgaz Doğa

Ph.D., Department of Electrical and Electronics Engineering

Supervisor: Prof. Dr. M. Kemal Leblebicioğlu

January 2024, 133 pages

Rotary-wing air vehicles present unique advantages over their fixed wing counterparts. Their operation capability in low flight speeds and ability to take-off and land from tight spaces make rotary wing air vehicles indispensable for military and commercial customers around the world. Despite these evident advantages, rotary wing aircraft are complex dynamical systems whose flight dynamics mathematical models are generally difficult to construct and validate. Classical type rotocrafts exhibit sophisticated phenomena that makes the mathematical modelling process troublesome. System identification methods for dynamical system modelling, can provide a solution to this modeling challenges. Both frequency and time domain identification methods have been used extensively either for directly modelling air vehicle motion or for validating the previously constructed physics-based models. Lately the academia and industry focus more on advanced methods that can work under an active feedback regulation. Identification with closed loop data not only makes system identification tests ever more safe than before but also makes identification possible for systems that has redundant controls or systems with control allocation strategies.

This thesis work focuses on the system identification of a rotary wing helicopter using

closed loop test data. A classical configuration rotorcraft is the system sought to be identified. The applicability and performance of joint input output approach, which can be used to identify both bare airframe and controller, is evaluated with simulation data and flight test data. A linear mathematical model for the bare airframe flight dynamics is identified and verified using closed loop flight test data.

Keywords: Rotorcraft, Helicopter, Flight Mechanics Modeling, Closed Loop System Identification, Frequency Domain Identification, Joint Input Output Approach

ÖZ

İNSANLI KLASİK KONFIGURASYON BİR HELİKOPTERİN KAPALI DÖNGÜ DİNAMİK SİSTEM TANIMLAMASI

Okcu, Ilgaz Doğa

Doktora, Elektrik ve Elektronik Mühendisliği Bölümü

Tez Yöneticisi: Prof. Dr. M. Kemal Leblebicioğlu

Ocak 2024, 133 sayfa

Döner kanatlı hava araçları, sabit kanatlı hava araçlarına nazaran özgün avantajlara sahiptirler. Düşük hızda operasyon kabiliyetleri ve dar alanlara iniş kalkış yapabilmeleri nedeniyle tüm dünyada askeri ve sivil müşteriler için vazgeçilmez durumdadır. Tüm bu avantajlarına rağmen döner kanatlı hava araçları karmaşık dinamik sistemler olmaları sebebiyle uçuş dinamiği matematik modellerini elde etmek ve doğrulamak oldukça zordur. Klasik tipte helikopterler dahi karışık dinamik etkiler sebebiyle modelleme konusunda zorluklar çıkartmaktadır. Sistem tanımlama yöntemleri bu modelleme zorluklarına çözüm sunabilmektedir. Frekans ve zaman uzayı sistem tanımlama yöntemleri hem dinamik sistem modeli oluşturmada hem de daha önceden oluşturulmuş fizik temelli modelleri doğrulamada kullanılabilir. Son zamanlarda akademi ve endüstri kapalı döngü verisi kullanılarak gerçekleştirilen sistem tanımlama yöntemleri üzerine yoğunlaşmıştır. Kapalı döngü verisi kullanılarak yapılan çalışmalar sadece yapılan sistem tanımlama testlerini daha güvenli kılmakla kalmayıp ayrıca gereğinden fazla eyleyiciye sahip sistemler ya da denetim paylaşmalı sistemler için de sistem tanımlama yöntemlerini uygulanabilir kılmaktadır.

Bu tez çalışması döner kanatlı bir hava aracının kapalı döngü test verisi kullanılarak uçuş dinamiği sistem tanımlamasına odaklanmıştır. Çalışma boyunca odadaki sistem, geleneksel yapıdaki bir helikopter olarak belirlenmiştir. Aynı anda hem açık döngü sistemi hemde denetleyici mekaizmasını tanımlayabilmek için kullanılabilen bileşik girdi/çıktı yönteminin uygunluğu ve performansı benzetim verisiyle farklı modeller kullanılarak değerlendirilmiştir. Daha sonra bileşik girdi/çıktı yöntemi ile kapalı döngü uçuş test verisi kullanılarak bir matematik model tanımlanmış ve doğrulanmıştır.

Anahtar Kelimeler: Helikopter, Uçuş Mekaniği Modellemesi, Kapalı Döngü Sistem Tanımlaması, Frekans Uzay Sistem Tanımlaması, Bileşik Girdi/Çıktı Yöntemi

Felix qui potuit rerum cognoscere causas

ACKNOWLEDGMENTS

I would like to express my sincere gratitude to my thesis supervisor Prof. Dr. M. Kemal Leblebiciođlu for his guidance and unwavering enthusiasm on practical dynamics and control applications. His belief and support made it possible for me to complete a graduate program in an initially foreign and intimidating department. Encountering different perspectives and overcoming new challenges in METU Electrical and Electronics Engineering Department broadened my perspective extremely. I would also like to thank my thesis jury members Prof. Dr. Ozan Tekinalp, Prof. Dr. Mehmet Önder Efe, Dr. Yakup Özkazanç and especially to Dr. Mustafa Mert Ankaralı. Dr. Ankaralı's aid and counsel made my graduation possible and I am deeply grateful for that.

Many thanks goes to my close friend Ali Can Özer for being a trustworthy comrade while pushing the human knowledge to its limits, for being there when I needed to *confabulate*, and for beating me to the graduation. His unique perspective have led many inspiring prospects during the course of this work and I believe, will continue to do so in the upcoming years.

Warmest thanks to my friends from METU Aerospace Engineering Department class of 2012, for keeping me sane over the course of this work, for all the summer vacations, snowboard lessons, concerts, theaters and much more.

A million thanks to engineers working in the Turkish Aerospace Helicopter Division and pilots and engineers working in the Turkish Aerospace Rotary Wing Flight Test Division without whom this work would not be possible. These people have built the aircraft manufacturing and flight testing infrastructure, designed and built the first indigenous Turkish classical configuration helicopter itself, its automatic flight control system, conducted the flight tests, created the research and development atmosphere in which this thesis work flourished. I truly have risen on the shoulders of the giants in this regard.

Endless thanks to my family for letting me to pursue what I want in life, for encouraging me in the way that leads to the positive sciences and basically making me who I am today. I truly believe that I am lucky to have Zühal Okcu and Yusuf Okcu as my parents, Işık Yılmaz Okcu as my brother and Esra Uyar Okcu as my sister-in-law. Their extraordinary attitude in life made me a better person overall in every regard I can think of.

Special thanks to my wife, Aslı Alp Okcu who has never known me outside my doctorate pursuits. During the long years while this thesis work is being conducted, I have never seen anything beyond support, understanding and partnership from her. Her commitment, determination and willpower have always been an inspiration for me. With the completion of this work a new chapter is beginning for us both in which, I believe, a lot of love, happiness and adventure awaits.

TABLE OF CONTENTS

ABSTRACT	v
ÖZ	vii
ACKNOWLEDGMENTS	x
TABLE OF CONTENTS	xii
LIST OF TABLES	xv
LIST OF FIGURES	xvi
LIST OF ABBREVIATIONS	xx
CHAPTERS	
1 INTRODUCTION	1
1.1 Motivation and Problem Definition	1
1.2 Proposed Methods and Models	5
1.3 Contributions and Novelties	17
1.4 The Outline of the Thesis	18
2 MODELS AND METHODS	21
2.1 Helicopter Flight Dynamics Models	21
2.1.1 Rigid Body Dynamics	22
2.1.2 Stability and Control Derivatives	28
2.1.3 Extended Helicopter Dynamics	32

2.1.4	The Platform: T-625	38
2.1.5	Non-linear Helicopter Model: TOROS	40
2.2	System Identification Methods	46
2.2.1	SISO Frequency Response Identification	46
2.2.2	MIMO Frequency Response Identification	48
2.2.3	Closed Loop Identification Approaches	50
2.2.4	Parametrization of Frequency Response Identification Methods	52
3	SYSTEM IDENTIFICATION APPLICATIONS	57
3.1	Introduction	57
3.2	Airplane Lateral Dynamics with Linear Simulation Data	58
3.3	Helicopter Lateral Dynamics with Linear Simulation Data	64
3.4	Helicopter Rigid Body Dynamics with Linear Simulation Data	68
3.5	Helicopter Rigid Body Dynamics with Non-Linear Simulation Data	78
3.6	Helicopter Rigid Body Dynamics Parameter Optimization	87
3.7	Helicopter System Identification with Real Flight Test Data	93
4	CONCLUSION	105
4.1	Conclusion	105
4.2	Future Work	106
	REFERENCES	109
	APPENDICES	
A	SIMULATION RESULTS	119
B	ADDITIONAL FREQUENCY RESPONSE COMPARISONS	125

CURRICULUM VITAE 131

LIST OF TABLES

TABLES

Table 2.1	T-625 Characteristics	39
Table 3.1	Identification Costs with Respect to Truth Model	87
Table 3.2	Identified Derivatives with Linear Simulation Data	88
Table 3.3	Identified Derivatives with Non-linear Simulation Data	91
Table 3.4	Flight Test Data	95
Table 3.5	Frequency Response Table	98
Table 3.6	Identified Derivatives from Flight Test Data - Normalized	100

LIST OF FIGURES

FIGURES

Figure 1.1	System Identification Methods	8
Figure 1.2	Classical Control Loop Block Diagram	13
Figure 2.1	Forward Flight Represented in Rigid Body Dynamics	32
Figure 2.2	Forward Flight Represented in Extended Helicopter Dynamics	32
Figure 2.3	Rotor Flapping Angle Definitions	33
Figure 2.4	Rotor Lag Angle Definitions	35
Figure 2.5	T-625 Helicopter	39
Figure 2.6	TOROS Linear vs Non-Linear Comparison Inputs	42
Figure 2.7	TOROS Linear vs Non-Linear Comparison Outputs	43
Figure 2.8	Simulator Environment	45
Figure 2.9	Simple SAS Block Diagram	49
Figure 3.1	LJ-25 Lateral Directional Dynamics Block Diagram	59
Figure 3.2	LJ-25 Simulation Inputs	60
Figure 3.3	LJ-25 Aileron to Roll Rate Frequency Response Estimation	62
Figure 3.4	LJ-25 Aileron to Side Slip Angle Frequency Response Estimation	63
Figure 3.5	LJ-25 Rudder to Roll Rate Frequency Response Estimation	63

Figure 3.6	LJ-25 Rudder to Side Slip Angle Frequency Response Estimation	64
Figure 3.7	T-625 Lateral Directional Dynamics Block Diagram	65
Figure 3.8	T-625 Lateral to Roll Rate Frequency Response Estimation . . .	66
Figure 3.9	T-625 Lateral to Yaw Rate Frequency Response Estimation . . .	66
Figure 3.10	T-625 Pedal to Roll Rate Frequency Response Estimation	67
Figure 3.11	T-625 Pedal to Yaw Rate Frequency Response Estimation	67
Figure 3.12	T-625 Rigid Body Dynamics Block Diagram with Feedback . . .	69
Figure 3.13	T-625 AFCS Functional Block Diagram	71
Figure 3.14	T-625 Rigid Body Dynamics Linear Simulation Excitation Signals	72
Figure 3.15	T-625 Rigid Body Dynamics Linear Simulation Bare Airframe Inputs	72
Figure 3.16	T-625 Rigid Body Dynamics Linear Simulation Outputs	73
Figure 3.17	T-625 Rigid Body Dynamics Linear Pitch Rate Response Com- parison	75
Figure 3.18	T-625 Rigid Body Dynamics Linear Roll Rate Response Com- parison	75
Figure 3.19	T-625 Rigid Body Dynamics Linear Yaw Rate Response Com- parison	76
Figure 3.20	T-625 Rigid Body Dynamics Linear Vertical Velocity Response Comparison	76
Figure 3.21	JIO Method Noise Sensitivity for Pitch Rate Identification Re- sults with Linear Simulation Data	77
Figure 3.22	T-625 10% Longitudinal Cyclic Sweep Non-linear Simulation Outputs	79

Figure 3.23	T-625 Pre-processed Sweep Non-linear Simulation Inputs	81
Figure 3.24	T-625 Pre-processed Sweep Non-linear Simulation Bare Air- frame Inputs	81
Figure 3.25	T-625 Pre-processed Sweep Non-linear Simulation Outputs	82
Figure 3.26	T-625 Non-linear Data Pitch Rate Response Comparison	84
Figure 3.27	T-625 Non-linear Data Roll Rate Response Comparison	85
Figure 3.28	T-625 Non-linear Data Yaw Rate Response Comparison	85
Figure 3.29	T-625 Non-linear Data Vertical Velocity Response Comparison .	86
Figure 3.30	T-625 Linear Simulation Identification Results	89
Figure 3.31	T-625 Nonlinear Simulation Identification Results	92
Figure 3.32	T-625 Simulation vs Flight Test Results for Collective to w	93
Figure 3.33	T-625 Simulation vs Flight Test Results for Longitudinal Cyclic to q	94
Figure 3.34	Identification Excitation and Bare-Airframe Inputs for Lateral Sweep Flight Tests	96
Figure 3.35	Lateral to Pedal Correlation	97
Figure 3.36	Flight Test versus System ID Model Bode Plots	101
Figure 3.37	Flight Test Validation Time Domain Step Responses	102
Figure 4.1	Engine Model Identification Framework Block Diagram	107
Figure A.1	LJ-25 Simulation Inputs	119
Figure A.2	LJ-25 Simulation Results	120
Figure A.3	T-625 Lateral Dynamics Linear Simulation Results	121

Figure A.4	T-625 Nonlinear Simulation Identification Results - SAS OFF . .	122
Figure A.5	T-625 Nonlinear Simulation Identification Results - SAS OFF . .	123
Figure B.1	T-625 Rigid Body Dynamics Linear Off Axis Lon. Cyc. Response Comparison	125
Figure B.2	T-625 Rigid Body Dynamics Linear Off Axis Lat. Cyc. Response Comparison	126
Figure B.3	T-625 Rigid Body Dynamics Linear Off Axis Pedal Response Comparison	126
Figure B.4	T-625 Rigid Body Dynamics Linear Off Axis Collective Response Comparison	127
Figure B.5	T-625 Rigid Body Dynamics Non-Linear Off Axis Lon. Cyc. Response Comparison	127
Figure B.6	T-625 Rigid Body Dynamics Non-Linear Off Axis Lat. Cyc. Response Comparison	128
Figure B.7	T-625 Rigid Body Dynamics Non-Linear Off Axis Pedal Response Comparison	128
Figure B.8	T-625 Rigid Body Dynamics Non-Linear Off Axis Collective Response Comparison	129

LIST OF ABBREVIATIONS

AFCS	Automatic Flight Control System
SAS	Stability Augmentation System
SCAS	Stability and Control Augmentation System
DTS	Development Test System
DoF	Degrees of Freedom
JIO	Joint Input Output
MIMO	Multi Input Multi Output
MISO	Multi Input Single Output
SISO	Single Input Single Output
M_a	Aircraft Mass
u	x axis velocity in aircraft body frame of reference
v	y axis velocity in aircraft body frame of reference
w	z axis velocity in aircraft body frame of reference
p	x axis angular rate in aircraft body frame of reference
q	y axis angular rate in aircraft body frame of reference
r	z axis angular rate in aircraft body frame of reference
ϕ	Euler Roll Angle
θ	Euler Pitch Angle
ψ	Euler Yaw Angle
μ_x	x axis normalized velocity of rotor hub in hub/shaft frame of reference
μ_y	y axis normalized velocity of rotor hub in hub/shaft frame of reference

μ_z	z axis normalized velocity of rotor hub in hub/shaft frame of reference
X	x axis force in aircraft body frame of reference
Y	y axis force in aircraft body frame of reference
Z	z axis force in aircraft body frame of reference
L	x axis moment in aircraft body frame of reference
M	y axis moment in aircraft body frame of reference
N	z axis moment in aircraft body frame of reference
$\hat{G}_{xx}(f)$	smooth auto-spectral density function
$\hat{G}_{xy}(f)$	smooth cross-spectral density function
$\tilde{G}_{xx}(f)$	rough auto-spectral density function
$\tilde{G}_{xy}(f)$	rough cross-spectral density function

CHAPTER 1

INTRODUCTION

1.1 Motivation and Problem Definition

The ability to fly and maneuver at low speeds makes rotary-wing flight vehicles indispensable for military and civilian applications like medical evacuation, troop relocation, oil rig transport which are impossible or highly inconvenient to perform with fixed wing aircraft. This unique ability of the rotary wing aircraft led an increasing interest on the helicopter platforms since the beginning of Vietnam War. Beyond all odds, the odd looking, unsymmetrical helicopter has strengthen its place in the aviation world in the following years but not without its problems. Industry and academia have been trying to improve the helicopter in terms of flight performance, maneuverability, stability and handling qualities for over 80 years now [1]. Great literature on different iconic helicopter programs like the infamous Sikorsky UH-60 Black Hawk [2] and Boeing–Sikorsky RAH-66 Comanche [3] mention the need of rigours mathematical modeling while revealing decades long helicopter research and development. Accurate, high fidelity descriptions of helicopter behaviour in air are required to support this research and development effort. Aircraft and flight control systems design, testing and certification can all benefit extremely from flight dynamics mathematical models. Steady state analysis for determining helicopter orientation and control positions during flight; ability to generate linear models for autopilot algorithm synthesis and inspection of aircraft stability characteristics, nonlinear simulations for maneuver assessment, load and controllability predictions; hardware-in-the-loop (HIL) and pilot-in-the-loop (PIL) simulator environment support are a short list of examples where a flight dynamics model can prove useful. The requirement for verified flight dynamics models for helicopters stems from these fundamentals.

Unlike its fixed wing counterparts, the classical configuration helicopter is an unsymmetrical vehicle with respect to its longitudinal axis. Not only the rotation of main rotor itself introduces the asymmetry, but also; the counter torque generating tail rotor placement and the usually asymmetric empennage design leads to coupling of primary controls. Especially the main rotor lift asymmetry is a major contributor to the maximum speed limit of classical configuration helicopters [4]. More recent tilt-rotor and co-axial helicopter designs [5, 6] address this asymmetry issue to overcome the speed limit which also helps the control coupling issue as a byproduct. Nevertheless, apart from some notable examples like the Bell Boeing V-22 Osprey [7], Boeing CH-47 Chinook [8] or Kaman K-MAX [9] majority of the helicopters in service today are of classical configuration i.e. they utilize a single main rotor and a tail rotor. A good example to the control coupling issue in a classical configuration helicopter is the heave to yaw coupling. When a helicopter tries to gain altitude it does so by increasing the torque on the main rotor, if this torque increase does not get compensated by the tail rotor, helicopter starts to yaw. That is why, an experienced helicopter pilot automatically compensates this excess torque by pedal controls while introducing a collective input to gain altitude. These kind of couplings makes it impossible to decouple longitudinal and lateral motions of the helicopter as opposed to the fixed wing aircraft [10]. The inability to uncouple, introduces two major problems. First, an AFCS is almost inevitable for reducing the pilot workload in classical configuration helicopters. Second, it is more complicated to come up with flight dynamics models for helicopters since the cross coupling derivatives are just as important as the primary response derivatives.

Although helicopters are complex, coupled multi-input-multi-output dynamical systems as explained above, it is surprisingly convenient to represent them using linear dynamic system models for certain limited flight regimes. This convenience makes system identification methods invaluable tools to extract linear models from helicopter flight test data for the helicopter flight dynamics engineer. System identification not only reflects the real aircraft demeanor since it is based on flight data; but also, it can produce linearized system dynamic relations that flight mechanics stability and control engineers loves to work on. The identified linear models can then be used to verify/validate first principles based helicopter mathematical models; they

can be used to gain insight about helicopter behavior around a certain flight regime; or they can be used very effectively to construct flight control algorithm development. Late literature is filled with system identification applications on aircraft for the purposes listed above. An excellent overview on the most recent system identification work on aircraft can be found for U.S. Army Combat Capabilities Development Command Aviation & Missile Center [11], NASA Langley Research Center [12], German Aerospace Center [13], Technical University of Munich [14], Delft University of Technology [15], Texas A&M University [16], Brazil Flight Test and Research Institute [17], Virginia Tech Nonlinear Systems Laboratory [18]. The cited references showcases the utilization of system identification methods for all of the purposes listed above and more. The diversity of the research institutes and universities around the world studying the aircraft identification underscores both the imperative nature and the rich potential inherent in this subject matter. System identification is a natural extension to helicopter flight mechanics modeling and a necessity when it comes to dynamic model validation.

Controllers by design try to suppress, or in some cases magnify, certain dynamics of the plant system, contaminating the identification data during system testing. That is why, system identification for dynamical systems is traditionally performed without any active controller or regulator so that system dynamics are not interfered with by the feedback mechanism. However, it may be impossible or too risky to collect aircraft system identification data without a feedback system [19, 20, 21, 22]. System identification testing generally requires specialized types of inputs to be injected to the system in question. Specifically for flight testing, when the bare airframe has unstable, lightly damped or highly coupled modes, execution of a frequency sweep or step response test without an active flight control system is generally considered to be too risky. For some systems it may be impossible to deactivate the feedback mechanism. For example, infamous UH-60 helicopter has a pitch bias actuator that modifies pilot inputs and can not be deactivated which prevents open loop testing altogether [23]. Moreover, some sub-component models inevitably require correlated inputs like the finite state inflow model which is used widely in helicopter flight dynamics modeling [24], which is analogous to interfering with the system with a controller. Additionally, in flight test programs, test data is often collected with something other than

system identification in mind, with an active flight controller. A closed loop identification method would made it possible to utilize the existing extensive flight test data for identification purposes. Ability to use existing flight test database would reduce the flight testing risk and cost immensely while providing the model development team more than enough data to produce a flight mechanics model. The utilization of closed-loop identification methodology presents numerous opportunities as listed above; however, it is accompanied by inherent challenges that needs careful consideration and resolution.

Main problems related with closed loop system identification are well documented in the literature [22]. Bias errors in frequency responses due to error feedback is an issue that should be taken into account especially for high gain, high performance controllers. Measurement noise can easily be amplified by the feedback, contaminating the plant input. Careful inspection of signal to noise ratio for the excitation signal is required to overcome this bias error issue [20]. Another major issue is the controller structure and controller parameter information. For reverse engineering projects controller information is rarely available to the system identification engineer. In such cases the indirect approach can not be used for closed loop identification as will be described later [25, 26]. Deciding on the excitation signal is also a problem for cases where the controller information is unknown. Higher amplitude excitations, where the controller suppresses system dynamics may be required to excite system dynamics sufficiently. Informative data sets are vital for meaningful identification of bare airframe [22]. For multi-input-multi-output (MIMO) systems, correlation of plant inputs due to controller feedback is a big concern [26, 20]. Unsurprisingly, system identification methods fail to distinguish between the effects of correlated inputs on system outputs. The reason is more obvious when looked from a least squares estimation problem formulation. Correlated inputs results in linearly dependent basis functions which requires ill conditioned matrix inversions for a solution to exist [19, 27].

Any approach that claims to be able to identify MIMO systems under feedback regulation should naturally or inherently solve identification problem under correlated inputs. Industry trends show that new rotorcraft designs that are unable to operate without correlated bare airframe inputs are about to be more popular than ever [28].

With the electric vertical take-off and landing (e-VTOL) revolution around the corner, aerial vehicles with redundant control effectors and redundant propulsion systems are becoming more and more popular [29, 30]. Redundant control is also becoming the norm for advanced rotary wing concepts for the turbine engine vehicles as well. Most famous and apparent concepts are the tilt-rotor and co-axial platforms [31, 32, 33]. After tackling and mostly solving the apparent control allocation problem related with the redundant controls that are encountered in practical situations, more recently; academia and industry are changing their focus to better understand the physical phenomena lying behind these new rotorcraft concepts. This focus shift inevitably requires a way to identify mathematical models under correlated inputs due to control allocation via redundant controls. Evidently, recent literature shows an increase in e-VTOL, co-axial, and tilt-rotor aircraft, as well as attempts at identifying them under correlated inputs or under feedback regulation [29, 26].

1.2 Proposed Methods and Models

Mathematical models for helicopter flight dynamics modelling can be categorized in several ways. First and most apparent distinction can be made by the means that the model is constructed. For this categorization there are two types of mathematical models: *first-principle-based* models and *system identification* models. In first-principle-based modelling, mathematical relations that represent the relevant physics are constructed from scratch, using the knowledge of underlying physical phenomena. Newtonian mechanics illuminates a bright way to construct mathematical relationships that can predict helicopter behaviour. For complex systems like helicopters, it is often customary to divide the system into force generating components and handle each component somewhat individually. That is why, first-principle based models are higher order, complex differential equations that have hundreds of system states to be solved. System identification models on the other hand, are generally simplified and parameterized versions of first-principle based models. The parameters in system identification models are determined with the help of information gathered from the input and output data. Resulting models are data driven; thus, they often do not need to have higher order complex differential equations to represent physical

phenomena, rather; real behaviour reveals itself in data driven parameters [34].

Second major categorization for mathematical models can be done by their linearity characteristics. Linear models allows the control and modelling engineer to be equipped with immense tools such as frequency response plots, pole zero maps, transfer functions, state space representations, etc. All these tools are the foundations of numerous frameworks within dynamic system modelling and control theory like modern control, robust control, stochastic control, optimal control, etc. However, real life models are rarely linear. Nonlinear behaviour is a natural and mathematically representable phenomena. Thus, it is always good practice to represent real life in nonlinear models, and linearize the nonlinear behaviour around certain interesting points so that linear modelling tools can be used. Helicopter mathematical models are no exception. It is common practice to construct a first principle based nonlinear helicopter model for design and development purposes. Then local linearized models are used for control law development or for aiding the design activities in a more informed manner. The dynamic validation of the mathematical model is often done by validating the linear models first with the flight test data since extracting linear model parameters from flight test data is handled better and is less prone to mistakes as opposed to extracting nonlinear model parameters. The nonlinear model is then validated by using verified linear models. This approach naturally leads to system identification being an integral part of first-principle-based model validation and verification activities.

Although there are non-parametric methods that do not require a model postulate, majority of system identification methods require a model structure [22]. A model structure comprises of the parametrized dynamic relations of the system to be identified. The question of selecting which dynamics to include and adequate parametrization of those dynamics is an intricate task. Apart from a strong familiarity with the system at hand, constructing suitable model structure involves determining the required frequency range of interest for the model and the number of dynamic states which are available for measurement [23]. The frequency range of interest is determined largely by the intended model application. For example, a typical flight mechanics simulation and simple handling qualities application model needs to be valid up to 12 rad/s [20]. That is, a simple 6 Degrees-of-Freedom (DoF) formulation would do the

trick. On the other hand, for control law development, a model should be accurate from one decade below to one decade above the cut-off frequency. This requirement puts the model applicability range up to 20 to 30 rad/s for models that will be used to develop high bandwidth flight controllers [23, 35]. For a frequency range up to 20 rad/s, flapping and lead-lag dynamics of main rotor should be included since these dynamics typically dominate the 20 rad/s frequency range. If validity up to 30 rad/s is sought, it would be appropriate they include engine, inflow-coning dynamics as well. [36] Thus, a coupled formulation including 6DoF, main rotor flapping, lead-lag, coning, engine and inflow dynamics should be used for a higher frequency range applicability. On the other hand, sometimes it is better to use a more simplified version of 6 DoF model for a deeper and more through analysis. Although helicopter dynamics do not really uncouple, for a fixed wing dynamic analogy it is possible to write the 6 DoF equations into two subsets: Longitudinal and Lateral-Directional dynamics [31, 37, 32]. For the validation part of this thesis work, such a simplification was performed. Closed loop identification approach applicability is tested for the lateral-directional part of a simple 6DoF fixed wing dynamics and then for a helicopter model. The model and the lateral and longitudinal decoupling are adapted from [31] and the details are given in the related sections.

As mentioned before, aircraft system identification has well documented applications for fixed-wing and rotary-wing systems both in time domain and lately more in frequency domain [19, 20, 21]. These applications draw their mathematical background from well established foundations on dynamical system identification [38, 39, 22]. Following discussion is a summary of all these foundational and application references. System identification methods can be broadly classified into two main groups: parametric and non-parametric system identification. Both have applications in frequency and time domain. Figure 1.1 shows a crude attempt to illustrate commonly used system identification methods in aircraft identification in an hierarchical way.

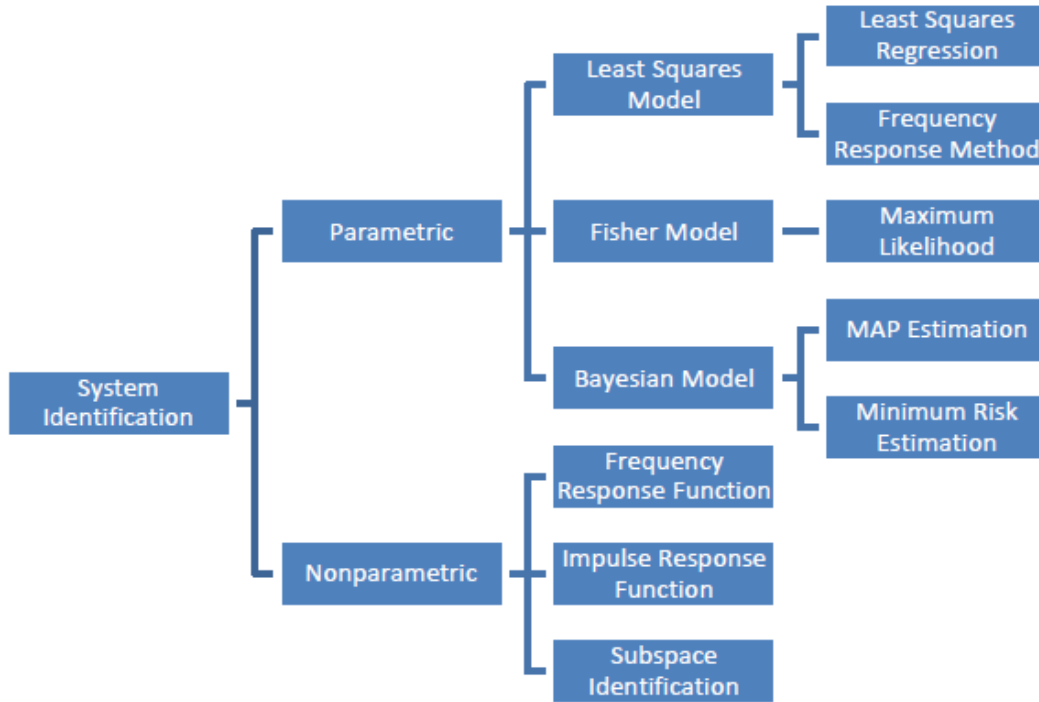


Figure 1.1: System Identification Methods

In parametric system identification, first a model postulate is constructed and parameterized according to the question at hand. Model parameters are pursued using input output information with an intelligent manner. The manner in which the parameters are defined and sought determines the parametric system identification problem formulation. After the model structure is determined and model is parameterized accordingly, system identification basically becomes a parameter estimation problem. The parameters of the given model structure are optimized based on a cost function that is determined by the selected system identification method. The selection of a system identification method or an estimation method depends on the assumptions made for the measurement noise and model parameters. The measurement noise or measurement error is almost always assumed to be random. The model parameters, on the other hand, can be assumed to be random variables or unknown constants. Based on the assumption on system parameters and measurement errors three different parameter estimation models can be proposed: Bayesian model, Fisher model and Least-Squares model [19]. The system identification problem formulation is given in equation 1.1 where $x \in \mathbb{R}^{m \times 1}$, is the state vector, $u \in \mathbb{R}^{n \times 1}$, is the input vector

$y \in \mathbb{R}^{k \times 1}$ is output vector, $z \in \mathbb{R}^{k \times 1}$ is measurement. $\nu \in \mathbb{R}^{k \times 1}$ is the measurement noise and Θ are the model parameters to be identified.

$$\begin{aligned}\dot{\mathbf{x}}(t) &= f[\mathbf{x}(t), \mathbf{u}(t), \Theta] & \mathbf{x}(0) &= \mathbf{x}_0 \\ \mathbf{y}(t) &= h[\mathbf{x}(t), \mathbf{u}(t), \Theta] \\ \mathbf{z}(t) &= \mathbf{y}(t) + \nu(t)\end{aligned}\tag{1.1}$$

$$E(\Theta) = \Theta_p \quad Cov(\Theta) = \Sigma_p \quad E(\nu) = 0 \quad Cov(\nu) = \mathbf{R}$$

Bayesian model assumes model parameters, Θ , and measurement noise, ν , are a vectors of random variables with probability densities $p(\Theta)$ and $p(\nu)$. Bayesian estimators require probability densities $p(\Theta)$ and $p(\nu)$ are known a priori. The posteriori, $p(\Theta|\mathbf{z})$, is calculated based on the Bayesian rule. Bayesian estimators include *Maximum A Posteriori* (MAP) estimation and *Minimum Risk* estimation [38]. It is possible to come up with sequential state estimators like *Kalman Filters* or *Particle Filters* in the context of a Bayesian problem formulation [40]. Despite the generality of Bayes estimator, the method has not found wide application in the aircraft parameter estimation. The main difficulty is finding an explicit statement about the parameters a priori probability densities [19]. Cost function is shown in equation 1.2.

$$J(\Theta) = \frac{1}{2}(\mathbf{z} - h(\Theta))^T \mathbf{R}^{-1}(\mathbf{z} - h(\Theta)) + \frac{1}{2}(\Theta - \Theta_p)^T \Sigma_p^{-1}(\Theta - \Theta_p) \tag{1.2}$$

In Fisher model Θ is a vector of unknown constant parameters. Measurement noise ν ; however, is treated as a random vector with probability density $p(\nu)$. Most common estimator for the Fisher model is the *Maximum Likelihood* (ML) estimator. In this method a likelihood function, which is equal to the conditional probability density of the measurements given the model parameters, is sought to be maximized. If there is process noise, states are estimated with a Kalman filter and compared with measurements which is called *Filter Error Method*. If no process noise is assumed, states are calculated by simple integration and compared with measurements which becomes the *Output Error Method*. If dynamic model is linear and all the states are assumed to be measured without error, in addition to the inputs that is called *Equation Error Method*. *Output Error Method* and *Equation Error Method* are identical to

nonlinear regression and linear regression respectively [19]. The likelihood function and the cost function are given in equation 1.3.

$$\begin{aligned}
 L(\mathbf{z}; \Theta) &= p(\mathbf{z}|\Theta) \\
 J(\Theta) &= \frac{1}{2}(\mathbf{z} - h(\Theta))^T \mathbf{R}^{-1}(\mathbf{z} - h(\Theta))
 \end{aligned}
 \tag{1.3}$$

In Least-Squares model Θ is assumed to be a vector of unknown constant parameters again. Measurement noise ν is a random vector of measurement noise. The cost function of the least-squares model is the simplest cost function since there is no information on the noise probability density function. Several estimator are built upon Least-Squares model formulation. *least squares regression* (LSR) method probably is the most commonly used estimator where on top of Least-Squares model assumptions, measurement noise is assumed to be uncorrelated. In cases where the measurement model can be formulated with linear relations LSR becomes a one-shot procedure rather than an iteration. LSR can be used with model structure determination tools like step-wise regression or orthogonal function modeling. However it can yield biased and inconsistent estimates in the presence of systematic errors and noise in the independent variables [19, 21, 38]. There are several examples from literature for LSR for helicopter identification [29, 41].

$$J(\Theta) = \frac{1}{2}(\mathbf{z} - h(\Theta))^T (\mathbf{z} - h(\Theta))
 \tag{1.4}$$

Frequency Response Method can be used for parametric identification under Least-Squares model assumptions as well. Nondeterministic noise on the measurements can be dealt with data consistency checks and data reconstruction methods where necessary. *Frequency Response Method* generates linear models since frequency response is a linear system property. When and if nonlinear models are required *model stitching* can be used to join multiple linear models [42]. Bias effects on measurements are effectively eliminated from the analysis as a byproduct of the Fourier Transforms involved in the process. Moreover coherence function provides a means to measure system excitation, data quality and system response linearity. Smaller number of points are included in iterative identification cost function calculations, which improves computational efficiency when compared with time domain methods. ML estimator

in frequency domain matches the Fourier transforms of the measured time histories. On the other hand, in frequency response method model and test frequency responses are matched for a selected number of frequency points [19, 38, 40, 21, 20, 43].

Non-parametric identification has a limited number of methods as opposed to parametric identification, however; eliminating the need for a model postulate offers a lot of flexibility while performing identification. It is common practice to use non-parametric methods first to determine model structure, then using that structure performing a parametric identification. Two methods worth mentioning for non-parametric identification are the *Subspace Identification* and *Frequency Response Function Estimation*. *Subspace Identification* is a non-parametric, non-iterative system identification method [39]. The measurement noise is assumed to be additive white or colored. Input/output data of a dynamic system is be stored in a Hankel matrix, which makes it possible to retrieve certain subspaces of the state space representation of the dynamical system in question. In addition to linear time invariant (LTI) system modeling, *Subspace Identification* is also suitable to use for linear parameter varying (LPV) systems and linear time periodic (LTP) systems both in time and in frequency domains [44]. There are several notable examples of *Subspace Identification* in helicopter flight dynamics modeling [45, 46, 47, 48, 49].

In this thesis work, the main identification method is selected as the *Frequency Response Method* due to its resilience offered by the redundance of a model postulate and its withstanding ability to identify helicopter dynamics [50]. Frequency domain system identification methods distinguish themselves from their time domain counterparts due to their computational efficiency, robustness to noise, applicability to common control-system design methods and flying qualities analysis, ability to provide physical acumen and possibility to be used in a non-parametric context and much more [51]. This identification work also utilizes frequency domain methods to take advantage of the listed strengths. Additionally, for rotorcraft flight dynamics modeling, where frequency domain analysis is traditionally much more practiced due to the periodic nature of the main tail rotor, frequency domain system identification is more easily comprehended and is a natural extension to the on-going helicopter development effort.

Up until now, system identification methods were summarized in a traditional sense where the system dynamics are assumed not to be under any feedback regulation. Being able to identify dynamic models under feedback regulation has tremendous advantages as stated in section 1.1; however, literature on closed loop ID is surprisingly scarce. Ljung classifies closed loop system identification approaches as the *direct approach*, the *indirect approach*, and *joint input output approach* [22, 25]. In direct closed loop identification approach, the system identification data is collected under feedback regulation active; but, the identification input output data set is selected as the plant input and plant output (u and y in Figure 1.2). Effectively disregarding the feedback signal makes it possible to use standard system identification methods to extract plant information but; this may also lead to insufficient plant excitation [22], bias due to noise feedback [20] or correlated plant inputs for MIMO systems [26]. In the indirect approach, identification is performed to construct the closed loop model from reference to output (r and y in Figure 1.2). In order to obtain plant model individually, the previously known controller part is subtracted from the identified model. Main drawback of the indirect approach is the dependency on controller knowledge. Any inaccuracy in controller information will manifest itself in plant model identified with the indirect approach [22, 25, 26]. Joint Input Output (JIO) approach; on the other hand, suffers no such disadvantage. JIO approach attempts to identify both the plant and feedback path simultaneously. The reference, plant input and output signals are used in JIO approach to this end. JIO approach can be used for identification under correlated plant inputs, which is a major issue for MIMO systems under linear feedback [26]. JIO approach can also be used for non-linear feedback which is almost always the case for operational flight controllers [25].

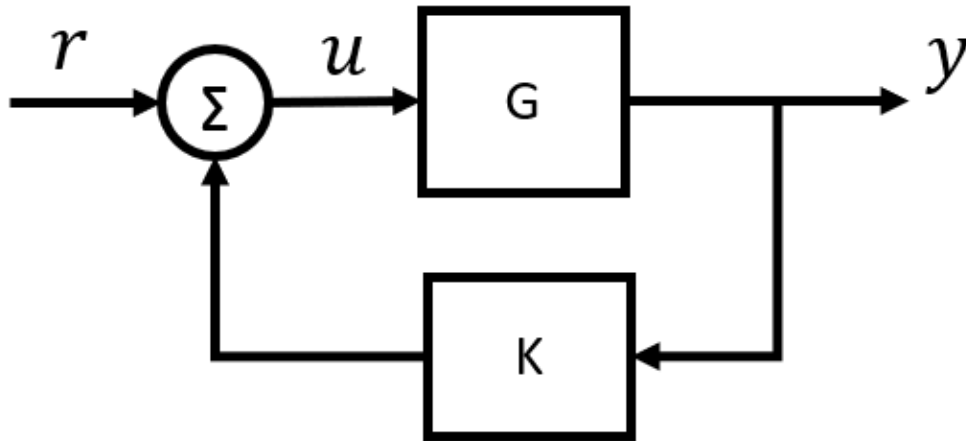


Figure 1.2: Classical Control Loop Block Diagram

JIO approach can be traced back to Akaike [52]. First practical use related to aircraft industry is the inflow identification work of Gennaretti *et. al.*. In an informative example of identification of inflow dynamics, Gennaretti manages to extract LTI models of main rotor inflow under correlated inputs utilizing the JIO approach [24]. Hersey *et. al.* improves on JIO identification of finite state inflow models and extends the study to co-axial inflow identification [53]. Initial application examples, utilized JIO approach in simulation environment specifically for sub-component identification like the inflow models that have correlated input sets. After JIO proved itself in identifying simulation models, it started to gain traction in aircraft dynamics identification field with real flight test data.

One of the first applications of JIO approach in whole aircraft identification is performed by Berger *et. al.* on fixed wing a business jet whose linear system model was available beforehand. To reduce the problem into a more manageable size while proving the JIO approach concept, only the lateral/directional dynamics of the business jet were identified. An identification is first performed with simulation data that is gathered in closed loop conditions which revealed direct approach fails to capture the underlying dynamics. On the other hand JIO approach shows excellent agreement with the known bare airframe model. JIO approach is also utilized with real flight test data to demonstrate JIO approach's ability to handle turbulence and noise in the data.

Results indicate JIO is able to generate correct dynamic models while direct approach fails to estimate Dutch roll mode damping [26].

Following the works of [26], a full mathematical model identification for fixed wing aircraft is performed for the infamous F-16 fighter jet. To come up with a full flight envelope model, multiple rigid body 6 degree of freedom models are identified, covering the flight envelope. Since the open loop dynamics of F-16 are unstable, JIO approach is not only suitable, but it is necessary for such an identification task. It is impossible for a pilot to control F-16 without an active AFCS assist, since the F-16 unstable dynamics are too fast to increase its maneuverability. Identification results are validated via doublet input response comparisons in time domain [54]. Lichota *et. al.* improves on the F-16 identification effort by utilizing simultaneous multi-sine input data in conjunction with JIO approach. Within a closed loop framework again, this time the aircraft is excited simultaneously from all input channels with signals that are designed to be uncorrelated. By doing so, it was possible to utilize JIO approach's advantages while completing the data collection in a single maneuver. The study was performed by using simulation data; nevertheless, it proved multi-sine excitation is possible for fixed wing aircraft identification with AFCS being active [55].

Fixed wing bare airframe identification using data collection with a feedback mechanism has also been a recent topic for the researchers at NASA as well. Grauer utilizes JIO approach with T-2 airplane simulation data and with X-56A flight test data. The excitation signal preferred is the phase optimized multi-sines. The ability to identify bare airframe with feedback is extended to cases where multi loop feedback is utilized. Additionally, real time computations of frequency responses using direct and JIO approaches are also presented. The importance of multi-sine excitation and recursive Fourier transform and ratios is emphasised for real time operation [56, 57, 58, 51].

One of the first examples of rotary-wing aircraft rigid body dynamics identification utilizing JIO approach is presented in [5] and [59]. V-280 tilt rotor platform is identified near hover flight conditions in V-280's helicopter mode. Being a tilt rotor, V-280 has highly coupled redundant control actuators and JIO approach is utilized to over-

come the input correlation issue. Berrigan *et. al.* demonstrates that JIO approach is feasible to use for identification of V-280 by using a hardware-in-the-loop simulation data. Then the study is improved in [5] by using flight test data. Frequency responses obtained by the JIO approach is used to improve a low fidelity Froude scale model, a physics based simulation model, and a high fidelity system integration lab. These studies showcase excellent examples of physics based model updates using system identification results.

Another use of JIO approach for unconventional rotary wing platforms can be found in [60]. Nadell *et. al.* performs a frequency domain system identification on a winged compound helicopter scaled demonstrator. The demonstrator is a 10% scaled version of a Piasecki X-49A compound helicopter. With redundant control actuators, high coupling between control axes and inevitable control mixing, the platform requires JIO approach for a rigid body dynamics identification. A composite model structure, explicitly incorporating the interconnected dynamics of the fuselage-rotor flapping and a first-order representation of RPM lag, was identified. A stitched model for using in the full flight envelope simulation model is also obtained.

Most recent use of JIO approach in a scaled technology demonstrator can be found in [61] where a compound UAV with intermeshing rotors is identified using both by JIO approach and by a modified subspace identification method. The excitation used is the generalized binary noise which provides advantages when used with subspace identification methods. No time domain step reponse validation was performed for the identified models however, eigenvalue analysis results indicate adequate hover linear models were obtained with JIO approach.

JIO approach with its ability to identify under correlated inputs finds itself an application area for systems that have redundant controls. Tilt-rotor platforms [5], unmanned aerial vehicles [60], highly complex technology demonstrators [58], experimental platforms that have redundant controls [62] have been identified by using JIO approach.

As the previous examples illustrate, JIO approach have been used for either tilt-rotor platforms or scaled technology demonstrators when considering rotary wing platforms. Literature lacks a classical configuration helicopter example because up until now, classical configuration helicopters were identified with AFCS off or degraded.

However, there are huge gains for classical configuration helicopters when JIO approach is utilized.

From a practical stand point JIO approach fits manned classical configuration helicopter system identification perfectly. First of all, classical configuration helicopters tends to have unstable bare airframe modes. Stabilizing the unstable modes with feedback not only helps the pilots during flight test immensely, but also makes first principle based model system identification possible on a desktop environment. Simulation model identification is used for model linearization and verification tasks; however, for unstable plants it is not possible to collect system identification data since there is no pilot compensation in the simulation. With JIO able to identify a closed loop model, it is possible to collect identification data in desktop simulations and come up with the bare airframe linearized models.

Secondly, JIO approach allows for identification of both plant and controller simultaneously. For helicopter development programs where both helicopter configuration and AFCS control laws keep changing, this provides a huge advantage. It is also possible to identify existing helicopters with feedback regulation without the need for the control law implementation. There may also be cases where the AFCS control law implementation is desired to be identified. For such reverse engineering tasks JIO provides an optional solution.

Third, for helicopter development programs where neither the bare airframe plant itself or the AFCS is certified and constantly go through envelope expansion tests, for which both systems constantly pushed to their extremes, JIO approach provides a measure to increase safety and data informativity.

Additionally, majority of helicopters in use today use limited authority automatic flight control systems (AFCS). The AFCS feedback control is added on top of the pilot inputs in a limited sense. It is possible for stability and control augmentation system (SCAS) servos to saturate in case of high angular rates, which makes the whole control response nonlinear in nature. In addition, many modern helicopter AFCS algorithms use switch case logic or complex voting and/or allocation strategies on top of linear control loops. These additional complexities inevitably makes the feedback nonlinear; however, even with such a nonlinear feedback, JIO approach

offers a way to identify bare airframe dynamics.

Lastly, since system identification tests may be conducted in a safe configuration where all the redundancies and control logic are active in the AFCS, JIO method may also eliminate the need for conducting dedicated system identification test all together. The main reason behind executing system identification flight tests is to obtain bare airframe data with AFCS deactivated. JIO eliminates this need, making any other available test data with sufficient control excitation, which should be abundant for new aircraft development programs, viable for system identification.

The implications of the listed advantages are tremendous. Being able to achieve all without a costly modification on the bare airframe or on AFCS but by simply recording the manipulation signals during flight tests and utilizing them in a resourceful manner is certainly captivating for a modeling, control and simulation engineer and it is an endeavor entailing persistent pursuit.

1.3 Contributions and Novelties

This work aims to identify the bare airframe dynamics of a medium sized classical configuration helicopter using the flight test data collected while the helicopters AFCS is active. To authors recollection, JIO method have never been used for identifying a classical configuration helicopter dynamics which has a limited authority control system before. This study utilizes closed loop identification, so that the system identification flight tests can be conducted with an active AFCS, mitigating the associated flight test risks of flying a manned helicopter in development phase. Risk mitigation during flight testing with and active AFCS happens through a number of factors. First, an active AFCS reduces the pilot workload considerably allowing the flight crew to better focus on the required test maneuver. Second, unstable bare airframe modes are stabilized by the AFCS removing the possibility of divergent flight conditions. Third, flight loads experienced by the aircraft are properly alleviated since the platform's response amplitudes are mitigated by the AFCS. An active AFCS also means larger amplitude excitation signals can be used to obtain rich, informative experimental data for identification, regardless of not generating that much system re-

sponse. JIO approach utilizes the manipulation signal content in order to make up for the reduced information content on aircraft bare airframe outputs. Being able to use closed loop data for system identification also allows the utilization of pre-existing test data, since typical system identification requires dedicated tests conducted with open loop dynamics.

To sum up, the main contributions of this work can be listed as:

- Application of JIO method to estimate a classical configuration helicopter dynamics from closed loop flight test data,
- Unstable bare airframe data gathering and identification by frequency response method,
- Simultaneous identification of both plant and controller for a given closed loop system,
- Increasing system identification flight test safety with and active controller without compromising data content,
- Creating a possibility to use preexisting flight test data for system identification purposes,
- Identification of bare airframe dynamics of a rotary-wing platform from closed loop data with a possibility of non-linear feedback.

1.4 The Outline of the Thesis

After stating the problem definition and motivation behind this thesis work, the proposed methods and models to overcome the problems in closed loop identification is given with possible contributions and novelties. Chapter 2 presents the mathematical models for helicopter flight dynamics representation with an increasing complexity and also explains the system identification methods and approaches utilized in this thesis work. Chapter 3 includes the application of JIO approach to a jet fighter aircraft proving that the closed loop identification is possible for air vehicles. Following

application of JIO approach is for a classical configuration helicopter. The applicability and suitability of JIO to helicopter flight mechanics identification is argued. Then an identification utilizing real flight test data is performed. The verification of the identification is performed by statistical metrics and the validation is performed using flight test data that is not used for identification. Concluding remarks for this research are given in Chapter 4.

CHAPTER 2

MODELS AND METHODS

2.1 Helicopter Flight Dynamics Models

Helicopter is a unique aircraft specifically due to its flight manoeuvrer capabilities. Unlike an airplane, a helicopter's movements in air are not dominated by aerodynamic forces and moments only. Inertial forces, specifically the centrifugal force plays an important role in helicopter controllability. Especially for helicopters that has modern articulated main rotors, the centrifugal force is by far the most dominant force that makes a helicopter manoeuvrable. Thanks to the complex and brilliantly designed main rotor and tail rotor systems, recent helicopter designs have the capability to generate moments that are beyond aerodynamic forces alone can provide, resulting in agile and highly manoeuvrable aircraft. On top of this, a helicopter is an asymmetric vehicle. The nature of a single rotating rotor system inevitably results in an aerodynamically asymmetric system. This asymmetry not only introduces dynamic cross couplings that are generally ignored for a fixed wing airplane; but also leads to asymmetric fuselage and empennage designs which contribute to cross coupling problem even more. These distinctions from fixed wing airplanes make helicopter flight dynamic modelling a new frontier filled with new challenges; be that as it may, one can still take advantage of the plentiful fixed wing modelling literature while attempting to represent helicopter behaviour. Following helicopter flight dynamic models does exactly that with increasing complexity and fidelity.

The first model named *rigid body dynamics* is also being used for fixed wing applications. As a matter of fact, *rigid body dynamics* represent any rigid body moving through space and thus can be used for both fixed wing and rotary wing applications,

even to represent spacecraft dynamics as well. For fixed wing applications it is customary to split the *rigid body dynamics* into two: the longitudinal dynamics which represent the motion in the aircraft along body x and z axes, and the lateral dynamics representing the helicopter behaviour on its body y axis. The second model called *extended helicopter dynamics* is an extension of the *rigid body dynamics* so is the name. This extension is to include states that are indigenous to helicopters like the flapping, the lead-lag, inflow dynamics. These two models are utilized as system identification model postulates in this work. Their derivations and linearized forms are provided in the following subsections. Apart from these system identification model postulates, a non-linear physical first-principles based helicopter flight dynamics model called TOROS [63] is used for system identification data gathering both with desktop simulations and piloted simulator tests. The structure of TOROS and its capabilities are also presented.

2.1.1 Rigid Body Dynamics

As mentioned before, *rigid body dynamics* are the common equation set that is used to represent the motion of any rigid body through space. Since the resulting equations has 6 degrees of freedom, the 3 translational and 3 angular displacements, this model is sometimes called the 6DoF model. The actual derivation is simply follows the Newton's 2nd law of motion and the version presented here is adapted from reference [31].

The dynamics of any rigid body moving in space can be given as;

$$\begin{aligned}
\dot{u} &= -(wq - vr) + \frac{X}{M_a} - g \sin \theta \\
\dot{v} &= -(ur - wp) + \frac{Y}{M_a} - g \cos \theta \sin \phi \\
\dot{w} &= -(vp - uq) + \frac{Z}{M_a} - g \cos \theta \cos \phi \\
I_{xx} \dot{p} &= (I_{yy} - I_{zz})qr + I_{xz}(\dot{r} + pq) + L \\
I_{yy} \dot{q} &= (I_{zz} - I_{xx})rp + I_{xz}(r^2 - p^2) + M \\
I_{zz} \dot{r} &= (I_{xx} - I_{yy})pq + I_{xz}(\dot{p} - qr) + N
\end{aligned} \tag{2.1}$$

The derivation of equations 2.1 can be found in Appendix 3A of reference [31]. Here, u, v, w represents the linear velocities of the aircraft decomposed in its body axis reference frame. p, q, r are the angular velocity vectors decomposed again in aircraft body axis system. ϕ and θ are the Euler pitch and roll angles respectively. Ma is the aircraft mass, I_{xx}, I_{yy}, I_{zz} are the rigid body second moment of inertias at respective axes. The capital letters X, Y, Z denote the external forces and L, M, N denote the external moments decomposed in aircraft body axis as well. Equation 2.2 complements equation 2.1 and denotes how the Euler angles progress over time for a rigid body in space.

$$\begin{aligned}\dot{\phi} &= p + q\sin\phi\tan\theta + r\cos\phi\tan\theta \\ \dot{\theta} &= q\cos\phi - r\sin\phi \\ \dot{\psi} &= q\sin\phi\sec\theta + r\cos\phi\sec\theta\end{aligned}\tag{2.2}$$

Apart from the state ψ , remaining 8 different variables in the equations 2.1 and 2.2 are commonly considered to be sufficient in order to represent an aircraft's dynamic state since the aircraft's translational position or its Euler angle ψ does not really affect the dynamic equations. That is, when subject to the same force and moments over time, an aircraft will behave the same regardless of its translational position and/or heading.

Although representing the full motion of a rigid body in space, equations 2.1 and 2.2 are non-linear in nature and still explicitly show the external forces and moments which are not easy to predict for a helicopter or a fixed airplane. The common solution to both problems is somewhat similar: small disturbance theory [10]. Assuming the behaviour around an equilibrium point can be represented with only linear relationships between the state variables constitutes the basis of small disturbance theory. The mathematical tool for such an assumption is the Taylor series expansion. Expanding the forces and moments with respect to state variables and neglecting the second order derivatives for conditions that are close to the equilibrium point provide a means for predicting the external forces and moments acting on the helicopter. Apart from states the forces and moments are also assumed to be effected from the pilot controls as well.

$$\dot{x} = Ax + Bu, x \in \mathbb{R}^8, u \in \mathbb{R}^4 \quad (2.3)$$

$$A = \begin{bmatrix} X_u & X_w - Q_e & X_q - W_e & X_v + R_e & X_p & X_r + V_e \\ Z_u + Q_e & Z_w & Z_q + U_e & Z_v - P_e & Z_p - V_e & Z_r \\ M_u & M_w & M_q & M_v & M_p & M_r \\ 0 & 0 & \cos\Theta_e & 0 & 0 & -\sin\Theta_e \\ Y_u - R_e & Y_w + P_e & Y_q & Y_v & Y_p + W_e & Y_r - U_e \\ L_u & L_w & L_q & L_v & L_p & L_r \\ 0 & 0 & \sin\Phi_e \tan\Theta_e & \Omega_a \sec\Theta_e & 1 & \cos\Phi_e \tan\Theta_e \\ N_u & N_w & N_q & N_v & N_p & N_r \end{bmatrix}$$

$$B = \begin{bmatrix} X_{\delta_{col}} & X_{\delta_{lon}} & X_{\delta_{lat}} & X_{\delta_{ped}} \\ Z_{\delta_{col}} & Z_{\delta_{lon}} & Z_{\delta_{lat}} & Z_{\delta_{ped}} \\ M_{\delta_{col}} & M_{\delta_{lon}} & M_{\delta_{lat}} & M_{\delta_{ped}} \\ 0 & 0 & 0 & 0 \\ Y_{\delta_{col}} & Y_{\delta_{lon}} & Y_{\delta_{lat}} & Y_{\delta_{ped}} \\ L_{\delta_{col}} & L_{\delta_{lon}} & L_{\delta_{lat}} & L_{\delta_{ped}} \\ 0 & 0 & 0 & 0 \\ N_{\delta_{col}} & N_{\delta_{lon}} & N_{\delta_{lat}} & N_{\delta_{ped}} \end{bmatrix}^T$$

$$x(t) = \begin{bmatrix} u & w & q & \theta & v & p & \phi & r \end{bmatrix}^T$$

$$u(t) = \begin{bmatrix} \delta_{col} & \delta_{lon} & \delta_{lat} & \delta_{ped} \end{bmatrix}^T$$

$$(2.4)$$

Additionally, calculating the first derivatives in matrix form or obtaining Jacobian matrix for equation 2.1, with the expansion for the external forces and moments depicted in equation 2.5 results in a linearized 6DoF equation set for any air vehicle. Equations 2.3 and 2.4 depict the infamous linear *rigid body dynamics* in 6 degrees of freedom. It should be noted that the parameters in 2.4 represents the deviations from equilibrium conditions since the general derivation procedure relies on the first order derivatives. In equation 2.4 subscript e denotes the equilibrium conditions. For example, the expansion for body x force X expended as,

$$X = X_e + \underbrace{\frac{\partial X}{\partial u}}_{X_u} \Delta u + \underbrace{\frac{\partial X}{\partial w}}_{X_w} \Delta w + \dots + \underbrace{\frac{\partial X}{\partial \delta_{lon}}}_{X_{\delta_{lon}}} \Delta \delta_{lon} + \dots \quad (2.5)$$

The partial derivative terms are labelled as shown in equation 2.5 and collectively they are called the stability derivatives.

As mentioned earlier, it is customary to divide the *rigid body dynamics* into two major subparts for fixed wing aircraft modelling. This division is possible because the fixed wing aircraft are generally symmetric with respect to their longitudinal axes which results in small stability derivatives on the non-diagonal parts of the A matrix. That is, the body lateral velocity v is approximately unaffected from the longitudinal states due to small stability derivatives like Y_u, Y_w, Y_q . The reason for these stability derivatives being small is rather apparent if one thinks about the nature of a conventional airplane. The stability derivative Y_u , for example, represents the change in body y force given a change in body x velocity. Since airplanes are symmetric vehicles it is obvious that a change in forward speed would not provide a change in side force and thus, Y_u can be neglected. The same thing goes for every cross-coupling stability derivative for a fixed wing aircraft. However, especially for low speed flight regimes, conventional helicopter stability derivatives can not be neglected. Following the same example, a perturbation in the forward speed of a helicopter would indeed cause a reaction that will result in a side force generation. A positive perturbation from the equilibrium body x speed, u will cause the inflow distribution on the rotor disc to tilt forward effectively increasing the angles of attack at the front of the main rotor and decreasing angles of attack at the back side. This angle of attack unbalance leads to

a longitudinal lift unbalance, which in turn causes main rotor to flap sideways due to the inherent *fundamental 90 degrees phase shift* [31]. The sideways tilt of the main rotor tip path plane, also tilts the main rotor thrust vector resulting in a net sideways force generation. Thus Y_u is a considerably large parameter for classical configuration helicopters at low speed flight regime. As the flight speed increases the inflow dominance on main rotor dynamics starts to diminish and Y_u can be neglected just as in the fixed wing case.

This cross-coupling of helicopters stems from their asymmetric design and prevents the partitioning of longitudinal and lateral dynamics at low speeds. However, it is still possible to distinguish longitudinal and lateral dynamics of a helicopter at relatively high speed regime. It is often admissible to model helicopter flight above 50 knots with separate longitudinal and lateral dynamics. This thesis work often utilizes lateral and longitudinal dynamics while trying to demonstrate proof of concept for system identification methods and approaches and thus, longitudinal and lateral dynamics will be presented for the sake of completeness.

After obtaining equations 2.3 and 2.4, derivation of lateral and longitudinal dynamic equations is a matter of selecting which stability derivatives to neglect. It is also assumed that the partitioning in the state space follows the commonly accepted fixed wing descriptions. Equations 2.6 show the decoupled *longitudinal dynamics* whereas, equation 2.7 shows decoupled *lateral dynamics* sometimes also called as the *lateral-directional dynamics* of an aircraft. The selected state and input variables are also presented for both equation sets. The derivatives that do not appear in equations 2.6 and 2.7 but are apparent in 2.4 are the ones that are neglected due to the nature of helicopter design.

$$\dot{x} = Ax + Bu, x \in \mathbb{R}^4, u \in \mathbb{R}^2$$

$$A = \begin{bmatrix} X_u & X_w - Q_e & X_q - W_e & -g \cos \Theta_e \\ L_v & L_p & 0 & L_r \\ M_u & M_w & M_q & 0 \\ 0 & 0 & \cos \Theta_e & 0 \end{bmatrix}$$

$$B = \begin{bmatrix} X_{\delta_{col}} & X_{\delta_{lon}} \\ Z_{\delta_{col}} & Z_{\delta_{lon}} \\ M_{\delta_{col}} & M_{\delta_{lon}} \\ 0 & 0 \end{bmatrix} \quad (2.6)$$

$$x(t) = \begin{bmatrix} u & w & q & \theta \end{bmatrix}^T$$

$$u(t) = \begin{bmatrix} \delta_{col} & \delta_{lon} \end{bmatrix}^T$$

$$\dot{x} = Ax + Bu, x \in \mathbb{R}^4, u \in \mathbb{R}^2$$

$$A = \begin{bmatrix} Y_v & Y_p + W_e & g \cos \Phi_e \cos \Theta_e & Y_r - U_e \\ Z_u + Q_e & Z_w & Z_q + U_e & -g \cos \Phi_e \sin \Theta_e \\ 0 & 1 & 0 & \cos \Phi_e \tan \Theta_e \\ N_v & N_p & 0 & N_r \end{bmatrix}$$

$$B = \begin{bmatrix} Y_{\delta_{lat}} & Y_{\delta_{ped}} \\ L_{\delta_{lat}} & L_{\delta_{ped}} \\ 0 & 0 \\ N_{\delta_{lat}} & N_{\delta_{ped}} \end{bmatrix} \quad (2.7)$$

$$x(t) = \begin{bmatrix} v & p & \phi & r \end{bmatrix}^T$$

$$u(t) = \begin{bmatrix} \delta_{lat} & \delta_{ped} \end{bmatrix}^T$$

As mentioned before decoupling of longitudinal and lateral dynamics generally holds true for fixed wing aircraft [64], helicopters on the other hand, have dynamics that is not suitable for decoupling for low speed flights. Decoupling assumption becomes more and more valid as the flight speed increases and for mid to high speed level flight regimes the lateral and longitudinal dynamics may generally be assumed to be uncoupled. Thus, same lateral-directional model for fixed-wing aircraft and helicopters may be used for mid to high speed flight regimes.

2.1.2 Stability and Control Derivatives

Here, it would be wise to discuss the nature of the stability and control derivatives that are apparent in the equations 2.3 and 2.4 above. 6-DoF rigid body model constitutes a good basis to gain insight about classical configuration helicopter behaviour and it reveals why, helicopter behaviour in air is unlike any other aircraft. Trying to come up with the signs and magnitudes of specific stability derivatives, leads to understanding of how the mechanisms and physics governing helicopter flight works, and is an endeavor every flight mechanics and control engineer needs to take at some point.

The standard 6-DoF set encompasses 36 stability derivatives and 24 control derivatives. A select number of pivotal derivatives will be explained, considering their variations in response to configuration and flight condition parameters. Each derivative is a composite of contributions from distinct aircraft components, like the main rotor, fuselage and empennage. Given the predominant role of the main rotor in helicopter flight dynamics, the ensuing discussion will place particular emphasis on main rotor behaviour and response. The discussion will mainly follow the arguments in [31] and group the derivatives into 3 categories as the transnational velocity derivatives, the angular velocity derivatives, and the control derivatives. Since helicopters change flight characteristics in and around hover and forward flight conditions, stability derivative characteristics for both low speed and high speed regimes will be discussed. Further details on stability derivatives and their values for example rotorcraft can be found in [50].

The velocity derivatives related to helicopter transnational motion are contingent upon the body velocities u , v , and w . Specifically, the derivatives X_u , Y_v , X_v , and Y_u exhibit close associations, particularly at low speeds. In high-speed flight, coupling derivatives become negligible, and the direct force damping terms, namely X_u and Y_v , linearly correspond with speed, reflecting the drag and side-force on the rotor–fuselage combination, respectively. At hover and low speeds, all four derivatives are of a comparable magnitude. The direct derivatives primarily stem from disc tilts in response to perturbations in u and v , tilting aft and port. While the direct derivatives are evident, the coupling derivatives are less apparent, necessitating an examination of the theory of nonuniform inflow, as mentioned in 2.1.1, to explain the notably

substantial values of X_v and Y_u around 40 knots forward flight. Similar characteristics are seen in the moment derivatives M_v and L_u due to nonuniform inflow. These strong cross-coupling derivatives are the main reasons behind the inter-axis coupling of helicopters.

The derivatives M_u and M_w , identified as speed and incidence static stability derivatives, exert a significant influence on longitudinal stability and, consequently, impact handling characteristics. In the context of fixed-wing aircraft operating at low subsonic speeds, the speed stability derivative is basically zero, as all aerodynamic moments correlate proportionally with dynamic pressure, resulting in a derivative proportional to the trim value of aerodynamic pitching moment, effectively yielding zero. Conversely, in helicopters, the main rotor moments due to speed variations remain relatively constant across the speed spectrum. However, the aerodynamic loads on the fuselage and empennage exhibit strong dependency on forward velocity. Specifically, the normal load on the horizontal stabilizer induces a substantial pitching moment at the center of mass, contributing to M_u in proportion to the trim load on the tail. During forward flight, a positive perturbation in normal velocity, w , leads to a greater lift increase on the advancing side of the disc than on the retreating side, causing the disc to flap back and generate a destabilizing, nose-up pitching moment. These pitching moments originate from three primary sources—the main rotor, the tailplane, and the fuselage. The tail's contribution to M_w is consistently stabilizing, wherein a positive incidence change results in increased tail lift, inducing a nose-down pitch moment. Conversely, the fuselage's contribution is predominantly destabilizing, as the aerodynamic center of the fuselage typically lies forward of the center of mass. The overall impact from the main rotor is contingent upon hub stiffness and center of gravity. The stabilizing influence of the tail is expected to offset the destabilizing contributions from the fuselage and main rotor.

Z_w is aptly referred to as the heave-damping derivative. Although the fuselage and empennage play roles in high-speed flight, the main rotor overwhelmingly influences Z_w across the entire flight spectrum and can be estimated through the thrust variation resulting from vertical velocity changes. Alterations in vertical velocity impact the local angles of attack at the blade sections of the main rotor, subsequently influencing the overall thrust. Consequently, rotors with higher blade loading tend to exhibit

smaller heave-damping derivatives.

Lateral/directional degrees of freedom are dominated by the sideslip derivatives—namely, the dihedral effect L_v and the weathercock stability N_v . The significance of these moments intensifies as sideslip increases, determining the lateral/directional static stability characteristics. A positive N_v value contributes to stability, while a negative L_v value has a stabilizing effect. Both exhibit analogous effects on rotary-wing and fixed-wing aircraft, with the distinctive inclusion of the tail rotor in rotary-wing aircraft, which can exert a substantial impact on both derivatives.

The magnitude of the tail rotor's contribution to the dihedral effect is contingent upon its height above the aircraft center of mass. Additionally, the fuselage can contribute to L_v when its aerodynamic center is vertically offset from the center of mass, commonly observed in deep fuselage hulls, resulting in a typically negative L_v component. However, the main rotor typically prevails as the dominant influence, particularly in helicopters equipped with hingeless rotors, where main rotor moments are amplified proportionally with rotor stiffness.

In hover, the L_v derivative is generated through aerodynamics akin to the pitch derivative M_u . As forward flight ensues, some fundamental similarities persist. Velocity perturbations expose the rotor blades to varying aerodynamic forces—the advancing blade experiences an uplift, the retreating blade a descent, and the one-per-revolution flapping response occurs approximately 90° around the azimuth. This imparts a rolling moment to port (or starboard for clockwise rotors) in response to lateral velocity perturbation and a pitch-up moment in reaction to a longitudinal velocity perturbation. The extent of the flapping response is influenced by rotor stiffness, Lock number, and trim lift on the rotor blades.

The directional stability derivative N_v is pivotal for both static and dynamic helicopter stability. Primary contributors include the tail rotor, vertical fin, and fuselage. The fuselage, typically destabilizing with the center of pressure ahead of the center of mass, contrasts with the stabilizing effects (i.e., positive N_v) exhibited by both the tail rotor and vertical fin. While these contributions are approximately linear with speed up to moderate forward speeds, the tail rotor's impact levels off at high speeds, while the contributions from the fin and fuselage persistently increase in positive and

negative senses, respectively.

It is important to start the discussion on the angular velocity derivatives with M_q , L_p , M_p and L_q as the direct and coupled damping derivatives collectively form one of the most pivotal groups within the system matrix. Primary damping derivatives gives character to the short-term, small to moderate amplitude handling characteristics, while cross-dampings assume a prominent role in determining the degree of pitch–roll and roll–pitch couplings. Despite being influential in handling qualities, their close association with short-term rotor stability and response introduces a degree of unreliability as handling parameters.

This cluster of derivatives is predominantly influenced by the main rotor response. The principal damping mechanism in a pitching helicopter arises from the aerodynamic moment generated by the flapping rate, occurring at azimuth positions of 90° and 270° when the rotor is pitching. The disc precesses due to aerodynamic forces at these azimuth stations, lagging behind the rotor shaft and producing a damping effect. The primary coupling mechanism involves the change in one-per-revolution aerodynamic lift when the rotor undergoes pitch or roll, thereby introducing an effective cyclic pitch.

Primary control derivatives can be listed as the derivative of thrust with main rotor collective, $Z_{\delta_{col}}$, the cyclic control derivatives, $M_{\delta_{lon}}$, $M_{\delta_{lat}}$, $L_{\delta_{lon}}$, $L_{\delta_{lat}}$, and the pedal control derivative $N_{\delta_{ped}}$.

The Z-force control derivative experiences a twofold increase in magnitude from hover to high-speed flight, representing the heave control sensitivity. Similar to the heave damping derivative Z_w , this sensitivity is predominantly influenced by blade loading and tip speed.

The direct and coupled moment responses to cyclic control inputs remain practically unaffected by forward speed and are directly influenced by rotor stiffness. Cross-moment derivatives emerge with nonzero stiffness, as the natural frequency of flap motion becomes less than one-per-revolution, resulting in a flap response phase of less than 90° . To counteract this initial coupling, cyclic controls are typically mixed at the swash plate.

2.1.3 Extended Helicopter Dynamics

With rigid body dynamics representation the forward acceleration of the helicopter is assumed to be progress as depicted in figure 2.1. It is as if the whole helicopter tilts forward reducing its pitch angle first to tilt the thrust vector so that the helicopter can gain longitudinal speed.



Figure 2.1: Forward Flight Represented in Rigid Body Dynamics

However, in reality when the helicopter tries to increase its speed with longitudinal cyclic control application, first tip path plane of the main rotor tilts forward also called as a longitudinal flapping. The longitudinal flapping is most apparent in the middle section of figure 2.2. The body pitch angle change and the thrust vector tilt follows this longitudinal flapping motion, resulting in a longitudinal acceleration of the whole aircraft. With extended dynamics the forward flight of the helicopter is accurately modelled resulting in a behaviour in the mathematical state space as depicted in figure 2.2.



Figure 2.2: Forward Flight Represented in Extended Helicopter Dynamics

Commonly used *rigid body dynamics* equations does not model flapping behaviour as previously stated. The main assumption being is the flapping is a much more faster motion with respect to rigid body motion. While working with the frequencies up to approximately 12 rad/s, it is safe to assume that there is no additional flapping state since the flapping of the main rotor reaches its steady state value so fast. However,

if one wants to push the frequency boundary further, the evidence suggests that a number of new state variables are needed, among flapping, to model high frequency motion of the helicopters. These extensions to *rigid body dynamics* are proposed by Tischler and Cauffman [20, 35], and have been used successfully by DLR as well [36]. DLR studies especially puts forward the advantages of using *extended helicopter dynamics* equations over using classical *rigid body dynamics* for helicopter system identification [65].

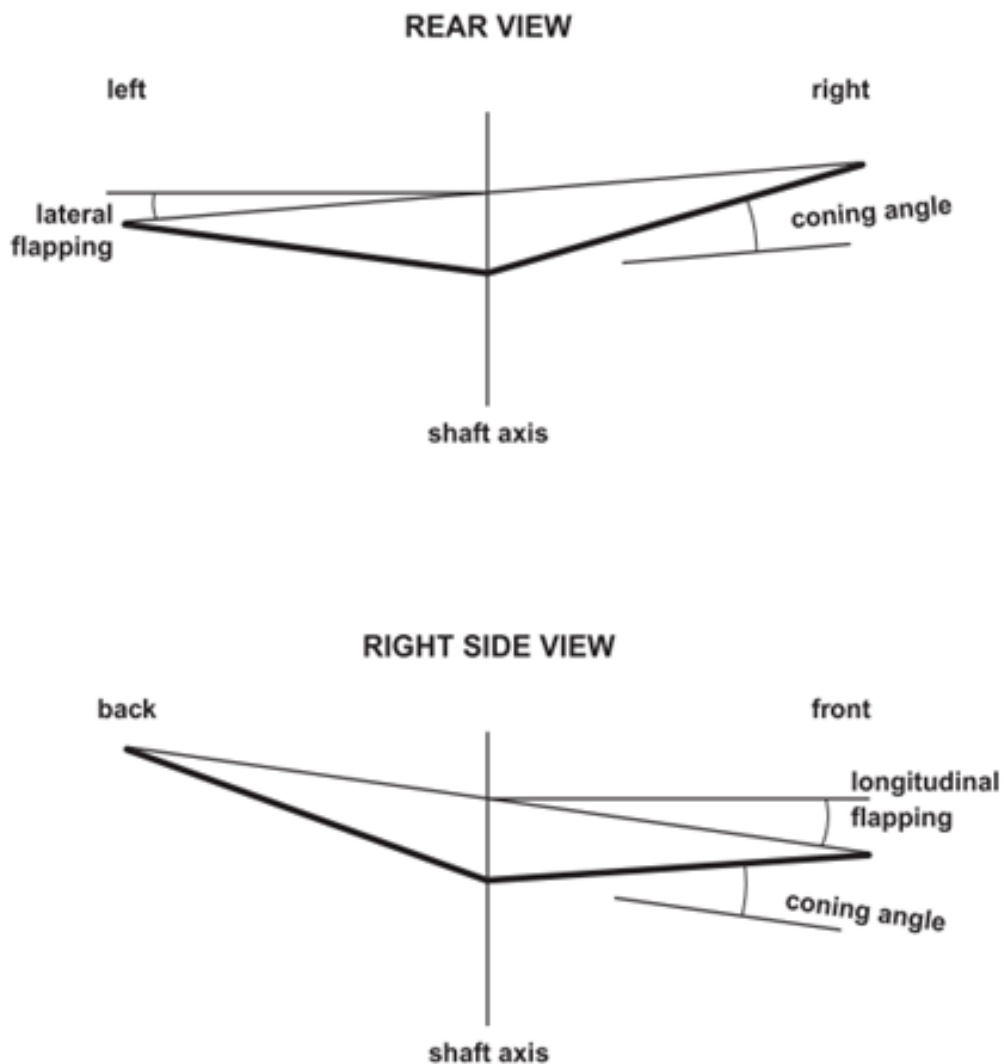


Figure 2.3: Rotor Flapping Angle Definitions [20]

First extension to *rigid body dynamics* is the inclusion of main rotor dynamics. Especially the main rotor regressive flapping couples with the fuselage roll and pitch

motion in stiff rotor helicopters [66]. Flap dynamics of the main rotor best described in the non-rotating frame [67, 68]. In this frame main rotor flapping has three degrees of freedom: longitudinal flapping (β_{1c}), lateral flapping (β_{1s}) and coning (β_0). These states are shown in figure 2.3 The forces and moments transferred from main rotor to fuselage depends on these three tip path plane angles. With some simplifications on the Chen's flapping equations [67, 68] and considering the Hefley's results about main rotor flapping dynamics [66], the regressive flap response of the main rotor can be modelled using two coupled first order equations.

$$\begin{aligned}\tau_f \dot{\beta}_{1s} &= -\beta_{1s} + Lf_{\beta_{1c}}\beta_{1c} + \tau_f p + Lf_{\delta_{lon}}\delta_{lon} + Lf_{\delta_{lat}}\delta_{lat} \\ \tau_f \dot{\beta}_{1c} &= -\beta_{1c} + Mf_{\beta_{1s}}\beta_{1s} + \tau_f q + Mf_{\delta_{lon}}\delta_{lon} + Mf_{\delta_{lat}}\delta_{lat}\end{aligned}\quad (2.8)$$

where the notations Lf and Mf are used to distinguish from fuselage roll and pitch moments L and M .

The rotor flap time constant τ_f can be estimated from geometric properties of the rotor like the hinge offset (e), lock number (γ) and rotor radius (R) using formula given by [66];

$$\frac{1}{\tau_f} = \frac{\gamma\Omega}{16} \left(1 - \frac{8e}{3R}\right) \quad (2.9)$$

where lock number is defined as the ratio of aerodynamic to inertial forces on a helicopter blade [31]¹;

$$\gamma = \frac{\rho ac R^4}{I_b} \quad (2.10)$$

With regressive flapping motion is defined as given above, it is not hard to couple these dynamics with the nominal *rigid body dynamics* equations of motion. The coupling is performed through translational and angular velocity equations. Replacing equations 2.11 with their respective counterparts in equations 2.4 takes care of the flapping coupling.

¹ An effective lock number definition is given by Curtiss which performs better in hovering cases. Detailed explanation on [20] section 11.7.1

$$\begin{aligned}
\dot{u} &= W_0 q + V_0 r - (g \cos \Theta_0) \theta + X_u u + X_v v + X_w w + X_r r + X_{\beta_{1c}} \beta_{1c} \\
&\quad + X_{\delta_{ped}} \delta_{ped} + X_{\delta_{col}} \delta_{col} \\
\dot{v} &= -U_0 r + W_0 p + (g \cos \Phi_0) \phi + Y_u u + Y_v v + Y_w w + Y_p p + Y_r r + Y_{\beta_{1s}} \beta_{1s} \\
&\quad + Y_{\delta_{ped}} \delta_{ped} + Y_{\delta_{col}} \delta_{col} \\
\dot{p} &= L_u u + L_v v + L_w w + L_r r + L_{\beta_{1s}} \beta_{1s} + L_{\delta_{ped}} \delta_{ped} + L_{\delta_{col}} \delta_{col} \\
\dot{q} &= M_u u + M_v v + M_w w + M_r r + M_{\beta_{1c}} \beta_{1c} + M_{\delta_{ped}} \delta_{ped} + M_{\delta_{col}} \delta_{col}
\end{aligned} \tag{2.11}$$

With only regressive flapping mode coupling added, total helicopter model consists of 10 states; $x = [u \ w \ q \ \theta \ v \ p \ \phi \ r \ \beta_{1c} \ \beta_{1s}]^T$.

The second extension to the flap/body coupled model is the inclusion of lead-lag dynamics. Main rotor blades also have an in-plane lead-lag degree of freedom made possible by the lead-lag hinges on the rotor hub. Lead-lag motion of the blades again easier to describe in the non-rotating frame. In non-rotating frame lead-lag motion again has three degrees of freedom; lateral shift of rotor blades (ζ_{1c}), longitudinal shift of the rotor blades (ζ_{1s}) and collective shift of the blades (ζ_0). These shifts of the blade's courses rotor centre of gravity to shift, which generates a sheer force and a moment to be imparted on the fuselage effecting flight dynamics [20].

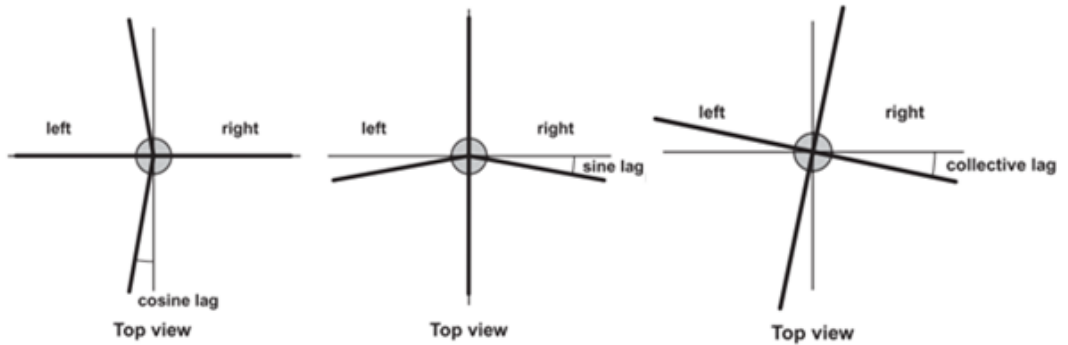


Figure 2.4: Rotor Lag Angle Definitions [20]

The complete state space equations for flap/lead-lag motion are complex [32]; however, previous work by Tischler shows including a closely spaced pole zero pair

(dipole) to the roll and pitch responses can capture the lead-lag effect on helicopter response [35]. Thus, lead-lag effect is modelled by appending two dipoles to pitch and roll responses. Explicit formulation can be followed from [23];

$$\begin{aligned}\frac{p'}{p} &= \frac{K_p(s^2 + 2\zeta_p\omega_p s + \omega_p^2)}{(s^2 + 2\zeta_{11}\omega_{11}s + \omega_{11}^2)} \\ \frac{q'}{q} &= \frac{K_q(s^2 + 2\zeta_q\omega_q s + \omega_q^2)}{(s^2 + 2\zeta_{11}\omega_{11}s + \omega_{11}^2)}\end{aligned}\quad (2.12)$$

This adds eight more identification parameters to the model structure. These dipoles implemented in canonical form contribute to four additional states: $\zeta_{p1}, \zeta_{p2}, \zeta_{q1}, \zeta_{q2}$ ².

Another extension is to include coupled fuselage conning inflow dynamics. The inflow dynamics equation can be written as [20];

$$\dot{\nu} = \frac{-75\pi\Omega}{32} \left(\bar{\nu}_0 + \frac{a\sigma}{16} \right) + C_0 + \nu + \nu_{\dot{\beta}}\dot{\beta}_0 + \frac{25\pi\Omega^2 R}{32} \left(\frac{a\sigma}{8} \right) C_0 K_{\theta_0} \delta_{col} \quad (2.13)$$

where trim thrust coefficient is defined as;

$$\bar{\nu}_0 = \sqrt{\frac{T_0}{2\rho\pi R^2(\Omega R)^2}} \quad (2.14)$$

and $C_0 = 0.639$ from [20]. K_{θ_0} transforms the collective stick input to blade pitch angle. Conning dynamics, ignoring the effect of hinge offset, for the blades can be written as³;

$$\ddot{\beta}_0 = -\frac{\Omega\gamma}{8}\dot{\beta}_0 - \Omega^2\beta_0 - \frac{\Omega\gamma}{6R}\nu + \frac{\Omega^2\gamma}{8}K_{\theta_0}\delta_{col} \quad (2.15)$$

The conning and inflow effects the helicopter thrust coefficient according to equation 2.16;

$$C_0 C_T = \frac{0.543}{\Omega^2 R} \dot{\nu} \frac{4\bar{\nu}_0}{\Omega R} C_0 \nu + \frac{4\bar{\nu}_0}{3\Omega} C_0 \dot{\beta}_0 \quad (2.16)$$

² Seher-Weiss et.al. has alternative formulations for the regressive lead-lag mode [36]

³ Seher-Weiss et.al. has the formulation with the effect of hinge offset added [36]

Coning inflow dynamics are coupled to the fuselage through thrust coefficient and vertical velocity equation. Again replacing equation 2.17 with its counterpart in equations 2.4 will constitute the coupling;

$$\begin{aligned} \dot{w} = & -V_0 p + U_0 q - (g \sin \Phi_0) \theta + Z_u u + Z_w w + Z_v v + Z_p p + Z_q q + Z_r r \\ & + \frac{-\rho \pi R^2 (\Omega R)^2}{m} C_T + Z_{\delta_{lon}} \delta_{lon} + Z_{\delta_{lat}} \delta_{lat} + Z_{\delta_{ped}} \delta_{ped} \end{aligned} \quad (2.17)$$

An extension regarding the engine dynamics is also available on reference [20]. The engine dynamics generally manifests itself as additional phase lag in angular rates of helicopter (p, q, r) to collective input (δ_{col}) Seher-Weiss has another engine modelling technique which can be incorporated from [36], equation 2.18 summarize this alternative model.

$$\begin{aligned} \ddot{\Omega}_{en} = & -2\zeta_{en} \omega_{en} \dot{\Omega}_{en} - \omega_{en}^2 \Omega_{en} + K_{\delta_{col}} \delta_{col} \\ \dot{\Omega} = & \dot{\Omega}_{en} - E_z \Omega_{en} + E_p \Omega \\ \dot{Q} = & R_{\dot{\Omega}} \dot{\Omega}_{en} - E_z R_{\dot{\Omega}} \Omega_{eng} + (R_{\Omega} + E_p R_{\dot{\Omega}}) \Omega + R_Q Q + R_{\delta_{col}} \delta_{col} + R_{\delta_{ped}} \delta_{ped} \end{aligned} \quad (2.18)$$

Engine dynamics couple body equations through yaw rate dynamics;

$$\dot{r} = N_r r + N_v v + N_p p + N_{\delta_{col}} \delta_{col} + N_{\delta_{ped}} \delta_{ped} + N_Q Q + N_{\Omega} \Omega \quad (2.19)$$

This concludes the *extended helicopter dynamics* formulation. There are 17 states and 76 parameters in the model. The initial values of the parameters for system identification purposes can be found from first principles based physical modelling [31, 37], simple low order model fits [20] or values for a similar type of aircraft [69].

Although hybrid model formulation is linear, this model structure can be used both for low-speed and high-speed cases. It should be kept in mind that, *rigid body dynamics* model is valid up to 12 rad/s , with only flapping dynamics extension frequency range goes up to 15 rad/s . Other extensions like inflow/coning and engine dynamics increase the validity range to 30 rad/s . It is possible to use *rigid body dynamics*

model with only flapping dynamics enhancement without lead-lag, or inflow dynamics, however the formulations were presented here for the sake of completeness.

The helicopter dynamic models presented up until now all show the mathematical structure involving the state variables and inputs. The numerical relationship between these variables is determined by the values of the stability derivatives. This work utilizes two different ways to come up with the numeric values of the stability derivatives and system identification is one of them. That is, the system identification applications illustrated in chapter 3 all eventually tries to come up with numeric values for the stability derivatives illustrated in one of the model structures presented above. In that sense the mathematical formulations given in equations 2.3, 2.4, 2.6, 2.7 are the mathematical model postulates for system identification applications in this work.

The other way to come up with the values of stability derivatives is to use a physics based first-principles non-linear mathematical model that is capable of generating linear models around selected equilibrium points in state space. This linear model generation is usually performed with numerical perturbations. Section 2.1.5 describes such a non-linear model that is utilized in this thesis work primarily for system identification data generation. Before that the helicopter platform used in this thesis work is introduced in the following section.

2.1.4 The Platform: T-625

The aircraft used for this work is the T-625 helicopter shown in Fig. 2.5. T-625 is a 6 ton 14 seat medium class utility helicopter and is being developed by Turkish Aerospace. It is powered by 2 LHTECH CTS-800 turboshaft engines rated 1030 HP each. T-625 have made its maiden flight in 2018 and is presently undergoing certification flight testing phase with 3 prototype helicopters. Vehicle characteristics are summarized in Table 2.1.

Although the prototype helicopters are heavily instrumented for platform certification, data required for rigid body system identification are gathered by the on board equipment that belongs to production helicopter. The pilot stick positions and AFCS

actuator inputs are recorded by the AFCS itself. Helicopter attitudes, rates and accelerations are collected by attitude and heading reference system or AHRS for short. Air data is collected through the air data computer. Prototype helicopters are also monitored with real time telemetry during flight tests to reduce the risks involved, especially when the flight envelope is being expanded. Telemetry is able to illustrate the on board equipment data like the AFCS and AHRS in addition to the specially placed flight test instrumentation data to the ground team.



Figure 2.5: T-625 Helicopter

Table 2.1: T-625 Characteristics

Parameter	English	Metric
Weight	13,340 lb	6050 kg
Rotor Diameter	43,3 ft	13,2 m
Length	52,1 ft	15,87 m
Max. Fuel	2,250 lb	1020 kg
V_{NE}	165 knot	306 km/h
V_{Cruise}	150 knot	280 km/h
Range	400 nm	740 km
Endurance	3,8 hours	
Service Ceiling	20,000 ft	6,100 m

2.1.5 Non-linear Helicopter Model: TOROS

The first-principle-based helicopter dynamics model is being developed by Turkish Aerospace to support T-625 program for a while now. The mathematical model is called the TAI Originated Rotorcraft Simulation or TOROS for short. Its use cases are demonstrated for flight mechanics analysis for helicopter design [63, 70, 71, 72, 73, 74], advanced control algorithms development and testing [75, 76, 77, 78, 79, 80], and pilot behaviour modelling [81, 82, 83]. TOROS has also been validated with commercially available tool FLIGHTLAB®.

TOROS is capable of simulating helicopter dynamics in a component based manner. The primary force and moment generating components of a helicopter are modelled separately like the main rotor, tail rotor, empennage, fuselage, etc. Then, forces and moments are summed up then the rigid body dynamics equations given in equation 2.1 are solved with these forces and moments to end up with helicopter rigid body states.

Main rotor and tail rotor models aerodynamics were developed following the widely used blade element theory [37, 31], with quasi-steady aerodynamics, yawed flow [32], and stall delay due to rotation [84] effects, to reflect 3D flow characteristics, are included. The inflow behaviour, which characterises the suction of the air induced by the main rotor rotation, is modelled utilizing the universally accepted Peters-He model [85]. The dynamics of main rotor include the rigid blade flapping, lead-lag and feathering motions; whereas, tail rotor does not have the lead-lag degree of freedom modelled.

The empennage and fuselage forces and moments are generated simply by using their respective aerodynamic database. This is the practice in the industry and proved to give satisfactory results [37, 31, 86]. For this purpose, aerodynamic lift, drag and moment coefficients of the empennage and fuselage are obtained by using computational fluid dynamics analyses.

Engine and drivetrain models are also implemented following references [31] and [87] to include the effects of variable main and tail rotor speeds.

Aerodynamic interference effects between the main rotor, tail rotor, empennage and fuselage are also considered. A finite state wake model following the works of Peters and He [85] is utilized as the default in TOROS. The most significant interference effects occurs between the main rotor and the horizontal tail, tail rotor and vertical tail and between main rotor and fuselage of the helicopter.

TOROS is capable of performing real time, non-linear simulations and has been used for piloted simulator tasks in the system integration laboratory (SIL) of T-625 for automatic flight control system (AFCS) development. TOROS is also the main model for AFCS control law development and thus needs to have a reliable linearization routine. Linear models are generated from the non-linear equations first by small disturbance theory to acquire the full order linear model [10], then the model truncation and reduction are performed by following the guidelines of reference [31], to obtain reduced order linear models. The behaviour of non-linear, full linear and reduced linear models are given in Figure 2.6 and 2.7. In order to check linear model validity doublet inputs in all available control channels are introduced to the helicopter model trimmed at hovering flight condition.

According Hartman – Grobman Theorem [88], behavior of nonlinear system around equilibrium points can be deduced from linearized model results at and around the equilibrium condition which is the hovering flight condition for this case. There are four different model outputs shown in figures 2.6 and 2.7. The nonlinear model results are self explanatory. The *Full Linear* model is the model obtained right after the small perturbation operation. It reflects the full model states, inputs and outputs. Full linear model is then goes through a truncation operation, where fast states are assumed to be at their steady-state values following a quasi-steady model assumption. Some states, that does not effect the rigid body modes, are omitted completely in this step, like the yaw angle, ψ , integrator. This omission is apparent in the last graph of figure 2.6, where only nonlinear and full linear model shows motion in ψ response. Lastly, *Truncated Linear* model order is again reduced to reflect rigid body 6 DoF states and this model is named as the *Reduced Linear* model. The inclusion of only the rigid body states shows itself in the control signals. Nonlinear, full linear and truncated linear model inputs are effected by the actuator dynamics which acts as a low pass filter. Reduced linear model inputs show no such low pass filter dynamics involved.

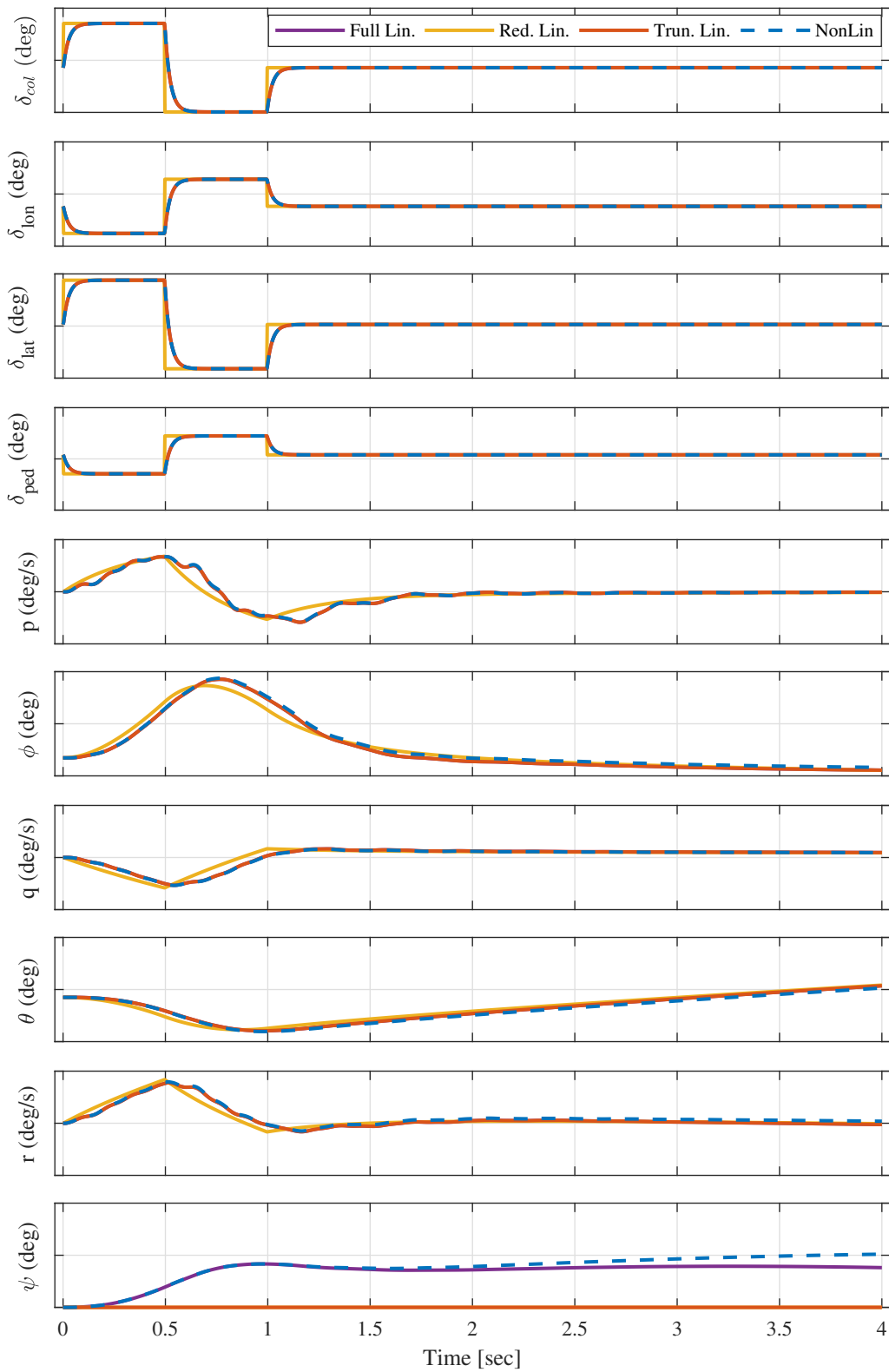


Figure 2.6: TOROS Linear vs Non-Linear Comparison Inputs

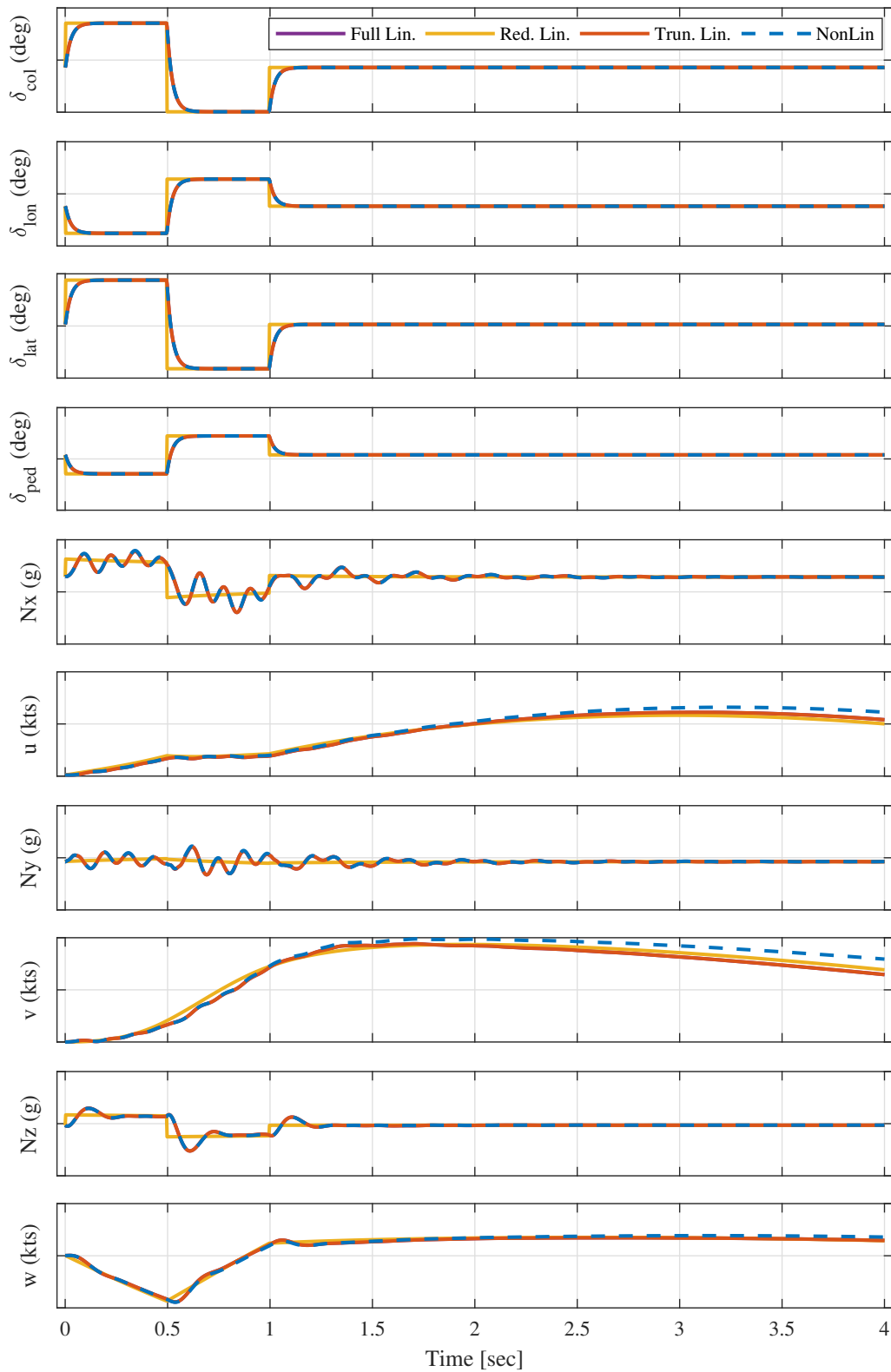


Figure 2.7: TOROS Linear vs Non-Linear Comparison Outputs

Figure 2.6 illustrates the angular response of linear and nonlinear models. The most obvious deduction is reduced linear models inability to capture faster dynamics that are exhibited by the nonlinear or higher order linear models especially in rate responses. The reduction in state space causes reduced linear model to be valid up to a certain frequency level. This is specifically apparent in the roll rate response. The nonlinear model response shows high frequency oscillations, reduced linear model does not. On the other hand, reduced linear model results shows good consistency with the nonlinear model response on both rate and angular responses.

Similar comments can be made for figure 2.7 as well. Although reduced linear model fails to capture faster dynamics above a frequency threshold, its overall response is satisfactory. The faster frequency responses are especially distinguishable in acceleration results which represent the faster dynamics in essence.

Since TOROS results for linear and non-linear models match adequately, it is safe to practice a system identification study with linear lateral-directional model of T-625 first. When the system identification method proves itself on the linear model, it will be ready for use with the non-linear simulation data. After the system identification approach proves itself with the non-linear simulation data, only then it will be ready for use with the real flight test data.

TOROS is also able to generate code that runs in real time for real time activities. It is the running model in the simulator environment of Turkish Aerospace helicopter division where it serves to facilitate both pilot-in-the-loop and hardware-in-the-loop tests for AFCS and airframe development purposes. The simulator, or the system integration laboratory, serves also as a flight training simulator environment where the pilots and flight crew can perform flight test missions prior to real flight, to perfect their procedures. Figure 2.8 illustrates the cockpit and image generator part of the fixed-based simulator during a piloted test section. Apart from real AFCS hardware the simulator environment also possesses the real airworthy equipment for the cockpit including the pilot displays, control panels, mechanical control system and so on for increased realism and testing capabilities.



Figure 2.8: Simulator Environment

This thesis work utilizes TOROS linear and non-linear simulation results for identification. The validation of system identification methods and closed loop identification approaches are performed using linear simulation results since there are less complications involved with using linear data for identification and results can be compared with linear model parameters rather easily. Non-linear simulation data is used for identification only after validation effort showed promising results with linear data. After both linear and non-linear identification results within closed loop framework culminates in satisfactory results, it was possible to use real flight test data in order to reveal real flight characteristics of T-625. To this end, AFCS performance test flight data were utilized. As explained earlier, closed loop flight test data would not be suitable for system identification if a traditional approach were to be used. However, JIO approach made it possible to identify bare airframe dynamics. Following is the explanation of frequency domain system identification methods and approaches utilized for this endeavour.

2.2 System Identification Methods

As explained in Chapter 1, frequency domain system identification is selected as the main identification method in this thesis work. Frequency domain system identification methods distinguish themselves from their time domain counterparts not only by their computational efficiency, robustness to noise, applicability to common control-system design methods and flying qualities analysis, but also it is possible to use them in a non-parametric context so that they provide physical acumen [12, 20].

To this end, in this section non-parameteric frequency domain identification techniques are explained both in SISO and MIMO sense. The main outcome of the non-parametric framework is the frequency response functions. Then, an optimization method for acquiring parametric models from frequency responses is introduced. Lastly, closed loop identification approaches that can be used with frequency domain methods are presented. Formulation for different methods is given and some basic rules of thumb are showcased for achieving the appropriate bare airframe linear model.

2.2.1 SISO Frequency Response Identification

The frequency response function estimation method is a widely used system identification modelling technique especially for helicopter system identification activities. The identification approach will be adopted from reference [20] and a summary of the approach can be given as follows. The Fourier transform as defined in equation 2.20 relates the Fourier coefficients of a systems input ($X(f)$), output ($Y(f)$) and the system's frequency response ($H(f)$) as given in equation 2.21.

$$X(f) = \int_{-\infty}^{\infty} x(t)e^{-j2\pi ft} dt \quad (2.20)$$

$$Y(f) = H(f)X(f) \quad (2.21)$$

That is, theoretically it is possible to come up with a system's frequency response

function using the Fourier transforms of its input and output signals. However, practically it is not possible to come up with the result of the analytic integral given in the equation 2.20. Firstly, the integral goes from minus infinity to infinity, essentially this poses an impossibility since all data record lengths will be finite. Secondly, equation 2.20 assumes a continuous signal however data records from digital computers are discrete. To overcome these problems reference [20] adapts the *Discrete Fourier Transform* (DFT) and spectral functions as a way of estimating the frequency response function. Equation 2.22 shows the auto-spectral and cross-spectral function estimates. The Fourier transform coefficients used for these estimates are the DFT outputs.

$$\begin{aligned}\tilde{G}_{xx}(f) &= \frac{2}{T}|X(f)| \\ \tilde{G}_{xy}(f) &= \frac{2}{T}|X^*(f)Y(f)|\end{aligned}\tag{2.22}$$

While estimating the spectral functions deterministic and nondeterministic errors lead noisy or rough results (denoted with overhead tildes). These errors are tried to be minimized by using *overlapped windowing* also called the method of *periodograms* so that resulting spectral function estimates become smoother. The windowing operation is actually a kind of averaging the rough data in a smart way. The time history segments of data are first multiplied with the window shaping function; then they are averaged over n window segments to result in smooth estimates. Equation 2.23 depicts the windowing operation. n_r is the window number.

$$\hat{G}_{xx}(f) = \frac{1}{0.612n_r} \sum_{k=1}^{n_r} \tilde{G}_{xx,k}(f)\tag{2.23}$$

It is straightforward to estimate frequency response function from the smoothed auto-spectral and cross-spectral densities. At each frequency point equation 2.24 is executed. From now on the hat and tilde notation from the equations will be dropped for clarity, and the following spectral density functions in equations are all smooth estimates unless otherwise specified. MIMO application of frequency response estimation is very similar to SISO case and extension to MIMO identification is fairly straightforward.

$$H(f) = \frac{\hat{G}_{xy}(f)}{\hat{G}_{xx}(f)} = \frac{\hat{G}_{yy}(f)}{\hat{G}_{yx}(f)} \quad (2.24)$$

2.2.2 MIMO Frequency Response Identification

MIMO frequency domain identification follows directly from SISO identification formulation. For single-input-single-output (SISO) systems, where $u \in \mathbb{R}$ and $y \in \mathbb{R}$, frequency response function can be estimated by using cross-spectral and auto-spectral functions as given in equation 2.24 [89, 20]. The extension of this frequency response to multi-input-multi-output (MIMO) systems is pretty straightforward. For $u \in \mathbb{R}^{n_i}$ and $y \in \mathbb{R}^{n_o}$;

$$\begin{aligned} \mathbf{H}(j\omega) &= \mathbf{G}_{uy} \mathbf{G}_{uu}^{-1} \\ &= \begin{bmatrix} \frac{y_1}{u_1}(j\omega) & \dots & \frac{y_{n_o}}{u_1}(j\omega) \\ \vdots & \ddots & \vdots \\ \frac{y_1}{u_{n_i}}(j\omega) & \dots & \frac{y_{n_o}}{u_{n_i}}(j\omega) \end{bmatrix} = \begin{bmatrix} G_{u_1 y_1} & \dots & G_{u_{n_i} y_1} \\ \vdots & \ddots & \vdots \\ G_{u_1 y_{n_o}} & \dots & G_{u_{n_i} y_{n_o}} \end{bmatrix} \begin{bmatrix} G_{u_1 u_1} & \dots & G_{u_{n_i} u_1} \\ \vdots & \ddots & \vdots \\ G_{u_1 u_{n_i}} & \dots & G_{u_{n_i} u_{n_i}} \end{bmatrix}^{-1} \end{aligned} \quad (2.25)$$

It is clear from Eq. (2.25) that the spectral matrix \mathbf{G}_{uu} should be invertible. Closer inspection will reveal, however; that correlated input sets result in degenerate \mathbf{G}_{uu} matrices; thus, MIMO identification could not be performed under such excitation. It is also sensible from a practical perspective, when there are correlated inputs for a linear system, it is impossible to distinguish their effects from one and other by looking only the outputs of the system. Controversially, if the inputs are uncorrelated, i.e., have different frequencies, it would be possible to establish their effects on the outputs individually.

For the sake of the following discussion, an example closed loop system would be beneficial. A sample representative block diagram for a stability augmentation system (SAS) algorithm can be seen in Figure 2.9 for a helicopter. Notice all the rigid body angular rates (p, q, r) are used as feedback signals in the control algorithm since the main objective is to dampen out angular rates. A pitch angle (θ) feedback is also utilized to improve the controller performance in longitudinal axis.

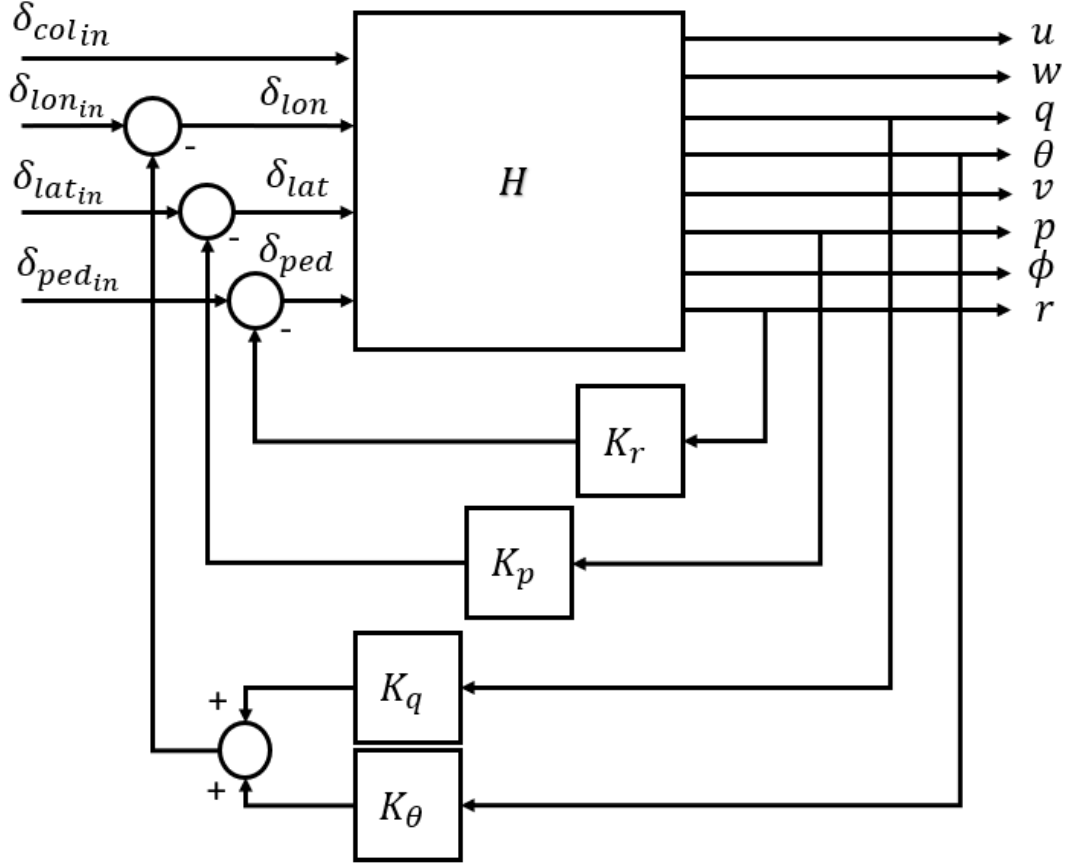


Figure 2.9: Simple SAS Block Diagram

Ref. [20], puts forward the multi-input-single-output (MISO) identification guideline based on the cross control correlations between inputs. Following the system given in figure 2.9, and defining the excitation inputs for system identification as; $\delta_{a_{in}} = [\delta_{col_{in}} \ \delta_{lon_{in}} \ \delta_{lat_{in}} \ \delta_{ped_{in}}]^T$ and bare airframe inputs as $\delta_a = [\delta_{col} \ \delta_{lon} \ \delta_{lat} \ \delta_{ped}]^T$, and noticing $\delta_{col} = \delta_{col_{in}}$ since there is no feedback on that channel, the MISO direct solution guideline can be represented for the case at hand as;

$$\left(\gamma_{\delta_{a_i} \delta_{a_j}}^2 \right)_{ave} < 0.5 \quad \text{for } i, j = 1 : 4 \quad \text{and } i \neq j \quad (2.26)$$

If the condition given in Eq. (2.26) does not hold, the MISO solution fails due to inversion of the ill-conditioned input spectral density function matrix in Eq. (2.25).

Even if there is high correlation between inputs, secondary inputs may be weak enough so their effects on outputs can be ignored and assumed they do not alter

identification results. That is, if the cross control correlation between the inputs is high but the secondary control auto-spectra is low then it may be possible to discard the secondary inputs and perform a SISO identification which was put forward as a guideline again [20].

$$\left(G_{\delta_{a_i}\delta_{a_i}}\right)_{ave} - \left(G_{\delta_{a_j}\delta_{a_j}}\right)_{ave} \leq -20dB \quad for \quad i, j = 1 : 4 \quad and \quad i \neq j \quad (2.27)$$

If the condition given in equation 2.26 holds then, MISO solution can be performed for all outputs recursively to obtain the whole MIMO solution. Alternatively, if the condition given in equation 2.27 is valid then a SISO solution, again for each output can be pursued to end up with MIMO solution. Nonetheless, generally neither condition holds for plant inputs in closed loop systems. That is the main reason why, system identification tests are performed without an active feedback regulation. When closed loop identification is unavoidable, there are a couple of approaches that can be utilized which are explained in the following section.

2.2.3 Closed Loop Identification Approaches

As explained in the chapter 1, closed loop identification approaches found in literature are the *direct approach*, the *indirect approach*, and *joint input output approach*.

The application of direct approach is fairly straightforward. Again using the block diagram given in Fig. 2.9, the definitions for $\delta_{a_{in}}$, δ_a , defining the output vector as $y = [u \ w \ q \ \theta \ v \ p \ \phi \ r]^T$ and since the feedback is effectively disregarded and assumed to be non-existent the solution becomes;

$$\mathbf{H}(j\omega) = \frac{y}{\delta_{a_{in}}} = \begin{bmatrix} G_{\delta_{col_{in}}u} & \cdots & G_{\delta_{ped_{in}}u} \\ \vdots & \ddots & \vdots \\ G_{\delta_{col_{in}}r} & \cdots & G_{\delta_{ped_{in}}r} \end{bmatrix} \begin{bmatrix} G_{\delta_{col_{in}}\delta_{col_{in}}} & \cdots & G_{\delta_{ped_{in}}\delta_{col_{in}}} \\ \vdots & \ddots & \vdots \\ G_{\delta_{col_{in}}\delta_{ped_{in}}} & \cdots & G_{\delta_{ped_{in}}\delta_{ped_{in}}} \end{bmatrix}^{-1} \quad (2.28)$$

Although practically uncomplicated, it is clear that this approach will yield incorrect results when the feedback gains are not negligibly small.

Indirect approach is a bit more computationally extensive, although still very practical. Identification is again performed through reference inputs to plant outputs but this time with the help of the controller frequency response, \mathbf{K} , the plant frequency response is calculated.

$$\mathbf{H}(j\omega) = \frac{\frac{y}{\delta_{a_{in}}}}{\mathbf{I} - \mathbf{K} \frac{y}{\delta_{a_{in}}}} \quad (2.29)$$

It is obvious from equation 2.29 that any inconsistency in the knowledge of \mathbf{K} will distort plant frequency response solution. Depending on the structure of the control algorithm and plant it would be problematic to understand how a certain error in \mathbf{K} will reflect on to the plant, making the identification parameters effect non-transparent during a possible defect correction.

The JIO approach emerged to address the specific correlation problem between the recorded bare airframe inputs during closed loop tests where MIMO identification is desired. It is possible to extract the bare airframe dynamics by only using uncorrelated inputs. Basic JIO approach can be defined as;

$$\mathbf{H}(j\omega) = \frac{y}{\delta_a} = \frac{y}{\delta_{a_{in}}} \left[\begin{array}{c} \delta_a \\ \delta_{a_{in}} \end{array} \right]^{-1} \quad (2.30)$$

Eq. 2.30 allows to identify frequency response matrix $\mathbf{H}(j\omega)$ even if the immediate inputs to $\mathbf{H}(j\omega)$ are correlated. Note that the frequency response matrices at the right hand side of Eq.2.30 both have the same inputs. MIMO identification is possible as long as there is an uncorrelated set of excitation signals, which can always be ensured with proper experiment design even under closed loop conditions. Two different operations following Eq. 2.25 can be performed to obtain the frequency responses from excitation signals to outputs and from excitation signals to bare-airframe inputs. Then $\mathbf{H}(j\omega)$ can be obtained by simply using the relation given in Eq. 2.30. By exciting the δ_{in} inputs sequentially with frequency sweeps, an uncorrelated excitation set can be guaranteed for JIO approach application for the helicopter bare-airframe identification case.

2.2.4 Parametrization of Frequency Response Identification Methods

For both SISO and MIMO identification, there exists a parameterized model which can simulate the identified frequency responses with correct parameters. Frequency responses offer a lot, even if there is no transfer function representation available. However, a parameterized linear model is often sought out for control development or model validation activities. Thus with a correct linear model postulate, like the ones given in equations 2.3, 2.4, 2.7, 2.6 or in equations 2.8 through 2.19, it is possible to fit the obtained frequency responses using a selected parameter set within these equations as optimization parameters. There are several optimization algorithms that can perform intelligent guesses for the optimization parameters, that will decrease a predetermined cost function [90, 91]. A commonly used cost function for quantifying the cost between two different frequency responses is given by reference [20].

$$J = \frac{20}{n_\omega} \sum_{\omega_1}^{\omega_{n_\omega}} W_g (|T_c| - |T|)^2 + W_p (\angle T_c - \angle T)^2 \quad (2.31)$$

The n_ω is the number of frequency points (typically selected as 20), ω_1 and ω_n are the first and last frequencies for the frequency range of interest. W_g and W_p are the gain and phase weightings respectively. The normal convention is to take $W_g = 1$ and $W_p = 0.01745$ which assigns a 1-dB magnitude error comparable with a 7.57 degrees of phase error. A rule of thumb for the cost function given in equation 2.31 is to aim a value less than a hundred ($J \leq 100$). A cost that is less than a hundred generally indicates an acceptable level of accuracy for flight dynamics. A cost of $J \leq 50$ reflects a match that is indistinguishable from one another. A straightforward extension of equation 2.31 to multiple frequency responses in order to use with MIMO systems is again can be found in reference [20].

$$J = \sum_{n_{TF}}^{l=1} \left(\frac{20}{n_\omega} \sum_{\omega_1}^{\omega_{n_\omega}} W_g (|T_c| - |T|)^2 + W_p (\angle T_c - \angle T)^2 \right)_l \quad (2.32)$$

n_{TF} is the total number of frequency responses, however; for most practical situations identification data does not have enough content for each input output pair of a MIMO system. In such cases several frequency responses are dropped from the cost

function calculations so that only the relevant relationships between input and output data are penalized. The overall accuracy of a MIMO cost function is quantified by the average cost function, $J_{ave} = J/n_{TF}$. The general rule of thumb for the MIMO case is to have an average cost function of $J_{ave} \leq 200$.

With a model postulate like the ones given in equations 2.3 and 2.4, it is possible to come up with a dynamic model by adjusting the model parameters that matches the frequency responses obtained from a flight test. When the parameters to be identified are determined within a given model postulate, it is only a question of what the values of the selected parameters should be, in order to match the test data frequency response or to reduce the cost given in equation 2.32. That is, if the parameters are to be collected together in an identification vector, $\Theta = [\theta_1, \theta_2, \dots, \theta_{n_p}]$, the parameter identification problem can be defined as;

$$\begin{aligned} & \underset{\Theta}{\text{minimize}} && J(\Theta) \\ & \text{subject to} && \dot{x} = Ax + Bu, \\ & && y = Cx + Du \end{aligned} \tag{2.33}$$

After the optimization problem is set out, any minimization algorithm can be used to come up with the values of the model parameters. For aircraft identification there are numerous examples of different algorithms such as secant method [20], Newton-Raphson [19], Gauss-Newton[21], Levenberg-Marquardt [90].

The precision or confidence level of the identified parameters, Θ , holds significant importance for several purposes. For starters, assessing the need for refining the model structure is one crucial aspect. When a parameter's confidence is notably low due to insufficient data or weak correlation with other parameters, it becomes beneficial to either remove that parameter from the model structure or substitute it with a value aligned with physical principles. This process significantly enhances the accuracy and dependability of the final model. Parameter accuracy is vital in designing and evaluating control systems to ensure their robustness. Various control design methods rely on estimated uncertainties during the design phase. These estimated uncertainties are later used to assess the anticipated deviation from nominal performance once the control system design is finalized. Comparing flight-test parameters

with simulation parameters necessitates understanding the confidence level associated with both sets of parameters. Having this knowledge is essential for evaluating apparent differences between the two sets of parameters.

Theoretical accuracy analysis can constitute a basis for the confidence levels of the identified parameters [20, 92, 93]. The method for theoretical accuracy analysis involves estimating the anticipated variation in parameters. It derives from a sensitivity examination of the finalized identification outcome. Theoretically, this mirrors the standard deviation of parameter estimates attained by running identification across multiple data sets. Additionally, this theoretical accuracy analysis yields extensive insights into the reasons behind parameter variability, aiding in the enhancement of the model structure. The foundation of the theoretical accuracy analysis lies in the Cramér–Rao inequality. This principle sets the Cramér–Rao bounds as the lowest anticipated standard deviation in parameter estimation achievable through numerous repetitive maneuvers.

$$\sigma_i \leq CR_i \tag{2.34}$$

The comparative Cramér–Rao bounds across the identification parameters play a crucial role in improving the model structure. When specific parameters exhibit significantly higher Cramér–Rao bounds in relation to others, it signifies a challenge in identifying them accurately. This situation indicates a poor level of identifiability and implies that these parameters might need to be removed or fixed within the model structure. The Cramér–Rao bound of a given identified parameter is determined from the inverse of the Hessian matrix.

$$CR_i = \sqrt{H_{ii}^{-1}} \tag{2.35}$$

where an $n_p \times n_p$ Hessian matrix is defined as;

$$H = \nabla_{\Theta}^2 J = \frac{\partial^2 J}{\partial \Theta \partial \Theta^T} = \begin{bmatrix} \frac{\partial^2 J}{\partial \theta_1^2} & \cdots & \frac{\partial^2 J}{\partial \theta_1 \partial \theta_{n_p}} \\ \vdots & \ddots & \vdots \\ \frac{\partial^2 J}{\partial \theta_{n_p} \partial \theta_1} & \cdots & \frac{\partial^2 J}{\partial \theta_{n_p}^2} \end{bmatrix} \quad (2.36)$$

The most effective representation of the Cramér–Rao bounds is in relation to the converged identification values, usually expressed as a percentage and they are given with their percentage values in related identification results in this work.

$$CR = \frac{CR_i}{\theta_i} \times 100\% \quad (2.37)$$

CHAPTER 3

SYSTEM IDENTIFICATION APPLICATIONS

3.1 Introduction

The identification applications performed in this thesis work use frequency methods with JIO and direct approaches as explained before. Since JIO is not the established procedure for dynamic system identification, a validation for the approach was sought. Initially, linear models both from literature and TOROS were used for validation studies. System identification data were collected by performing time marching simulations with linear models in a closed loop setup. Open loop frequency responses for bare airframe were calculated using JIO and the direct approach. Comparison of identified frequency responses with the linear model bode plots made it possible to compare the JIO and direct approaches performances. Later, a validation with non-linear simulation data was performed, again first by comparing the frequency responses of bare airframe models obtained from JIO and direct approaches. Reference frequency responses for identification results were acquired from perturbation based linear models provided by TOROS again.

After frequency response comparisons proved that the JIO approach was able to predict open loop dynamic responses adequately, a complete system identification is achieved by parameter optimization of adequate model postulates. Parameter optimization aims to reduce the difference between the frequency responses obtained from flight test and their model postulates as explained in Chapter 2. The parameter optimization is performed only for T-625 rigid body dynamics, using linear and non-linear simulation data. Unlike the frequency responses, having identified system models also made it possible to perform validation comparisons in time domain where,

step responses obtained from simulation models and system identification models were analysed to evaluate the overall system identification performance. Subsequent to the JIO approach and model parametrization validations, the same frequency response generation and model parameter optimization practice is followed by utilizing real flight test data yielding a system identification model for T-625 helicopter in 70 knots level flight conditions.

The applications follow an increasing complexity. Initial proof of concept is the lateral fixed wing linear dynamics with a single proportional feedback. The linear model and control structure was found from literature and implemented in a simulation environment. Then, lateral rotary-wing linear dynamics with two proportional feedback on two channels is used. This linear plant model is obtained from TOROS and a controller is designed for identification purposes. After JIO was proved to be successful in producing correct frequency responses for bare airframe dynamics with two different lateral dynamic models, a full rotary-wing rigid body linear model, obtained again from TOROS, is used. This time the control structure consists of 2 proportional and a proportional integral feedback. The feedback controller was designed so that it will stabilize the naturally unstable plant in the longitudinal axis. Before moving on the nonlinear model for validation, a noise sensitivity study is performed within linear rigid body dynamics section to get a notion of how much noise can be tolerated when applying this approach to real flight test data. Then, a closed loop system identification with the nonlinear simulation data is performed. After all of these method validations are performed a full rigid body dynamics solution for the rotary-wing platform is performed with real flight test data. Frequency domain method with JIO approach proved to be satisfactory for all of these use cases.

3.2 Airplane Lateral Dynamics with Linear Simulation Data

Learjet-25 is a fixed wing jet propelled aircraft that has a maximum take off weight of 6800 kg, a cruise speed of 464 KTAS, a maximum range of 1535 nautical miles, and a service ceiling of 45,000 feet [94]. Fixed wing aircraft dynamics are suitable for decoupling in the lateral and longitudinal motion domains since they are symmetrical vehicles in the sense that their right and left hand sides are exact mirror images.

Learjet-25's lateral dynamics are selected for the first validation case of this thesis because it is suitable for application of JIO and frequency response estimation methods and the lateral dynamics linear model is available in literature [26]. Within this application, two closed loop identification methods will be compared. The direct method will be used to identify bare airframe model using the bare airframe input and output data, disregarding the feedback loop. The direct method is employed in a SISO sense since attempting to MIMO direct method application is impossible due to bare airframe input correlation as explained in section 2.2.2. The JIO method, on the other hand, is utilized in a MIMO setting, since it is specifically designed to overcome the bare airframe input correlation issue.

Figure 3.1 shows the block diagram of lateral directional dynamics of a Learjet-25 fixed wing aircraft. The bare airframe dynamics can be considered as the same as given in equation 2.7. The control and stability derivatives that constitute the open loop dynamic model are taken from reference [26]. The closed loop lateral dynamics for the LJ-25 has a simple proportional feedback on rudder input. This feedback mechanism is designed to suppresses the dutch-roll mode of the aircraft.

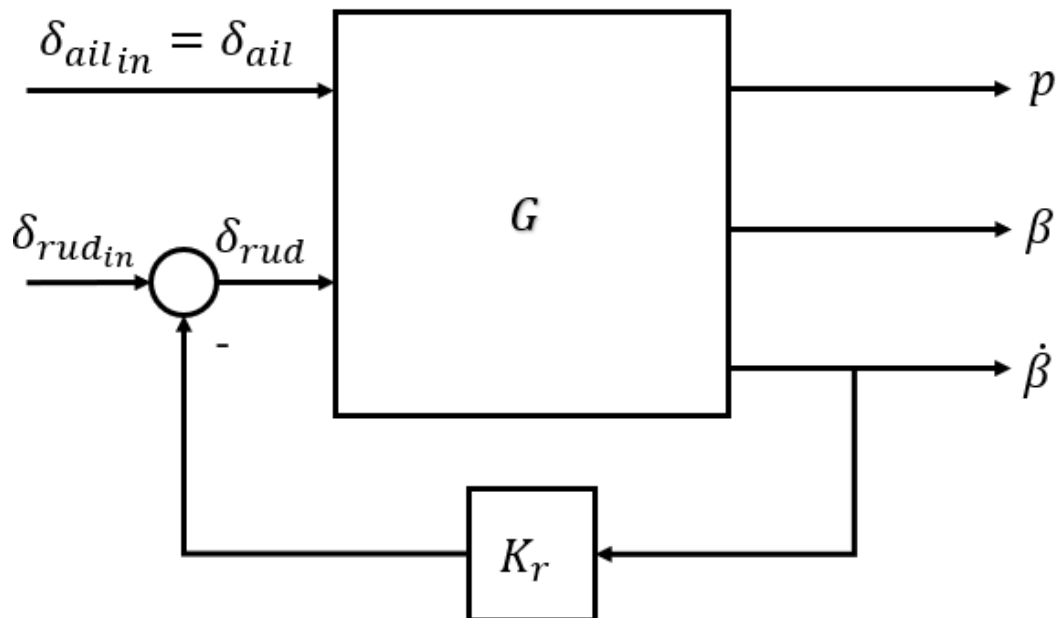


Figure 3.1: LJ-25 Lateral Directional Dynamics Block Diagram

The identification inputs are selected as frequency sweeps. The frequency of the sweeps changes exponentially with time to avoid going over slower frequencies rapidly. A complete guide on construction computer generated frequency sweep inputs can be found in reference [20]. Frequency range of interest is selected as 0.8 rad/s to 15 rad/s to cover the lateral rigid body dynamic mode natural frequencies. The excitation signals also utilizes a fade-in-fade-out (FIFO) part which adjusts excitation amplitude at the start and end of the excitation. The FIFO is not really necessary for linear model simulations, however; it plays a critical role during non-linear simulations or real flight tests to avoid losing the trimmed flight condition quickly. The excitation signals were given in conjunction with one and other from the ports labelled as $\delta_{ail_{in}}$ and $\delta_{rud_{in}}$ in block diagram. Excitation signals and resulting bare airframe inputs are shown in Figure 3.2.

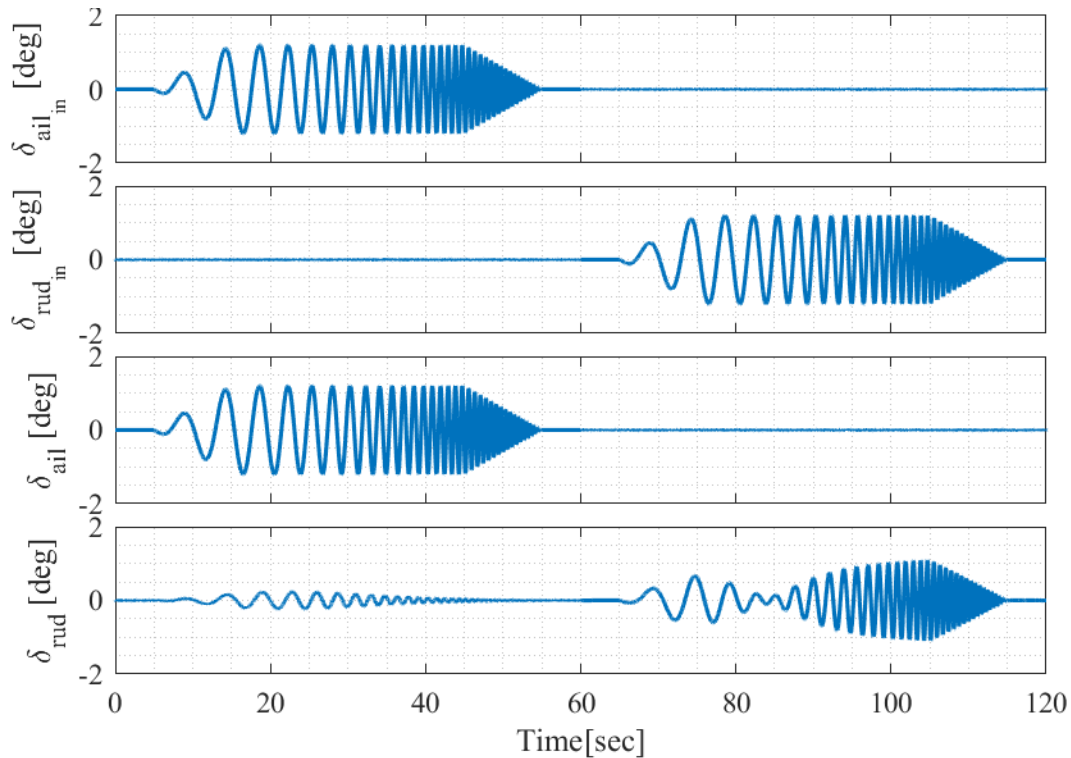


Figure 3.2: LJ-25 Simulation Inputs

As can be seen from Figure 3.2, especially during aileron excitation the bare airframe inputs show high levels of correlation due to rudder feedback. If this correlation were not present, MIMO direct approach would have been implemented as shown

in equation 3.2. However the correlation between inputs makes the matrix inversion impossible for the second matrix at the right hand side of the equation. That is, the conditions given in equations 2.26 does not hold. Thus, MIMO direct method is not applicable to this case and direct approach results are only available as SISO solutions. Direct approach responses follow equation 2.24 and for this specific case become;

$$\begin{aligned} \frac{p}{\delta_{ail}} &= \frac{G_{\delta_{ail}p}}{G_{\delta_{ail}\delta_{ail}}} & \frac{p}{\delta_{rud}} &= \frac{G_{\delta_{rud}p}}{G_{\delta_{rud}\delta_{rud}}} \\ \frac{\beta}{\delta_{ail}} &= \frac{G_{\delta_{ail}\beta}}{G_{\delta_{ail}\delta_{ail}}} & \frac{\beta}{\delta_{rud}} &= \frac{G_{\delta_{rud}\beta}}{G_{\delta_{rud}\delta_{rud}}} \end{aligned} \quad (3.1)$$

MIMO frequency response generation from simulation data follows equations 2.25. Two separate frequency response set are generated for the problem at hand, one from excitation signals to outputs and one from excitation signals to bare airframe inputs.

$$\begin{bmatrix} \frac{p}{\delta_{ail_{in}}} & \frac{p}{\delta_{rud_{in}}} \\ \frac{\beta}{\delta_{ail_{in}}} & \frac{\beta}{\delta_{rud_{in}}} \end{bmatrix} = \begin{bmatrix} G_{\delta_{ail_{in}}p} & G_{\delta_{rud_{in}}p} \\ G_{\delta_{ail_{in}}\beta} & G_{\delta_{rud_{in}}\beta} \\ G_{\delta_{ail_{in}}\dot{\beta}} & G_{\delta_{rud_{in}}\dot{\beta}} \end{bmatrix} \begin{bmatrix} G_{\delta_{ail_{in}}\delta_{ail_{in}}} & G_{\delta_{rud_{in}}\delta_{ail_{in}}} \\ G_{\delta_{ail_{in}}\delta_{rud_{in}}} & G_{\delta_{rud_{in}}\delta_{rud_{in}}} \end{bmatrix}^{-1} \quad (3.2)$$

$$\begin{bmatrix} \frac{\delta_{ail}}{\delta_{ail_{in}}} & \frac{\delta_{ail}}{\delta_{rud_{in}}} \\ \frac{\delta_{rud}}{\delta_{ail_{in}}} & \frac{\delta_{rud}}{\delta_{rud_{in}}} \end{bmatrix} = \begin{bmatrix} G_{\delta_{ail_{in}}\delta_{ail}} & G_{\delta_{rud_{in}}\delta_{ail}} \\ G_{\delta_{ail_{in}}\delta_{rud}} & G_{\delta_{rud_{in}}\delta_{rud}} \end{bmatrix} \begin{bmatrix} G_{\delta_{ail_{in}}\delta_{ail_{in}}} & G_{\delta_{rud_{in}}\delta_{ail_{in}}} \\ G_{\delta_{ail_{in}}\delta_{rud_{in}}} & G_{\delta_{rud_{in}}\delta_{rud_{in}}} \end{bmatrix}^{-1} \quad (3.3)$$

JIO approach is completed by utilizing the two set of frequency responses together. Again referring back to section 2.2.3, equation 2.30 for this problem becomes,

$$\frac{y}{\delta_a} = \frac{y}{\delta_{a_{in}}} \left[\frac{\delta_a}{\delta_{a_{in}}} \right]^{-1} \quad (3.4)$$

where,

$$\begin{aligned}
y &= [p \quad \beta \quad \dot{\beta}]^T \\
\delta_a &= [\delta_{ail} \quad \delta_{rud}]^T \\
\delta_{a_{in}} &= [\delta_{ail_{in}} \quad \delta_{rud_{in}}]^T
\end{aligned} \tag{3.5}$$

It is possible to use MIMO frequency response estimation as given in equation 3.2 for both frequency response from $\delta_{a_{in}}$ to y and from $\delta_{a_{in}}$ to δ_a since the excitation inputs ($\delta_{a_{in}}$) are not correlated in either case. The excitation can be given in a controlled and predetermined manner so that it is never correlated. This ability to excite the system from any given point in the block diagram without introducing any correlation, and still being able to identify bare airframe with two different frequency response function estimate matrices, make JIO approach such powerful tool. In situations like these, where the direct approach fails, JIO is still applicable. What is more, the results show greater agreement with the truth data for JIO approach rather than the SISO direct method.

Frequency response results are depicted in Figures 3.3, 3.4, 3.5, and 3.6.

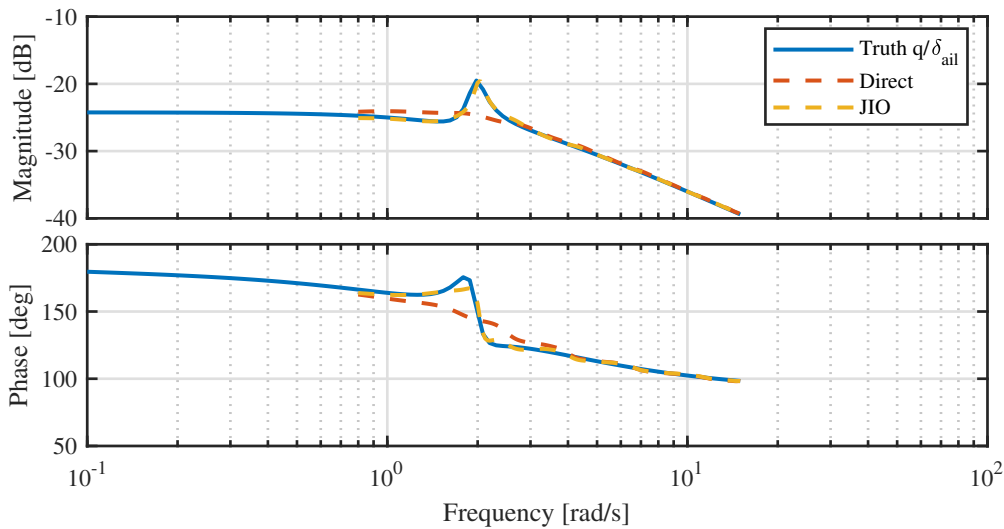


Figure 3.3: LJ-25 Aileron to Roll Rate Frequency Response Estimation

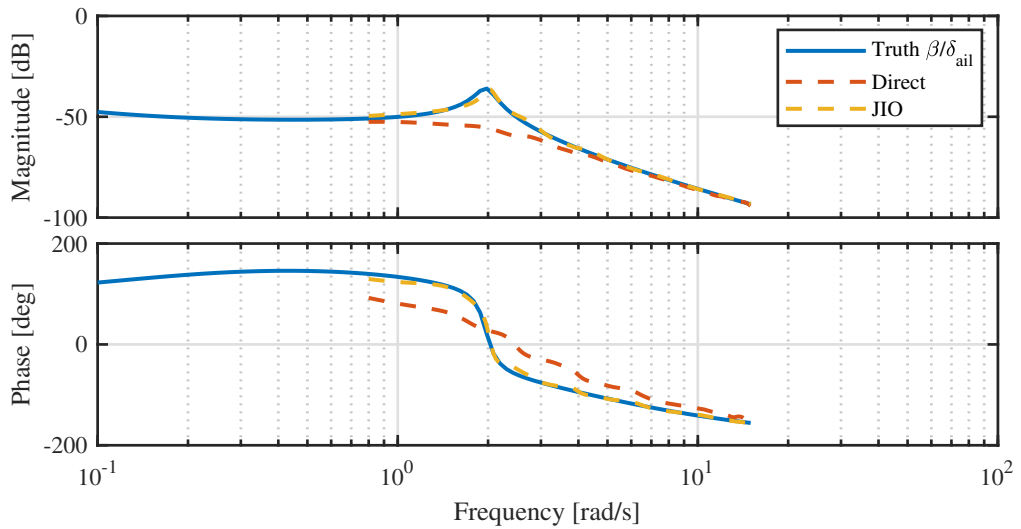


Figure 3.4: LJ-25 Aileron to Side Slip Angle Frequency Response Estimation

It is apparent from figures that direct approach fails to capture dutch-roll mode; whereas, JIO approach captures the effects. Direct approach tries to estimate the dynamics while the pedal feedback tries to suppress the dutch-roll mode dynamics; that is why, direct approach results show a higher damped dutch-roll mode compared to JIO approach results.

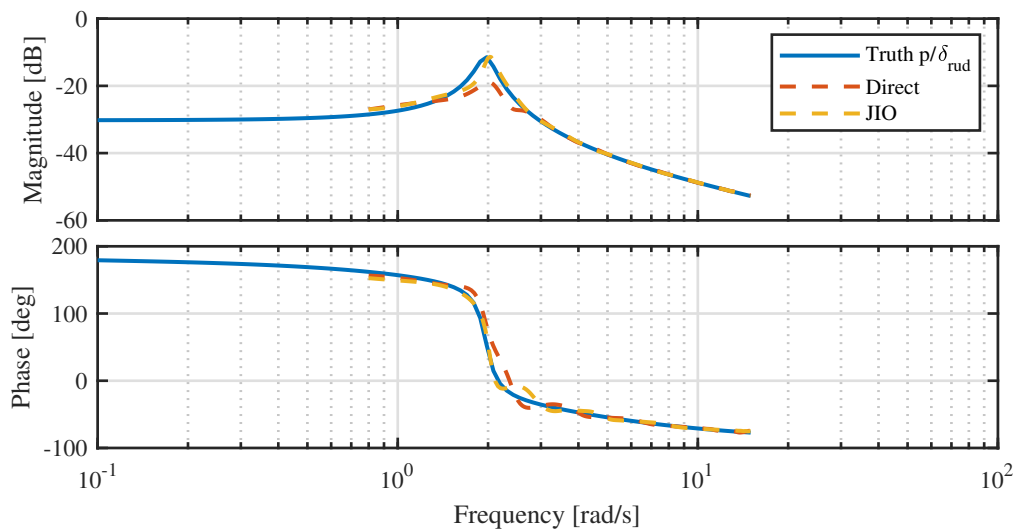


Figure 3.5: LJ-25 Rudder to Roll Rate Frequency Response Estimation

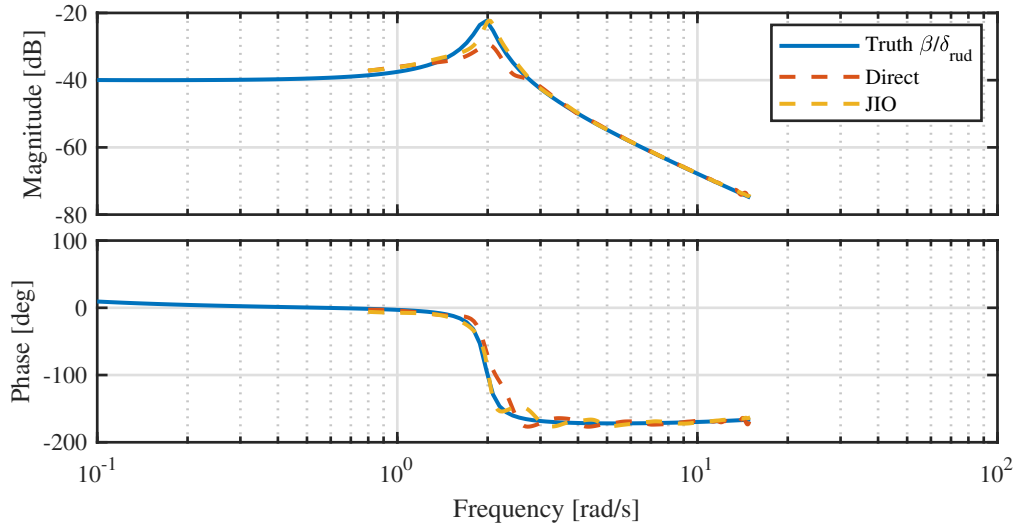


Figure 3.6: LJ-25 Rudder to Side Slip Angle Frequency Response Estimation

Frequency response estimations seems to be on point for JIO approach for all of the response pairs shown in both magnitude and phase. Direct approach, on the other hand; manages to capture the truth model response in high frequency region; however, around the dutch-roll mode cross over fails to capture the true behaviour of the system. This failure is mainly due to the assumption about not taking the feedback signal into account during direct approach frequency response generation. The time histories for LJ-25 linear simulation can be found in appendix section A.

3.3 Helicopter Lateral Dynamics with Linear Simulation Data

T-625 is a medium weight classical configuration helicopter being developed by Turkish Aerospace as explained in section 2.1.4. Its maximum take of weight is 6 tons and will be able to carry up to 12 personnel excluding the pilot and the copilot. It has a conventional limited authority control system that is still being developed. T-625 prototypes are also equipped with a *development test system* (DTS) which is able to inject excitation inputs and record all the signals within the control system. This section tires to extend the results of LJ-25 lateral dynamics identification using closed loop data with JIO method to T-625 lateral dynamics since the benefits of such and identification capacity would be colossal.

The bare airframe lateral dynamics of T-625 can be assumed to be the same as given in equation 2.7. Most basic function of the AFCS is the stability augmentation system (SAS). For lateral dynamics, SAS operates by utilizing proportional feedback loops on roll and yaw rates of the helicopter. A block diagram representation for T-625 lateral dynamics is shown in Figure 3.7, analogous to LJ-25 case. However, unlike LJ-25, T-625 has two distinct feedback loops on both lateral and pedal inputs. T-625 lateral dynamics identification is a direct extension to LJ-25 case both in regards of fixed-wing to helicopter dynamics transition and from SISO feedback loop to MIMO feedback loop. One of the major advantages of JIO approach reveals itself at this point. Since JIO approach requires no knowledge of the feedback mechanism, from an analytical stand point, no change is required when compared with LJ-25 case, to come up with the frequency responses of the bare airframe.

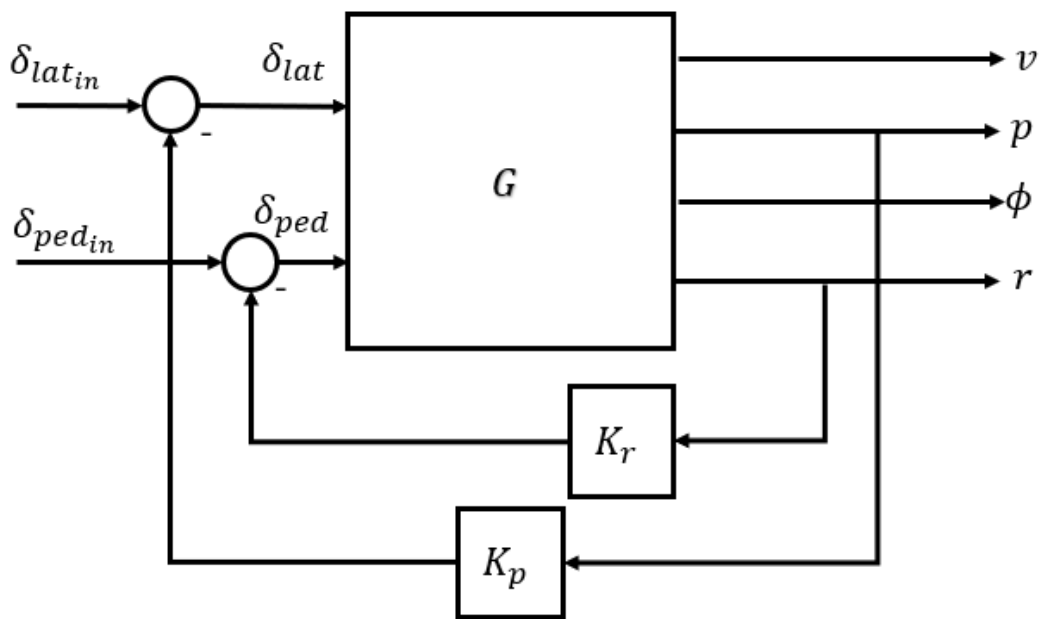


Figure 3.7: T-625 Lateral Directional Dynamics Block Diagram

Just as in LJ25 case the, frequency responses from the excitation signals to outputs and from excitation signals to bare airframe inputs are identified using spectral functions with periodogram windowing as depicted in equation 2.25 and processed as the JIO method dictates. The excitation, bare airframe input and output terms in equation 2.30 need to be updated for this case . The output, excitation and bare airframe in-

put signals are $y = [v \ p \ \phi \ r]^T$, $\delta_a = [\delta_{lat} \ \delta_{ped}]^T$ and $\delta_{a_{in}} = [\delta_{lat_{in}} \ \delta_{ped_{in}}]^T$. Simulation time histories can be found in appendix section A. Frequency response comparisons for the truth model, JIO and direct approaches are illustrated in Figures 3.8, 3.9, 3.10, and 3.11.

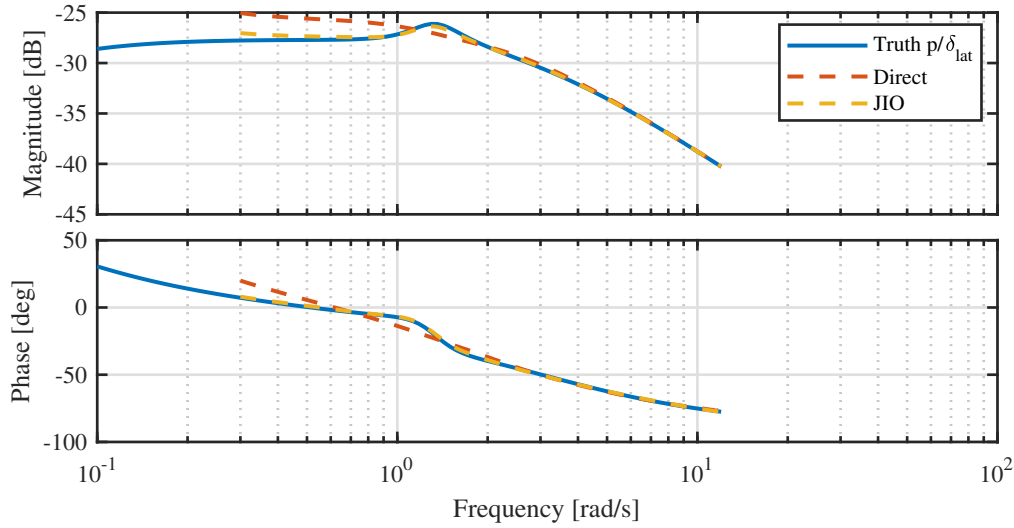


Figure 3.8: T-625 Lateral to Roll Rate Frequency Response Estimation

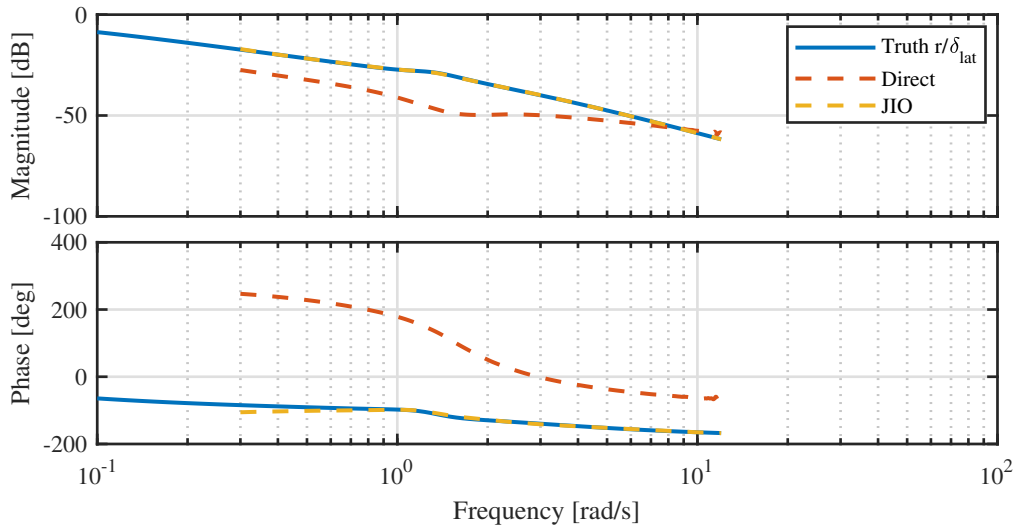


Figure 3.9: T-625 Lateral to Yaw Rate Frequency Response Estimation

Direct method fails considerably especially for lateral to yaw rate frequency response. JIO method shows good compliance with truth models for all cases.

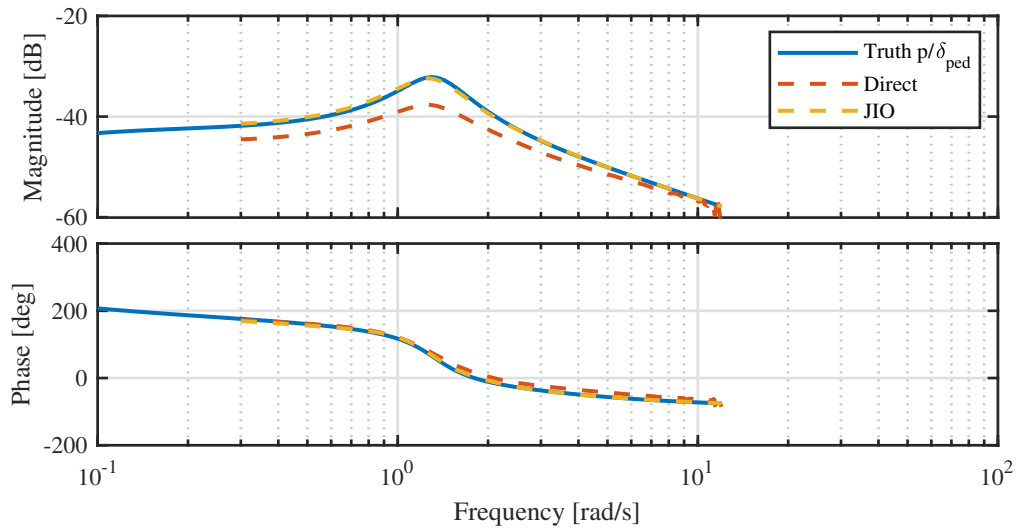


Figure 3.10: T-625 Pedal to Roll Rate Frequency Response Estimation

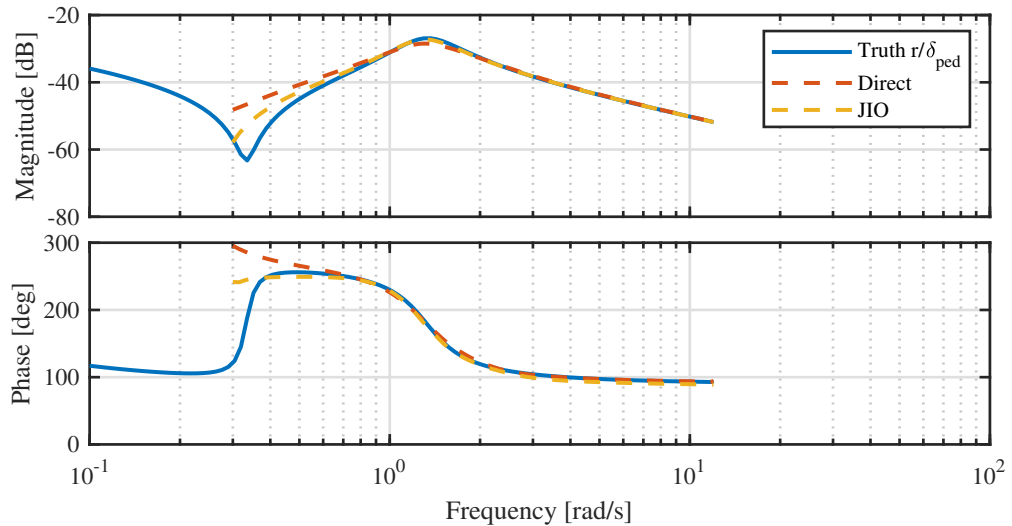


Figure 3.11: T-625 Pedal to Yaw Rate Frequency Response Estimation

Again just as in LJ-25 case, JIO method shows superior compliance with truth model data. These results show JIO method is able to predict bare airframe dynamics from closed loop data for helicopters as well. What's more having a SISO or MIMO feedback does not have any effect on the applicability of JIO method. It is able to operate under different feedback mechanisms entirely. Thus, JIO method has no restrictions on the feedback signal structure. The lateral dynamics results prove JIO method can predict correct bare airframe responses for data collected under feedback regulation.

3.4 Helicopter Rigid Body Dynamics with Linear Simulation Data

Rigid body dynamics of T-625 describes the coupled longitudinal and lateral behaviour of the helicopter as given in equation 2.1. The six degree of freedom rigid body dynamics of the helicopter extends the previous lateral dynamics example by adding extra degrees of freedom that represent the longitudinal motion to linear model. These extra longitudinal degrees of freedom introduces two new modes of motion to helicopter dynamics. These dynamics are traditionally known as the *short period* and *phugoid* modes. *Short period* and *phugoid* modes are named by analogy to fixed-wing aircraft longitudinal dynamics; however, unlike fixed-wing aircraft, classical configuration articulated rotor helicopters occasionally suffer from an unstable *phugoid* mode. This is the case for the T-625 helicopter linear model at hand as well. Additionally, a simple proportional rate feedback is not sufficient for stabilizing the *phugoid* oscillation. An elementary alternative is to use pitch angle feedback as well, analogous to using a proportional-integral control loop for longitudinal dynamics. Added integral action results in a stabilized closed loop system, which presents a perfect case for close loop identification applications. Rigid body dynamics of T-625 complicates the identification problem further not only by adding extra states, controls, and outputs to open loop plant, but also using a more complicated feedback structure compared to the previous application examples. The overall feedback structure is depicted in figure 3.12.

The feedback structure shown is the extension of the SAS to cover longitudinal dynamics as well. As mentioned earlier in section 3.3, SAS is the most basic function of the AFCS that aims to aid the pilots during flight by adding rate damping and stabilization to helicopter rigid body modes of motion. There are four control inputs to rigid body motion of a helicopter: collective, longitudinal and lateral cyclic, pedal. The cyclic and pedal inputs are the primary controls to command helicopters body angular rates in three orthogonal axes. That is why, The AFCS manipulates the cyclic and pedal controls to add damping and angular stabilization to the helicopter. The pilot control ports are used and depicted for excitation signal inputs for rigid body dynamics for simplicity since mathematically there is no difference between introducing the excitation signals from pilot ports. The excitation and pilot inputs are the

same labelled as $\delta_{a_{in}} = [\delta_{col_{in}} \ \delta_{lon_{in}} \ \delta_{lat_{in}} \ \delta_{ped_{in}}]^T$. Since there is no feedback on the collective control the collective excitation and the bare airframe inputs are the same and they are used interchangeably for this specific application case, $\delta_{col_{in}} = \delta_{col}$. The bare airframe inputs are, $\delta_a = [\delta_{col} \ \delta_{lon} \ \delta_{lat} \ \delta_{ped}]^T$ and the output vector of the bare airframe plant is $y = [u \ w \ q \ \theta \ v \ p \ \phi \ r]^T$. With the excitation signals, bare airframe inputs and plant outputs defined, it is again pretty straightforward to implement JIO approach using equation 2.30. At this point however, it is best to consider the practical implications for collecting time history data for identification.

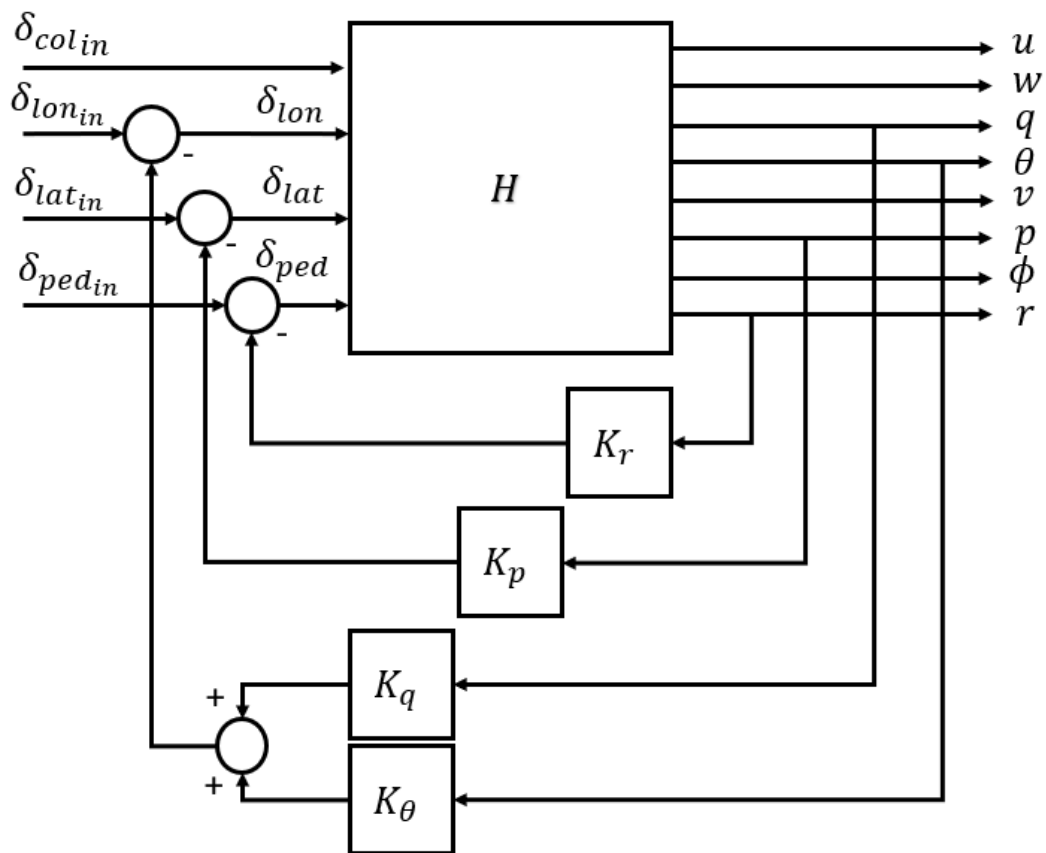


Figure 3.12: T-625 Rigid Body Dynamics Block Diagram with Feedback

What we have in hand, is an open loop unstable system that can be stabilized by utilizing two proportional control loops for lateral dynamics, and a proportional-integral control loop for longitudinal dynamics. It would be, at best impractical, probably impossible to perform a frequency sweep system identification test in both simulation

and flight test with this unstable open loop dynamics if one tries to pursue classical open loop techniques. As MIMO plant requires each control to be injected with a frequency sweep, gathering system identification data for an unstable system seems increasingly out of reach. It is obvious that, a closed loop identification makes collection of time history data possible and the overall procedure would result in a faster and safer test execution phase.

From a practical stand point, it should be noted that T-625 has a limited authority flight control system. AFCS has two main control actuators on each channel (longitudinal and lateral cyclic, pedal and collective). Parallel or trim actuators are located under pilot control sticks and are responsible for supplying the slow AFCS inputs to the bare airframe. Series or SCAS actuators on the other hand are located under the swashplate and are responsible for fast AFCS inputs to the bare airframe. Although AFCS actuation signals are calculated all together in a classical sense, the actuation is executed after a procedure called frequency splitting which differentiates fast and slow frequencies on the actuation signal and passes fast signals to SCAS actuators and slow signals to trim actuators. Both SCAS and trim actuators has rate and position saturation limits. Especially SCAS actuators has a position saturation limit which is the most probable non-linearity to be encountered during normal helicopter operation. Different AFCS modes uses SCAS and trim servos. SAS mode utilizes only the SCAS servos. SAS also serves as a basis functionality to higher AFCS control modes which completes each other in a cascaded manner. Considering this architecture it follows that, SAS is the core of the AFCS control algorithms, on which everything else is built and it is a perfect starting point to test JIO method applicability on helicopter flight mechanics.

The applicability of JIO method requires the ability to infuse excitation signals into required ports of AFCS. Luckily T-625 being a development program, the prototype helicopter has the DTS which is capable of injecting necessary inputs to helicopter for the JIO method from the ports labeled as $\delta_{col_{in}}$, $\delta_{lon_{in}}$, $\delta_{lat_{in}}$ and $\delta_{ped_{in}}$ in Figure 3.12. Figure 3.13 illustrates the functional diagram of T-625 automatic flight control system (AFCS). The DTS injection points are the lines going from FCC's to main rotor and tail rotor servo actuators, which makes JIO method excitation plausible. Main and tail rotor servo actuator positions are also recorded during flight tests, fulfilling another

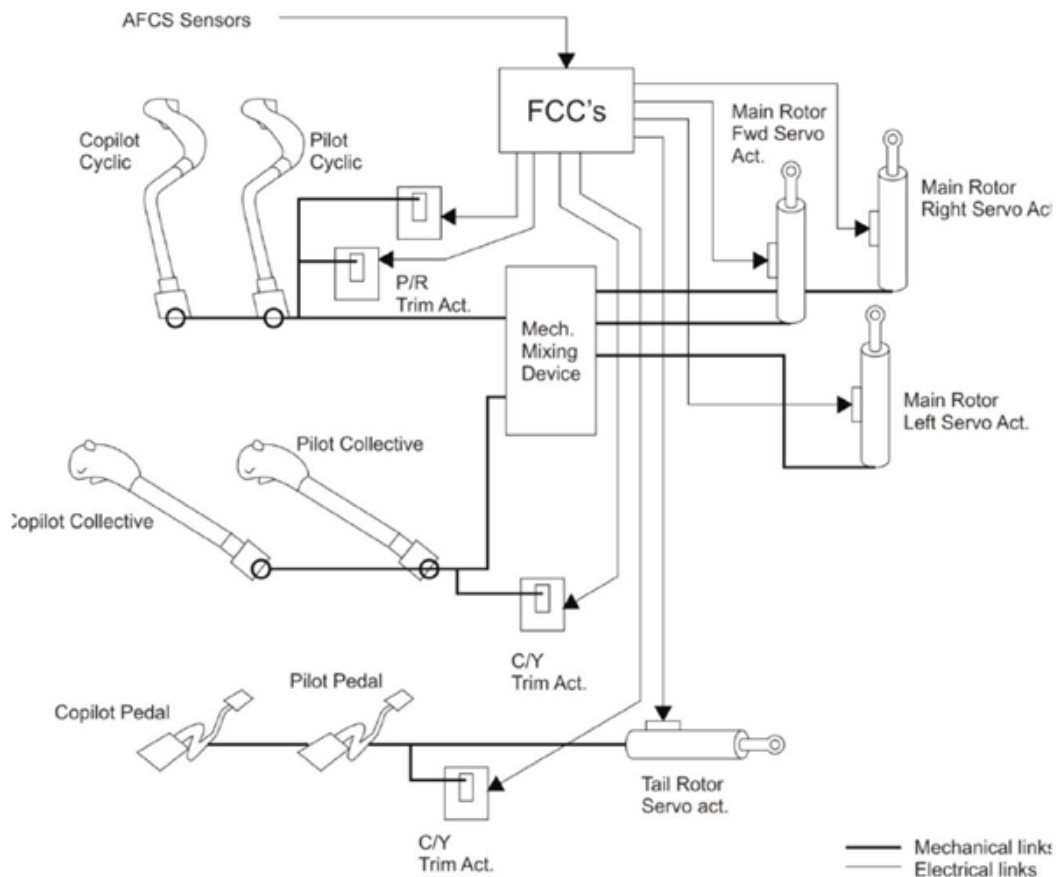


Figure 3.13: T-625 AFCS Functional Block Diagram

requirement for JIO method. What is more, DTS system is available on a simulator level in the system integration laboratory of T-625, which makes it perfect to test and evaluate JIO method with different inputs, excitation levels, or for different flight regimes as well. Being able to practice the system identification data gathering tests in a simulator environment also ensures that all parties involved in the test (i.e. flight test engineers, pilots, design engineers, operations support personnel, etc.) are on the same page and helps mitigate the flight test risks immensely. After the method is perfected on a system integration laboratory level, it becomes possible to collect flight test data in development tests and apply the procedure to identify both bare airframe dynamics and the controller dynamics.

For the linear simulation TOROS model was utilized. Nonlinear differential equations were linearized around 70 knots level flight conditions. The identification data is generated by using the linear model of the helicopter with feedback signals.

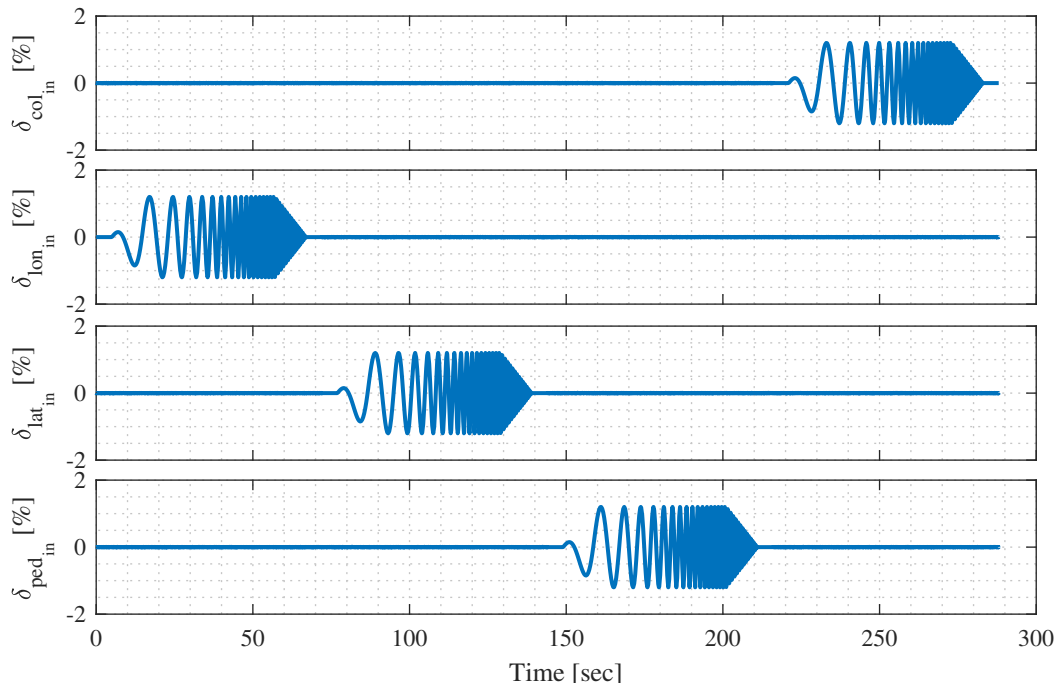


Figure 3.14: T-625 Rigid Body Dynamics Linear Simulation Excitation Signals

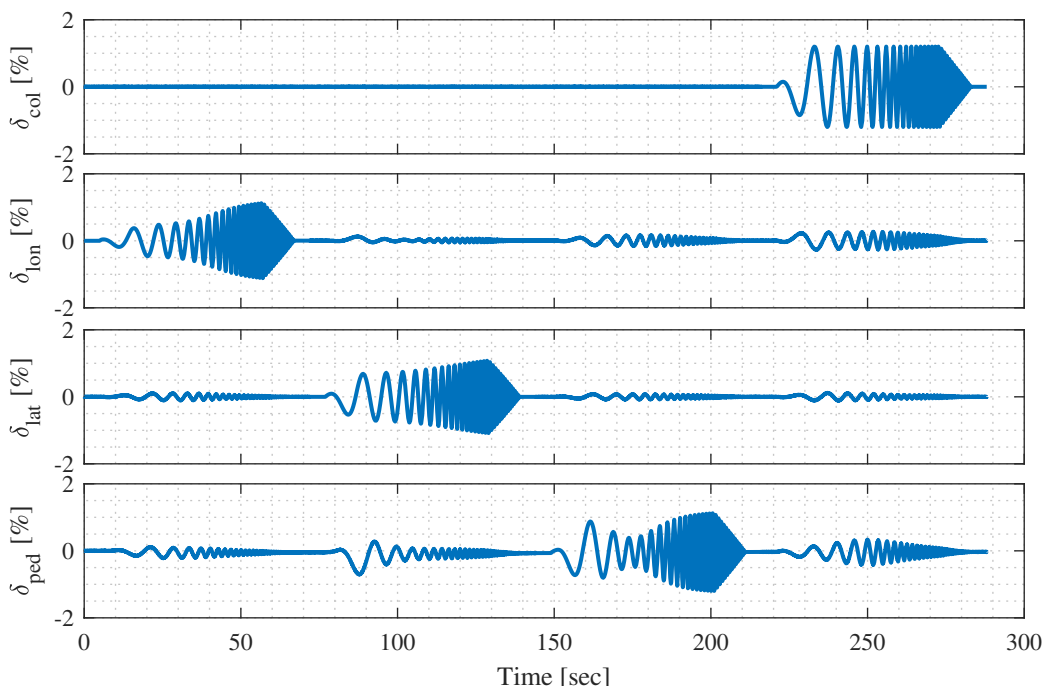


Figure 3.15: T-625 Rigid Body Dynamics Linear Simulation Bare Airframe Inputs

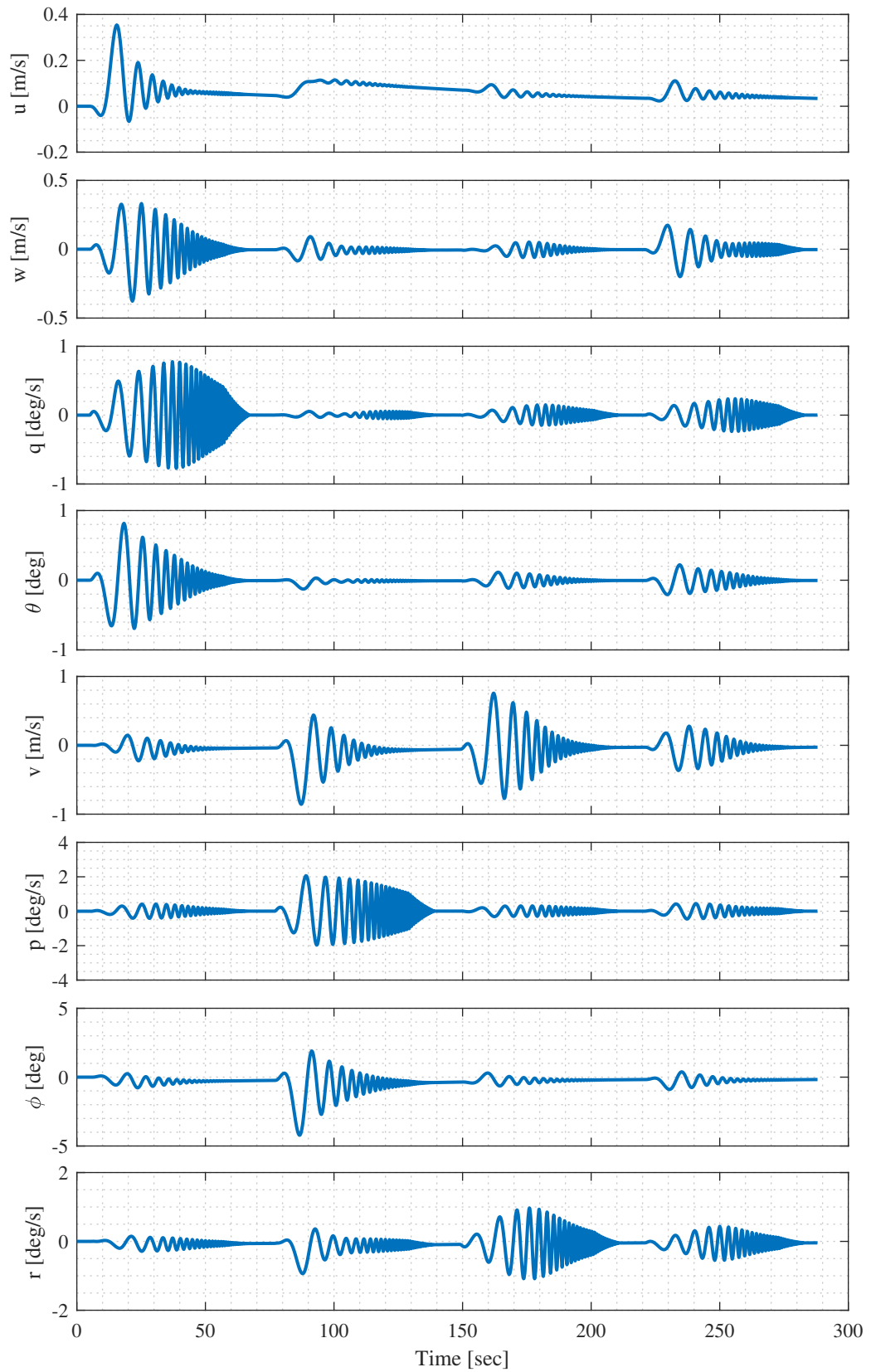


Figure 3.16: T-625 Rigid Body Dynamics Linear Simulation Outputs

Identification excitation signals cover the frequency range from 0.3 rad/s to 12 rad/s as in the lateral dynamics case before. This frequency range is generally adequate for helicopter rigid body dynamics [20]. The excitation is introduced consecutively to each individual channel, just as in the previous applications. That is, four different consecutive simulations were completed for system identification data gathering.

It is evident from time results shown in figure 3.15 that bare airframe inputs are correlated. This correlation makes SISO identification methods incapable of predicting the bare airframe dynamics adequately just as in previous cases.

Input output sets are once again used for identification with JIO approach and SISO direct approach for comparison purposes. On axis frequency response results are given in the following figures. The on axis responses represents the intended control actuation of the pilot. For example when the longitudinal cyclic is pushed forward, main expectation is for helicopter to exhibit a pitch down angular rate. Thus, on axis response is from the longitudinal cyclic control to pitch rate. In the same manner, the primary on axis responses can be listed as from lateral cyclic to roll rate, from pedal to yaw rate, and from collective control to body vertical velocity. However, as mentioned before, helicopters exhibit highly cross coupled responses and predicting off axis behaviour is a major concern for any system identification effort as well. Inspecting the whole input output pair responses is both impractical and unnecessary since significant off axis responses are foreknown for a given helicopter. For the T-625 primary off axis responses are determined as the cross coupled cyclic controls to angular body rates due to main rotor phase angle and gyroscopic moments, from pedal control to pitch rate due to canted tail rotor configuration and from collective to yaw rate because of the main rotor torque. The off axis frequency response results can be seen in the appendix section B and their related cost functions are tabulated in table 3.1.

On axis results for cyclic and pedal to helicopter body rates and collective control to helicopter body z linear velocity shows JIO approach is able to predict the truth model very closely in each case; whereas, the SISO direct approach fails to do so. The JIO approaches ability to predict the frequency response near the dominant modes continues to present itself in the 6 DoF rigid body case as well. Apart from collective to

vertical velocity response, direct approach actually shows some promising results for the cyclic input frequency responses. However, disregarding the feedback signal results in the estimation of completely inaccurate frequency responses for the collective channel for both on and off axis responses. The cost of these frequency response results are tabulated in table 3.1 also shows JIO approach's cost values are considerably lower for every input output pair.

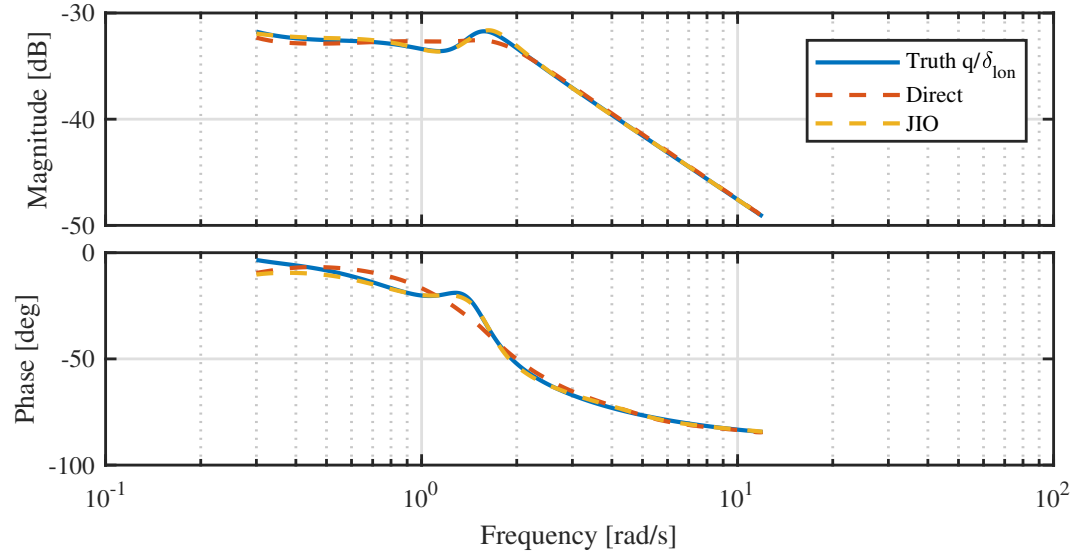


Figure 3.17: T-625 Rigid Body Dynamics Linear Pitch Rate Response Comparison

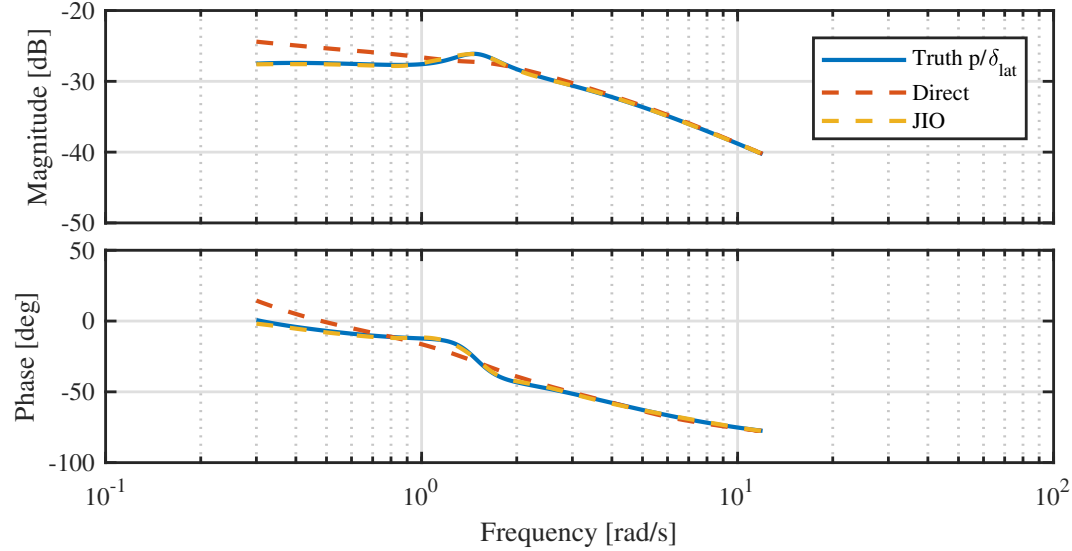


Figure 3.18: T-625 Rigid Body Dynamics Linear Roll Rate Response Comparison

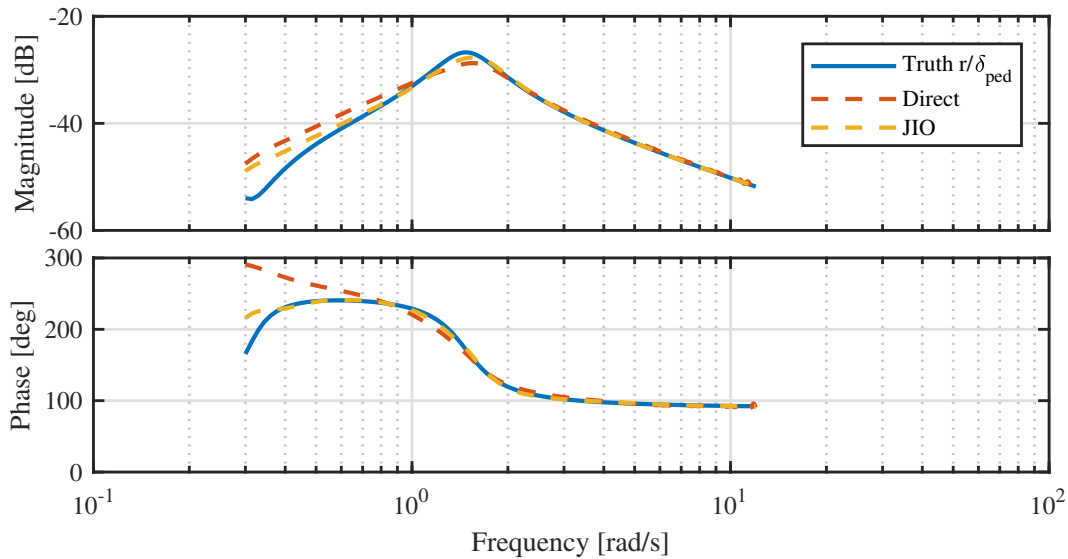


Figure 3.19: T-625 Rigid Body Dynamics Linear Yaw Rate Response Comparison

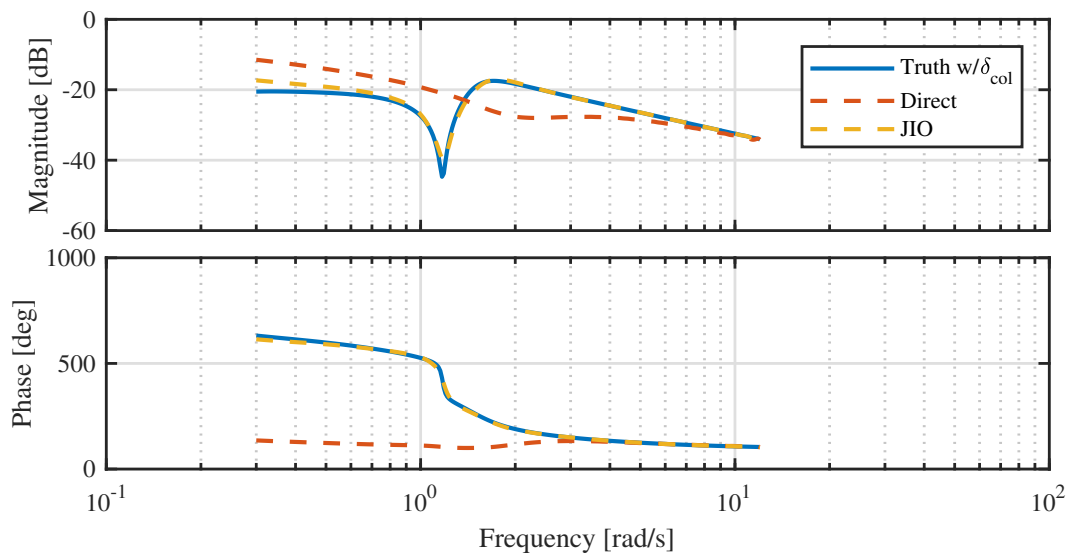


Figure 3.20: T-625 Rigid Body Dynamics Linear Vertical Velocity Response Comparison

It is seen that JIO approach outperforms the SISO direct approach once more when applied utilizing a higher order system with 8 states and 3 feedback signals. It should also be considered that the 8 state linear model is highly coupled. Even with a coupled longitudinal and lateral motion, JIO approach shows encouraging results with linear simulation data. At this point, before proceeding with the non-linear simulation data,

it was decided to check the noise sensitivity of JIO approach.

Figure 3.21 illustrates the noise sensitivity study conducted with linear simulation model for the 6 DoF rigid body case. Sample noise signals are introduced to sensor measurements at each channel with varying strength. The concern was, with the feedback regulation active, sensor measurement noise could lead to some undesired behaviour. To check noise sensitivity, longitudinal cyclic to pitch rate frequency response is inspected. The solid line in figure Figure 3.21 indicates the frequency response obtained without any noise present. When the noise level rises, some scatter or random error is apparent. However, on average the identification tracks the true response, so that there is no significant bias error. However it is also indicative that the as the noise level increases the random error becomes considerable. That is, as expected there is an upper allowable noise limit for frequency response identification and it can be considered to be nearly 30% from this simple noise sensitivity analysis. Luckily, the sensor suits that are used in modern aircraft has much lower noise levels and as long as the identification data is not collected under extreme turbulent weather conditions, sensor noise should not pose a problem.

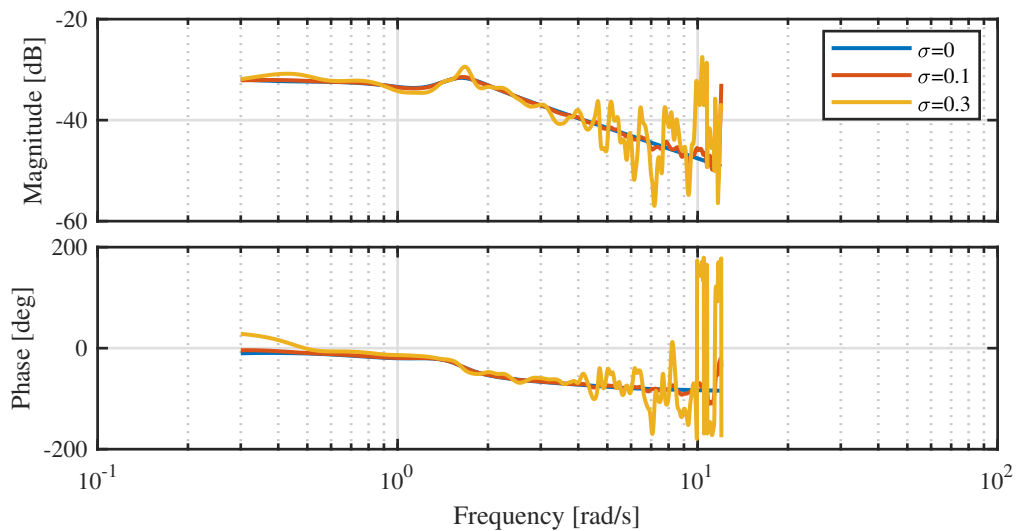


Figure 3.21: JIO Method Noise Sensitivity for Pitch Rate Identification Results with Linear Simulation Data

3.5 Helicopter Rigid Body Dynamics with Non-Linear Simulation Data

As the last validation check identification with non-linear simulation data is performed. Since the linear simulation results showed satisfactory results, the most labour intensive part of using non-linear simulation data was the data collection and data pre-processing parts. System identification data collection with the non-linear model is not straight forward since at the flight condition and configuration selected for identification the helicopter with stability augmentation system on is not stable. It is acceptable for a SAS to leave some dynamic modes unstable with really large periods or time constants, since the helicopters are designed to have a pilot in the cockpit at all times. A human operator can easily stabilize a slow divergent mode, thus the SAS does not need to do all the stabilization. However, this situation proves to be a problem of offline data gathering for system identification in a desktop simulation. Since there is no human pilot involved with the desktop simulation, each frequency sweep data was obtained by trial and error. Figure 3.22 shows a sample frequency sweep outputs to a 10% longitudinal cyclic input in a non-linear desktop simulation. Even with the controller active, helicopter strays away from its trim condition at the end of the frequency sweep. Thus, performing consecutive sweep inputs for each channel during simulation is not an option.

The preferred way to construct the required system identification data is to performed the frequency sweep for each channel separately, starting the simulation from the same trim condition each time. Then the gathered data can be concatenated together for system identification purposes. This concatenation can be done as much as needed since it also enriches the frequency information content.

One other point while looking at figure 3.22 is that the states are not moving around zero as in the linear simulation case. For linear simulations, the trimmed flight condition is represented by the origin of the state space; that is, every state starts form zero for a linear simulation and the deviations from zero actually represents the deviations from the equilibrium or trim condition. Since the identification is performed in frequency domain, and the end goal here is to come up with frequency responses, each variable should start from zero indicating a trimmed flight condition at the start of the data record. This initial value reset should also be handled during data pre-processing.

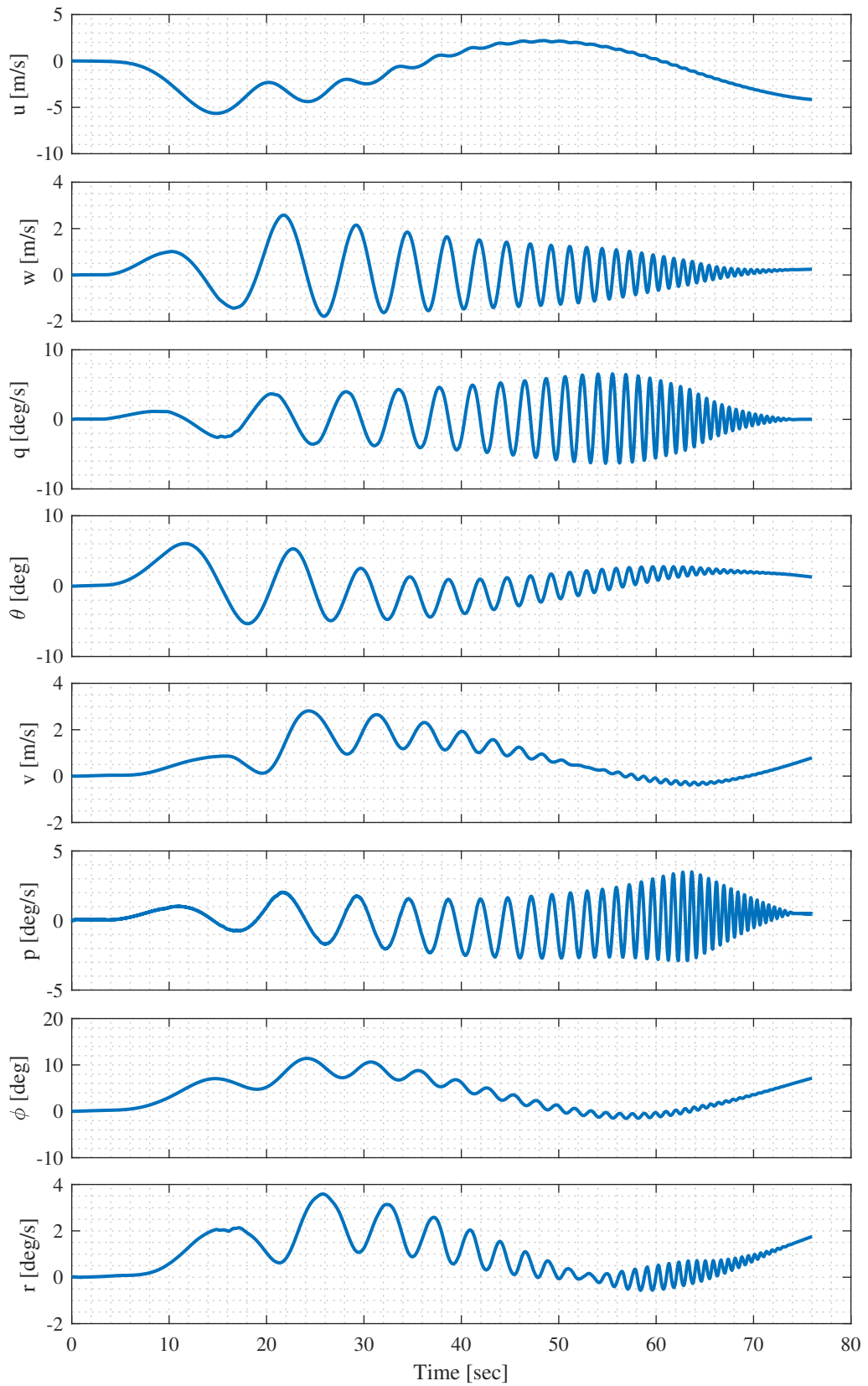


Figure 3.22: T-625 10% Longitudinal Cyclic Sweep Non-linear Simulation Outputs

Following figures 3.23 , 3.24, and 3.25 illustrate a set of concatenated data whose initial condition is reset for frequency domain system identification data gathering. The solid vertical black lines indicate boundaries of different simulation data. Figures show a total of four different simulation runs, each exciting a different control axis so that the excitation signals will be uncorrelated with one and other. The frequency range for the excitation signals are the same: $0.3rad/s$ to $12rad/s$. Each simulation run has a 2 second trim duration at the start and at the end. Only the longitudinal axis excitation, applied from the longitudinal cyclic channel has a magnitude of 10%, all other excitation amplitudes are selected as 5%. The reason for a higher amplitude, longitudinal cyclic input is due to the high second moment of inertia of the helicopter in pitch axis of rotation. Compared to pitch inertia, roll inertia of the helicopter of much smaller, thus requires a lower magnitude input to respond. The aim was to acquire approximately 5 degrees of second body angular rates for the respective axis for cyclic and pedal excitation and a 3 meters per second body z velocity change for the collective excitation. These values are lower than the typical 10 degrees of second rule of thumb suggested by reference [20]; however, they are considered to be enough since the non-linear simulations does not have any noise and the identification data is collected within a closed loop configuration.

The simulation model is trimmed at 70 knots level flight condition and so pitch angle, roll angle and body transnational rates are not zero during this trimmed flight condition. However, figure 3.25 illustrates that all states initial conditions are zero indicating an equilibrium state at the start of each simulation run marked by the vertical black lines. This is achieved by subtracting the trim value of each state indicating that the simulation results show only the perturbations from trim values.

Another important point to make is the correlation between the bare airframe inputs that is obvious in figure 3.24. With no noise content in the signals, event the smallest similarities in bare ariframe inputs lead to undetermined matrix inversions which makes the utilization of JIO approach an obligation. Especially collective excitation creates correlated signals in all channels and lateral excitation creates a highly correlated pedal input.

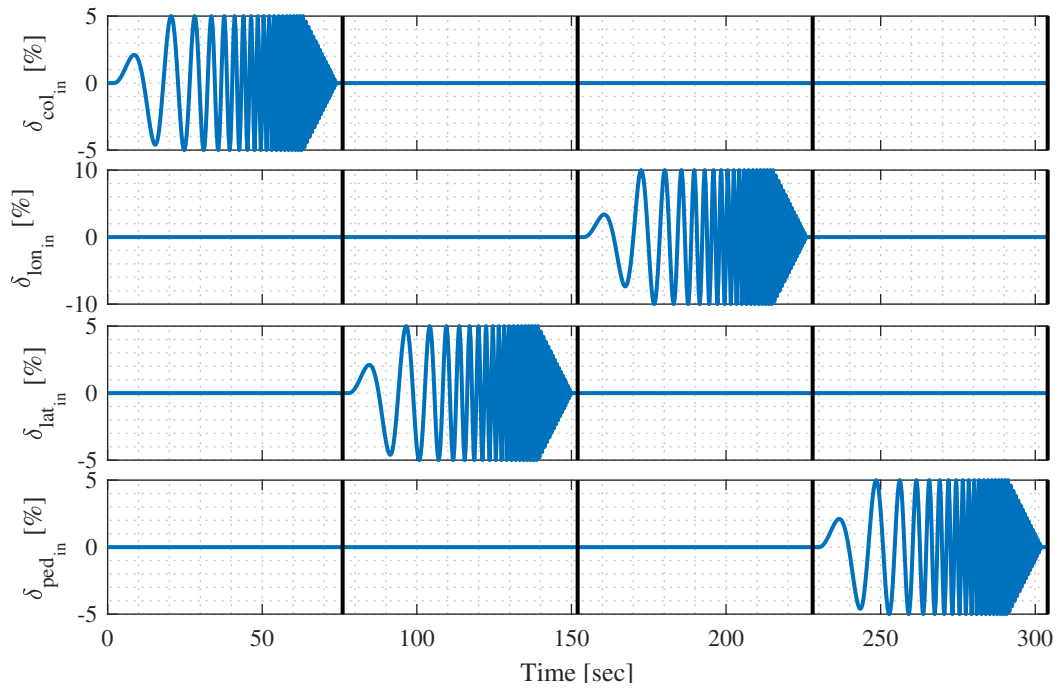


Figure 3.23: T-625 Pre-processed Sweep Non-linear Simulation Inputs

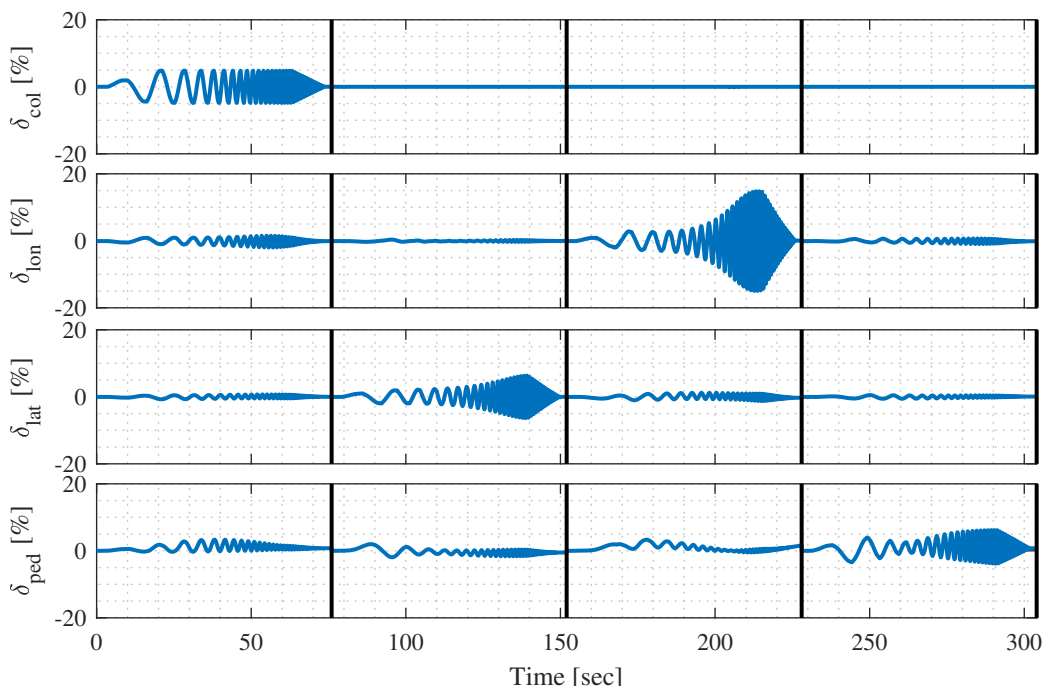


Figure 3.24: T-625 Pre-processed Sweep Non-linear Simulation Bare Airframe Inputs

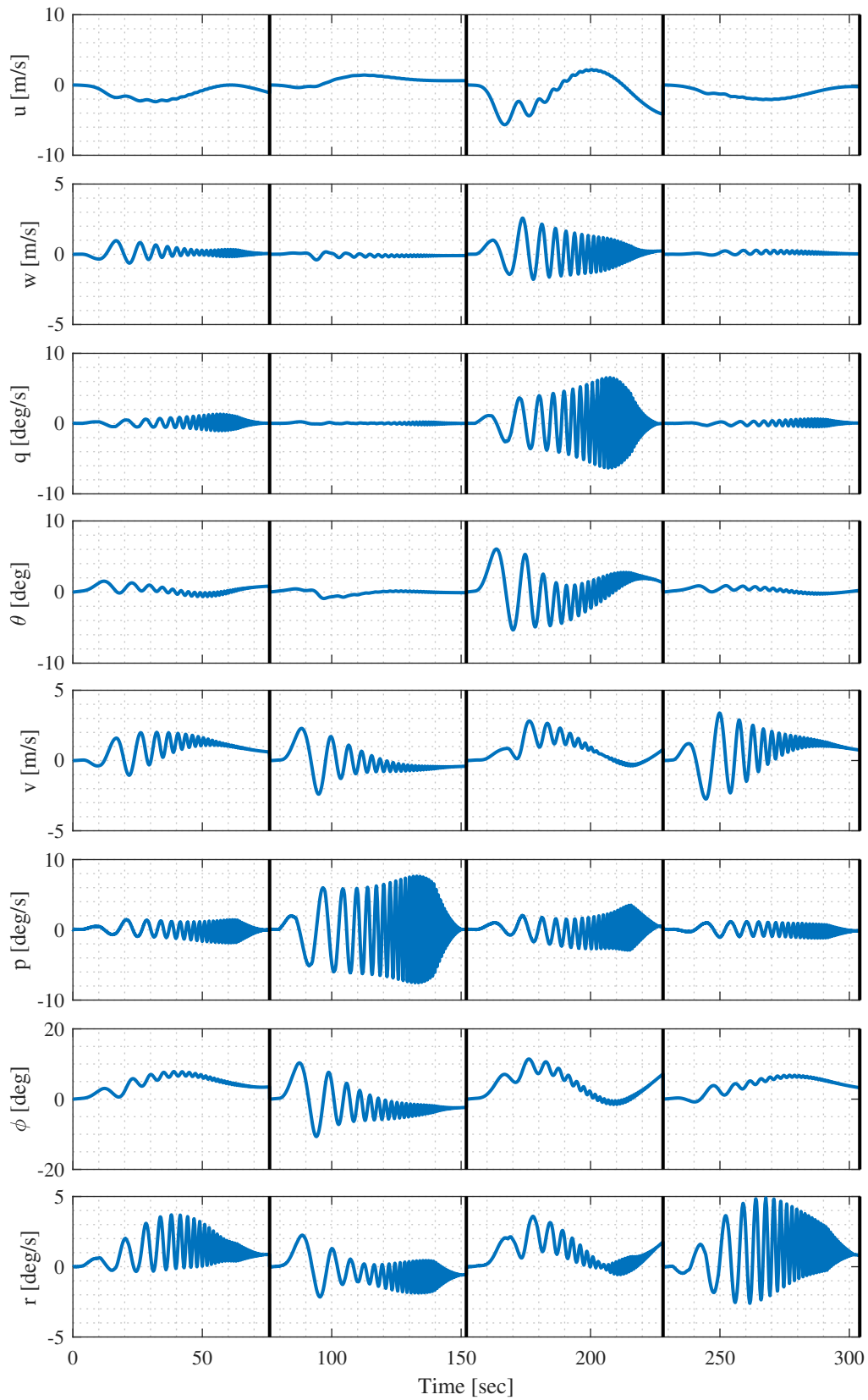


Figure 3.25: T-625 Pre-processed Sweep Non-linear Simulation Outputs

Ideally the helicopter should remain around the selected equilibrium during the excitations and at the end should go back to the initial trim condition. This ideal response condition was indeed the case for the linear simulation runs; however, non-linear simulation data exhibits divergence from the trim condition. Low frequency excitation is especially disruptive in this sense. This disruption is most apparent in the body x velocity u output data. Starting with the low frequency portion of the input, body x velocity u distorts and its mean value shifts either positively or negatively. This mean value shift is not optimal and could lead to some discrepancies in the identification procedure. There are several other parameters that show a similar distortion from the trimmed flight condition. Nonetheless, these shifts are likely to occur due to associated non-linearities of the model and probably will manifest themselves in real flight data as well. Thus, any identification procedure should be able to handle such a sub-optimal data.

The merged data is used with JIO approach and direct approach again just as in the previous cases to compare both approaches. The identification results are again given as frequency responses for the on-axes. The truth data for frequency responses is generated by utilizing the perturbation based linearization approach of TOROS. With the non-linear simulation data figures 3.26, 3.27, 3.28 and 3.29 shows that JIO approach is again performs sufficiently well compared to direct approach notably for low to mid frequency range of interest. However, JIO approach results starts to show some deviations from the truth model especially at higher frequencies. Direct method generally fails to capture the dynamic response pole locations because it does not account for the feedback mechanism in the system. Feed back mechanism is designed specifically for suppressing the magnitude increase in the frequency response near the system poles. For this, direct method results are understandable. However; the deviation of frequency responses at higher frequencies for both direct and JIO approaches requires further investigation. The high frequency roll off in the identification results may very well be due to shortcomings of the truth model itself. It is a good point to remember that the truth model is actually a reduction of a perturbation based linear model and it lacks important elements like the actuator or sensor dynamics. These missing dynamics in the perturbation based truth model are actually a part of the non-linear model from which the identification data is generated. That is why the iden-

tification results show a steeper roll off especially at higher frequencies whereas the truth model can not because the truth model just do not have enough states to represent a steeper high frequency roll of. This is exactly the reason why it is more suitable to use system identification methods for linearization rather than perturbation based methods [20]. This argument is also makes more sense if one remembers the perfect accuracy between the perturbation based truth model and the JIO approach that was obtained with the linear simulation results depicted in figures 3.17 through 3.20. If one examines the linear model structure given in equations 2.3 and 2.4, it would become obvious why the perturbation based model fails to capture higher order dynamics. It would become more apparent when the search for parametrized models start.

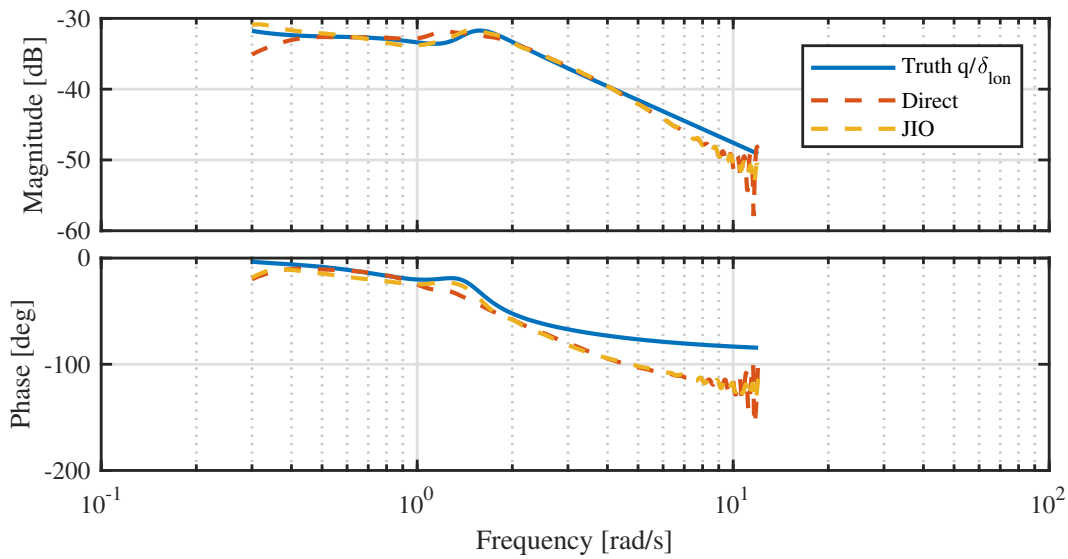


Figure 3.26: T-625 Non-linear Data Pitch Rate Response Comparison

Unlike other channels, collective to body z velocity frequency response identification shown in figure 3.29, shows a constant shift throughout the entire frequency range. Although JIO result is following the correct trend, JIO approach over predicts the magnitude response starting from mid frequencies up to high frequencies. This may be due to insufficient excitation amplitude. The non-linear response data for w shows only a 3 meters per second deviation and this may just be not enough to rightfully characterise the magnitude response. On the other hand, predicted zero and pole locations by the JIO approach do seem close to truth values.

The off-axis frequency response results are again not presented here for the sake of

simplicity. However, it should be noted that off-axis results also show consistent behaviour with the truth data. Off axis response comparisons can be found in the appendix section B.

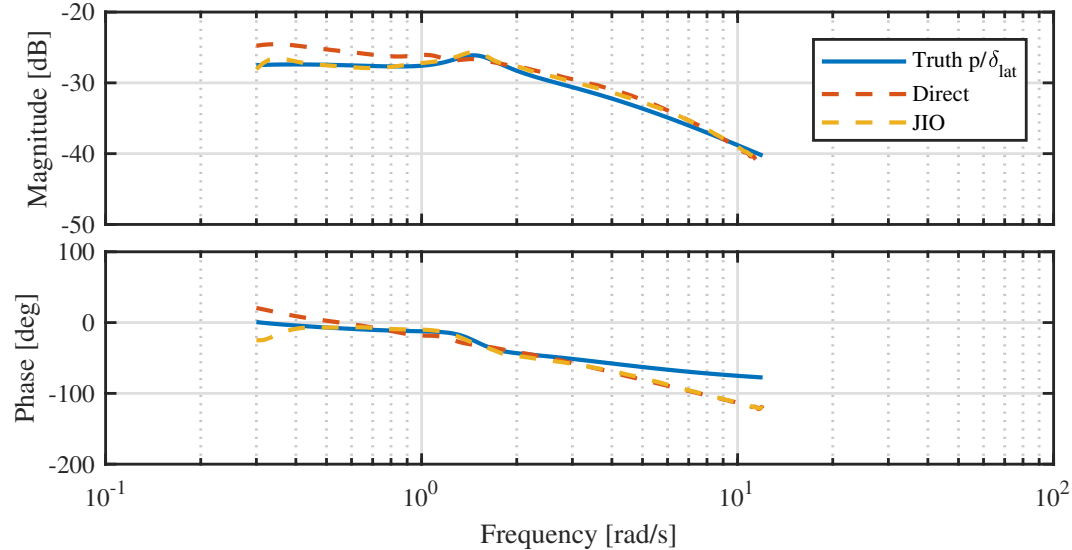


Figure 3.27: T-625 Non-linear Data Roll Rate Response Comparison

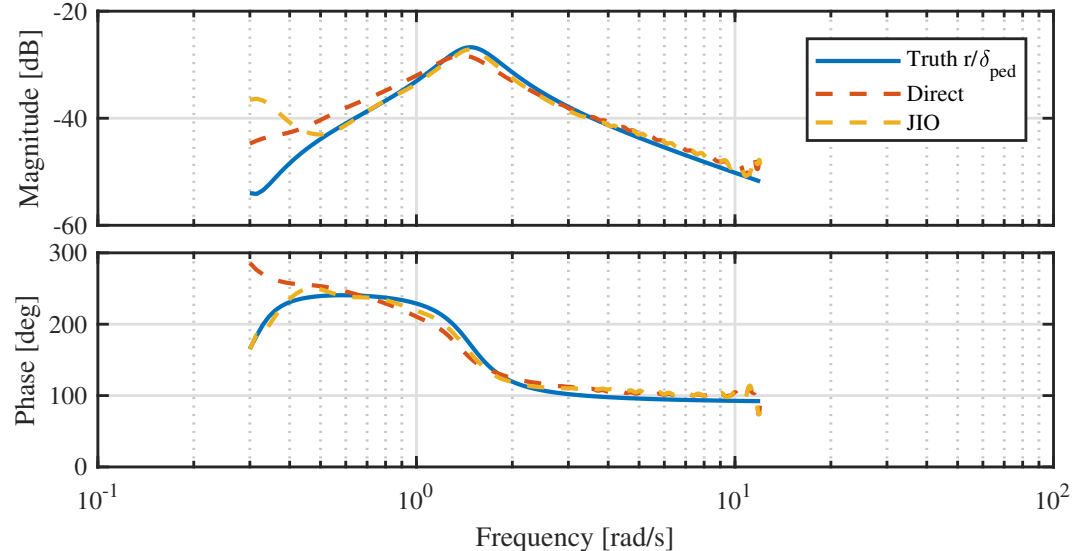


Figure 3.28: T-625 Non-linear Data Yaw Rate Response Comparison

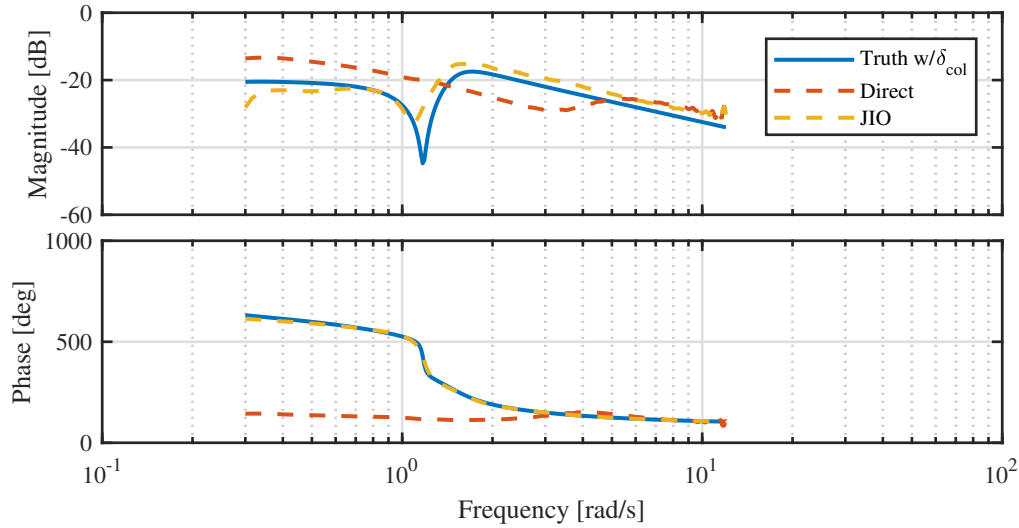


Figure 3.29: T-625 Non-linear Data Vertical Velocity Response Comparison

To quantify the results more properly a cost function table is prepared. Table 3.1 summarizes the cost values for each frequency response for both direct approach and JIO approach against the truth model utilizing the cost function definition of equation 2.31. Linear identification costs for JIO approach shows excellent agreement between the identified responses and the truth data. As mentioned previously guidelines suggests a cost value $J \leq 50$ will end up in a response indistinguishable from one and other and linear JIO results indicate such a situation. Direct approach results for linear identification suggest results are not suitable for further use. Every transfer function in question indicates a cost value far above the upper limit of a hundred suggested by the guidelines except for the linear lateral to roll rate response identification case. Same comments can be made for the non-linear direct identification results as well. For both linear and non-linear identification JIO method shows far more superior cost values for all channels involved. For the non-linear JIO approach results, the reason for the high cost values may be the limitations of the truth linear model may have as explained earlier. That is why, the cost values are all above the general rule of thumb of a hundred for the non-linear simulation results. It is safe to conclude that JIO approach is able to predict bare airframe dynamics from closed loop identification test data, thus; the model parametrization and time domain verification effort will be done only with the frequency responses obtained by the JIO approach.

Table 3.1: Identification Costs with Respect to Truth Model

Freq. Response	Linear Simulation		Non-linear Simulation	
	Direct	JIO	Direct	JIO
q/δ_{lon}	2.32	0.29	364.5	342.5
p/δ_{lat}	7.70	0.15	262.4	240.8
r/δ_{ped}	47.44	9.52	101.1	105.5
w/δ_{col}	6280	8.23	6015	1052
p/δ_{lon}	132.5	23.19	1494	1007
q/δ_{lat}	1030	1.41	2839	1860
q/δ_{ped}	478.7	2.76	904.2	37.81
r/δ_{col}	767.9	10.92	1012	1055

It should be noted that it is possible to concatenate more test data together to increase the identification precision. Different input types, other than the frequency sweep have been suggested [21, 95] and utilized successfully in prior work [36, 46, 65, 41]. For JIO approach with frequency domain identification, it is possible to concatenate test data that utilizing different input types like doublet, multistep inputs or possibly even random excitations. Overall, JIO method was able to capture the true nature of the helicopter model utilizing non-linear response data under feedback regulation is active. While doing so, it does not require any knowledge about the feedback gains or the feedback structure.

3.6 Helicopter Rigid Body Dynamics Parameter Optimization

The results shown in table 3.1 and all figures from 3.17 to 3.29 all indicate with data gathered in a closed loop context, JIO approach is able to yield physically meaningful results; whereas, direct approach fails to do so due to high correlation among the bare airframe inputs. With these implications, it is only logical to start thinking about model parametrization and parameter optimization. Up until now, only frequency response data are identified, which captures the relationship between the input and output pairs. However such a non-parametric identification fails short if one needs to

utilize the identification results for further simulation or tries to validate the identification results with dissimilar response data in time domain.

Table 3.2: Identified Derivatives with Linear Simulation Data

Param	Val.	CR-%	Param.	Val.	CR-%
X_u	-0.054	39.7	X_{col}	0.013	7.2
X_w	0.025	38.2	X_{lon}	-0.034	4.8
X_q	-0.95	16.1	Z_{col}	-0.24	3.1
Z_u	0.007	549	Z_{lon}	-0.074	20.0
Z_w	-0.64	6.3	M_{col}	0.014	2.7
Z_q	36.67	3.1	M_{lon}	0.043	2.5
M_u	-0.003	40.4	Y_{lat}	0	104.0
M_w	-0.017	8.1	Y_{ped}	0.022	53.5
M_q	-1.2	4.2	L_{lat}	0.126	3.1
Y_v	-0.16	13.9	L_{ped}	0.015	4.1
Y_p	1.4	25.2	N_{col}	0.014	3.5
Y_r	-40.8	2.8	N_{lat}	0.014	5.3
L_v	-0.05	4.1	N_{ped}	-0.030	2.6
L_p	-2.8	3.1	τ_{col}	0	173.8
L_r	0.12	45.4	τ_{lon}	0	246.4
N_v	0.036	3.4	τ_{lat}	0	264.3
N_p	-0.32	6.6	τ_{ped}	0	335.8
N_r	-0.69	4.3			

With a correct model postulate, frequency response data obtained by JIO approach can be used to come up with model parameter values. The model postulate to be used for T-625 rigid body dynamics is the one given in equations 2.3 and 2.4. Model parameters to be determined are naturally the stability derivatives additional four time delay parameters are added to the model structure as optimization parameter to cover any un-modelled high order dynamics. The optimization problem can be defined as given in equation 2.33 and for this work the secant method as adapted by reference [20] is utilized. The resultant important stability derivatives after the parameter search is tabulated in table 3.2 for the linear identification case.

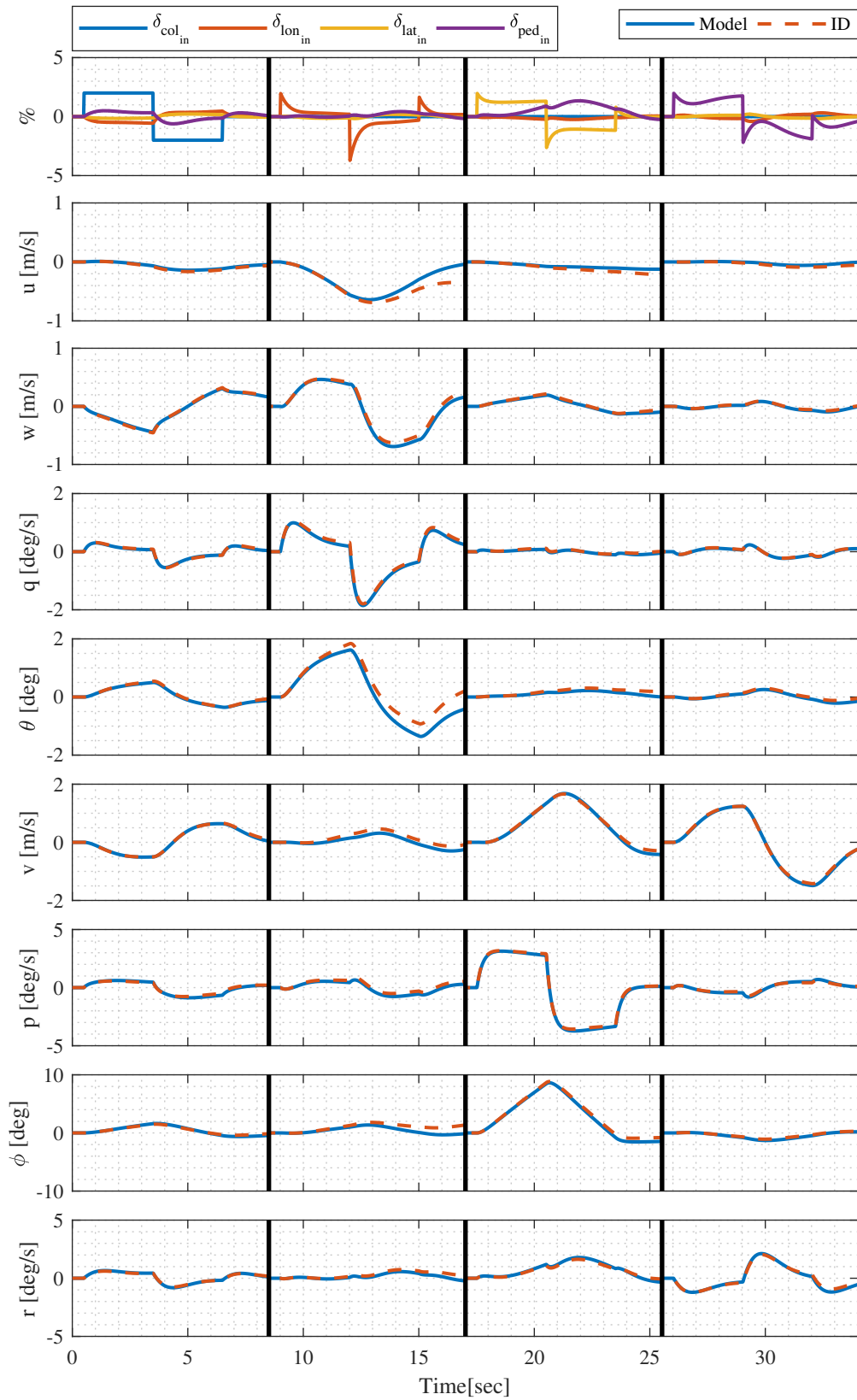


Figure 3.30: T-625 Linear Simulation Identification Results

Stability and control derivative parameter values are given with their respective Cramer-Rao values. A lower CR value indicates a lower uncertainty about the identified parameter. A high CR value often indicates the identification data in hand does not have a rich enough content to be able to identify the said parameter. Linear parameter fit results illustrate low CR values overall since there is little uncertainty in the identification data. However, there are certain exceptions. For example Z_u, Y_{lat}, Y_{ped} are parameters that have high CR bounds indicating that the simulation data does not contain enough information to identify these particular parameters, or more probably these parameters should be eliminated from the model structure. It is also important to note that, parameter optimization did not require to fit any time delay to the model ($\tau_{col} \tau_{lon} \tau_{lat} \tau_{ped}$) to capture any higher order un-modelled dynamics since the generated identification data and the identification model structure is exactly the same.

Validation cases in time domain, exciting all available control channels are completed and results are shown in figure 3.30. Same control signals are introduced to the linear 6DoF model and the identified model. The responses show excellent alignment with one and other indicating a perfect match between the system identification model and the linear model. It is important to note that this validation data is not used during system identification effort, guaranteeing the identified models predictive capability.

Same parametrization and time domain validation cases are run for the non-linear simulation results as well. Results are tabulated in Table 3.3. Non-linear parameter identification results show higher uncertainty bounds than the linear results overall which is expected since with non-linearity the uncertainty in the identification data becomes elevated. The highest CR bound is on Y_p which is different than the linear case. Additionally, the parameter optimization ended up identifying significant values for the time delays, which helps identification model to capture un-modelled higher order dynamics. These higher order dynamics are the reason for the mismatch between the linear and identified frequency responses given in figures 3.26 , 3.27, 3.28 and 3.29.

Table 3.3: Identified Derivatives with Non-linear Simulation Data

Param	Val.	CR-%	Param.	Val.	CR-%
X_u	-0.11	16.5	X_{col}	0.033	6.2
X_w	-0.035	31.1	X_{lon}	-0.060	4.7
X_q	-0.44	50.5	Z_{col}	-0.26	3.5
Z_u	-0.20	20.0	Z_{lon}	-0.040	44.3
Z_w	-0.59	6.8	M_{col}	0.016	2.7
Z_q	44.5	3.3	M_{lon}	0.043	2.5
M_u	-0.002	35.7	Y_{lat}	-0.057	19.4
M_w	-0.011	10.5	Y_{ped}	0.085	15.0
M_q	-1.3	4.1	L_{lat}	0.16	3.3
Y_v	-0.20	11.5	L_{ped}	0.025	4.2
Y_p	-0.44	108.7	N_{col}	0.018	3.0
Y_r	-41.63	2.8	N_{lat}	0.016	5.6
L_v	-0.082	4.1	N_{ped}	-0.029	2.8
L_p	-4.0	3.3	τ_{col}	0.11	2.9
L_r	-0.22	41.9	τ_{lon}	0.13	2.8
N_v	0.030	3.8	τ_{lat}	0.12	3.4
N_p	-0.42	6.4	τ_{ped}	0.023	17.1
N_r	-0.65	4.5			

Non-linear time validation results are given in figure 3.31. The same procedure is again followed for this comparison. Since these input output data is not utilized in the system identification process, the predictions of the identified models are genuine and reflects the system identification models capability of predicting unprecedented behaviour. The overall on axis time domain response is satisfactory for every control channel; however, slight deviations in off axis responses seems to present themselves. General behaviour and response of the identified model is satisfactory, proving that JIO approach can yield adequate results with non-linear simulation data as well. Additional time domain validation comparisons for linear and nonlinear identified models in SAS OFF conditions are given in appendix section A.

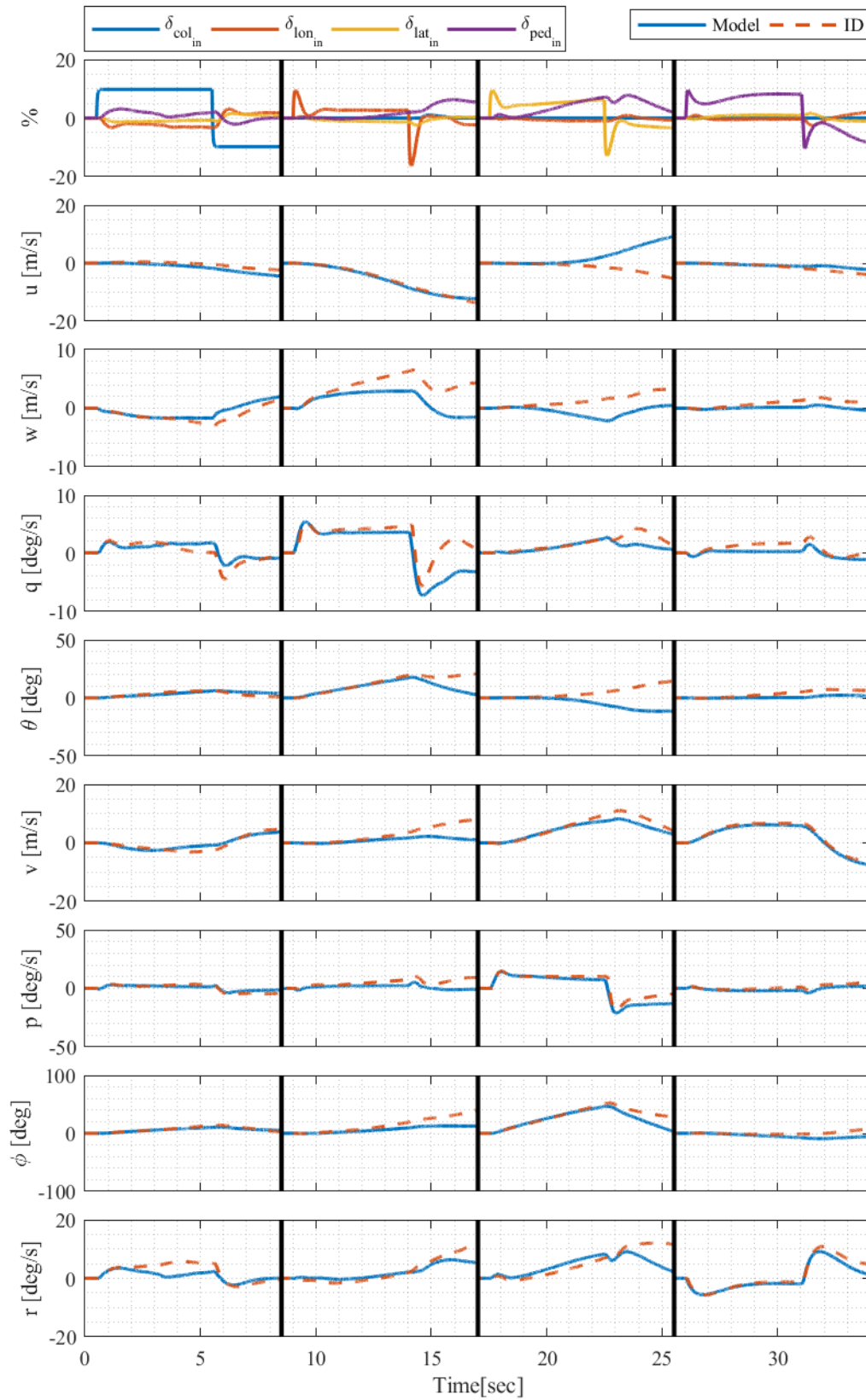


Figure 3.31: T-625 Nonlinear Simulation Identification Results

3.7 Helicopter System Identification with Real Flight Test Data

After validating the identification method with linear and non-linear simulations, logical next step is to perform identification with real flight test data. To this end, several flight tests which were conducted within the development test flight program of T-625 helicopter were sought to be used. These tests were originally conducted for AFCS performance evaluation and it was assumed they were suitable to be utilized for bare airframe identification as well. However, the information content of the test flights were found to be very low as indicated by the coherence values in figures 3.32 and 3.33.

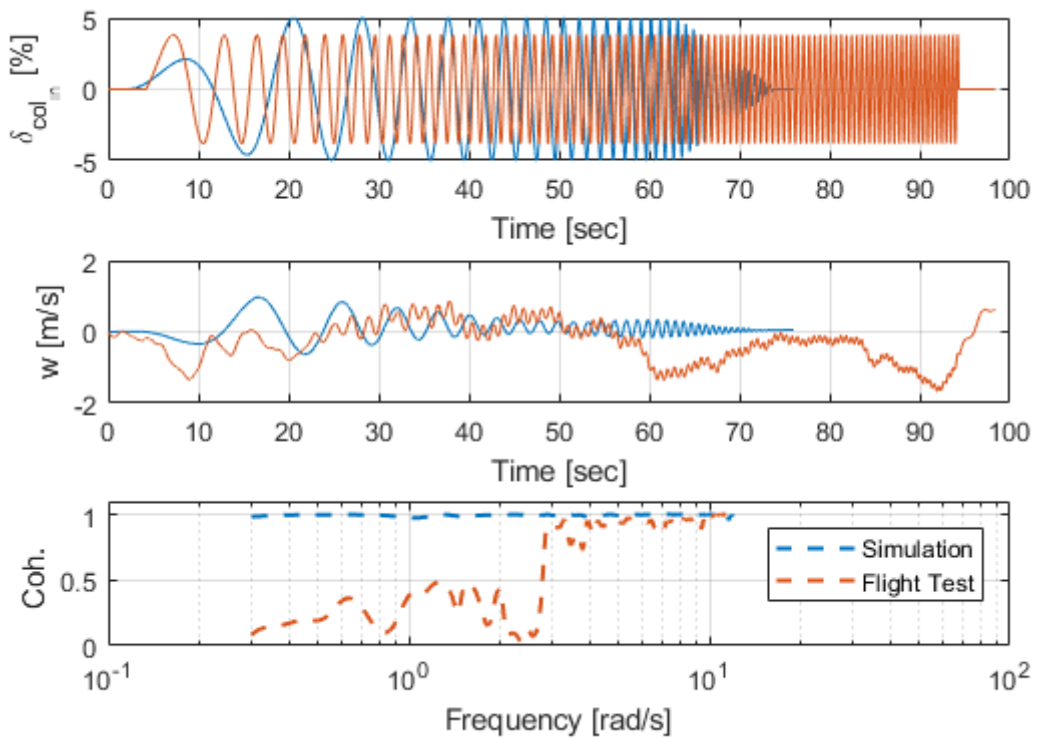


Figure 3.32: T-625 Simulation vs Flight Test Results for Collective to w

A comparison with simulation data revealed that although the excitation amplitudes are similar the frequency is varied linearly in the flight test, whereas; it is varied exponentially in the simulation runs. This difference resulted in poor data for identification especially in lower frequency regions as indicated by the coherence plot in figure 3.32. The lack of information in the identification data in low frequency region is also illustrated in the time domain response. The response amplitude in the

lower frequency region is much lower for real flight when compared to simulation data. Same conclusions may be drawn from the longitudinal cyclic excitation as well as indicated by figure 3.33.

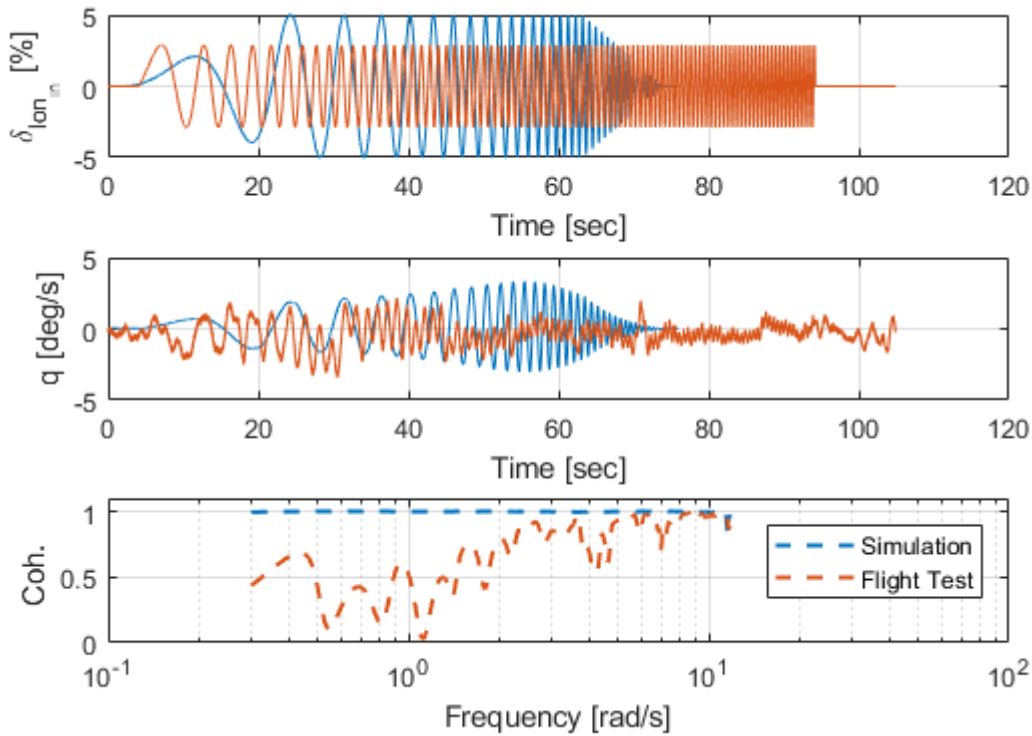


Figure 3.33: T-625 Simulation vs Flight Test Results for Longitudinal Cyclic to q

Armed with the knowledge of exponential frequency sweeps vitality, a series of system identification flight tests were planned and executed. Flight tests were performed as a benchmark in the same flight conditions that the simulation studies were performed; that is, 70 knots level flight conditions. T-625 flew a total of 3 flight hours in 2 different sorties for the 70 knot level flight system identification tests. Frequency sweep inputs for all four axis of control and step, doublet responses for validation were performed. Test points summary can be found in Table 3.4. Since the frequency sweep test were performed with AFCS active, they can also serve to the AFCS development effort, which is just another added advantage of utilizing JIO approach for system identification. Flight test were closely and carefully monitored in real time with a telemetry and the excitation signals' amplitude and frequency range is adjusted if necessary after each test point, especially for frequency sweep test points. Some of the test points were also repeated without any changes on the excitation signal content

in order to have a rich flight test database, negating the uncertainty and randomness associated with flight testing as much as possible. Further testing for different flight conditions are being performed with the know how gathered from this study.

Table 3.4: Flight Test Data

Axis	Sortie - Test Point	Excitation
Collective	Sortie A - TP 22	5% Fr. Sweep
	Sortie A - TP 23	10% Fr. Sweep
	Sortie A - TP 24	10% Doublet
	Sortie A - TP 25	10% Doublet
Lateral	Sortie A - TP 14	5% Fr. Sweep
	Sortie A - TP 15	5% Fr. Sweep
	Sortie B - TP 19	5% Fr. Sweep
	Sortie B - TP 20	5% Fr. Sweep
	Sortie A - TP 17	10% Doublet
	Sortie A - TP 16	10% Doublet
Longitudinal	Sortie A - TP 10	10% Fr. Sweep
	Sortie A - TP 11	10% Fr. Sweep
	Sortie B - TP 14	5% Fr. Sweep
	Sortie B - TP 15	10% Fr. Sweep
	Sortie A - TP 12	10% Doublet
	Sortie A - TP 13	10% Doublet
Pedal	Sortie A - TP 18	10% Fr. Sweep
	Sortie A - TP 19	10% Fr. Sweep
	Sortie B - TP 23	10% Fr. Sweep
	Sortie A - TP 20	10% Doublet
	Sortie A - TP 21	10% Doublet

The frequency sweep excitation signal is constructed just as in the validation cases to cover the $0.3 - 12 \text{ rad/s}$ frequency range. The computer generated automated test signals are introduced to the helicopter via SCAS actuators which is possible by the DTS as explained earlier. The FIFO during the start and end of the excitation

signals drastically helped the pilots to maintain the aircraft around the predetermined trim condition of 70 knots level flight. However, from time to time especially the low frequency portion of the sweep signals caused the helicopter to deviate too much from the trim conditions. Pilot intervention in such cases were inevitable not only for data quality but also for the safety of flight. For such cases flight crew was informed to use sharp corrective inputs in order not to contaminate the frequency region of interest too much. Nevertheless, pilot corrections are not much of a problem from a theoretical point of view since they are treated as part of the excitation signals. Fig. 3.34 shows a lateral cyclic excitation test with corrective pilot inputs.

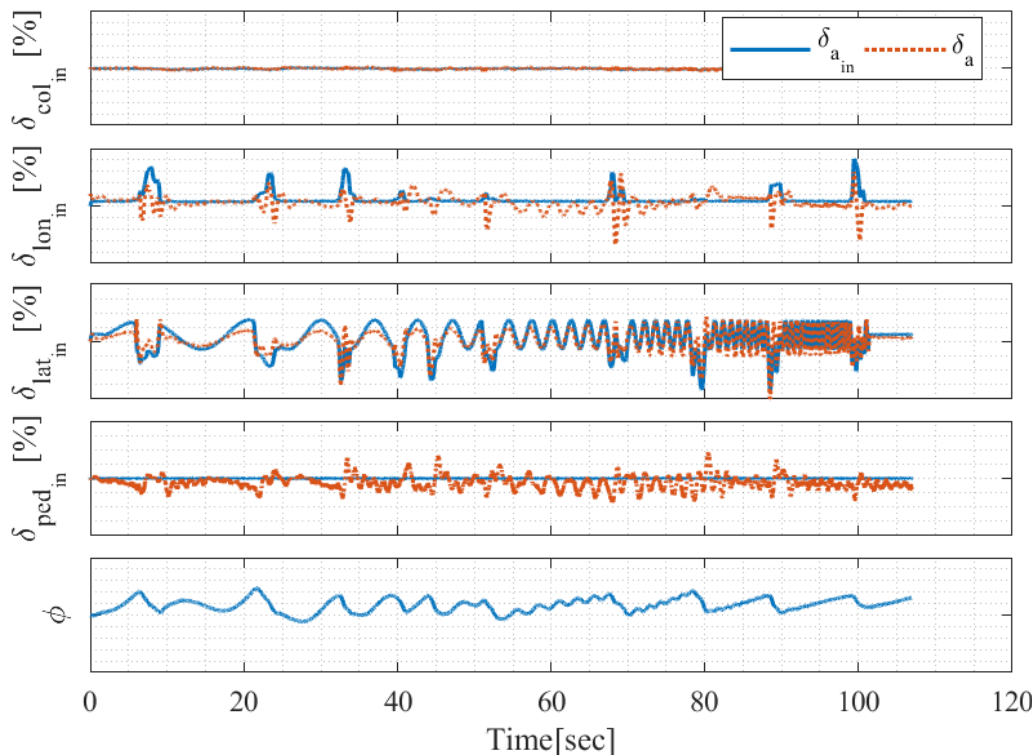


Figure 3.34: Identification Excitation and Bare-Airframe Inputs for Lateral Sweep Flight Tests

Pilot intervention is visible whenever the helicopter exceeds the predetermined roll angle limits. The unintentional pilot inputs to longitudinal stick is also apparent in the data which is practically inevitable, since it is almost impossible to move the cyclic stick in single axis precisely during. Pilot inputs seems like they contaminate the excitation inputs in the lateral axis since the nice sinusoidal shape seems distorted with every time roll angle limits exceeded; however, resulting data showed good coherence

values indicating the corrective pilot actions do not corrupt the identification data that much. Unlike the simulation cases the correlation between the bare airframe inputs are hard to detect by simply looking at the simulation time domain data. Detailed data analysis for the lateral cyclic sweep tests revealed that the correlation between lateral cyclic input, δ_{lat} , and pedal input, δ_{ped} , is higher than the threshold defined in Eq. (2.26); thus, an attempt for MISO identification will fail. Additionally, secondary control, δ_{ped} , auto-spectra is not low enough according to 2.27 to permit for a SISO identification as well. Fig. 3.35 shows the recorded identification data against the limits given in Eq. (2.26).

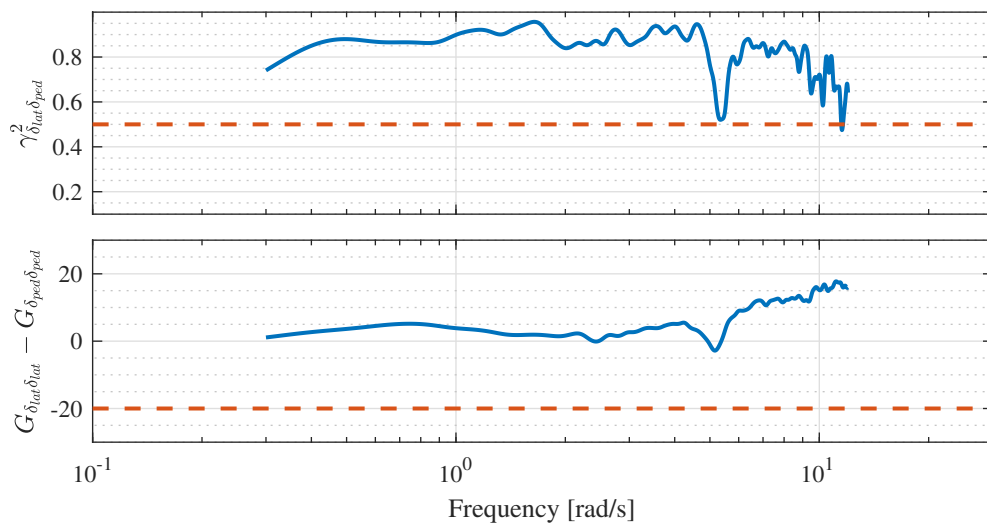


Figure 3.35: Lateral to Pedal Correlation

The entire frequency sweep data utilized in the flight tests follows the automatic signal generation guidelines of [20]. The available flight test data was inspected for a coherence evaluation and results are summarized in Table 3.5. The values in the table represents the frequency range of applicability after obtaining the bare-airframe frequency responses using 2.30. Table 3.5 basically states that not all of the input output pairs have linearly dependent relationships. For example, it was not possible to find a linear dependency between the collective input to the body x velocity output. This may be due to the fact that for a given helicopter this relation is a weak correspondence or the system is not excited enough to reveal an underlying relationship if there is any. Each pair of input output is inspected in this manner and only marked as *none* if there is belief that the input output pair in question is indeed an negligible one for

a given classical configuration helicopter.

Table 3.5: Frequency Response Table

Measurement (Output)	Control (Input)			
	δ_{col}	δ_{lon}	δ_{lat}	δ_{ped}
u	none	0.3-2	none	none
v	none	none	0.8-5	0.4-5
w	5-12	0.3-12	none	0.4-4
p	none	none	0.3-12	4-12
q	1-12	0.3-12	none	0.4-12
r	2-6	none	none	0.3-12
ϕ	none	none	0.3-5	none
θ	2-12	0.3-7	none	0.5-4

The model postulate is utilized as given in equations 2.3 and 2.4; however, following the information in Table 3.5 some of the stability and control deviates that are associated with frequency response pairs marked as *none* in the table are omitted from parameter optimization process. For example the frequency response from δ_{lat} to u does not contain enough information content, this is probably due to the fact that for a helicopter in forward flight a change in lateral input does not physically effects the longitudinal velocity of the helicopter, so stability derivatives X_p , X_r control derivative X_{lat} are dropped from the parameter optimization process. This reduction is performed for every frequency response pair that has low information content.

Initial condition for the parameter optimization was selected so that the parameters are close to the linear models obtained from TOROS, which was the best available guess at the start of the parametric identification process. The parameter optimization resulted in an overall cost of $J_{ave} = 202$, which is considered as adequate and should result in satisfactory time domain simulations. During the parameter optimization the insensitive parameters are further omitted from the parameter list. Resultant parameter list and their normalized values for the identified model is given in Table 3.6. The CR bounds for each parameter is also provided in the table. A lower CR bound refers to a more accurate identification result. The parameters with the highest CR bounds

are Y_v and L_r , both of them are important stability derivatives that can not be omitted from the identification process. However, it seems the identification data does not have rich enough content for the identification of these parameters. There are other proposed methods for coming up with this individual stability derivatives. Y_v can be determined from kinematic relations like the ones proposed in reference [20] for determining the speed stability derivatives and L_r can be determined with additional stability tests such as *turn-on-one-control* tests[96]; however, these prospects are not pursued in the scope of this work.

Frequency responses from the test data and the frequency responses of the identified model are illustrated on top of each other in Fig. 3.36. The primary on axis control plots at the top four shows satisfactory matches with the flight test data. Several noteworthy off-axis responses for a helicopter in forward flight are selected and illustrated in the bode comparison figure. The collective to yaw rate relation is selected because due to torque balance this relation is always a strong coupling for classical configuration helicopters. The longitudinal to roll rate is selected to investigate if the aerodynamic phase angle of the rotor system is captured correctly. Pedal to pitch rate is included to see the effect of cant angle on the tail rotor and pedal to roll angle is included due to the tail rotor placement above the helicopter cg. The overall off-axis response match with the flight test data is again competent.

Lastly, for validation doublet input tests are compared with the system identification model outputs. Fig 3.37 shows the results for two different doublet inputs per control axis. Longitudinal doublet on-axis and off axis results show decent resemblance although the roll rate and roll angle outputs display slight differences. Lateral doublets seem to generate considerable amount of pedal control as well, since the SAS mode of the AFCS is active. The lateral axis responses seem satisfactory despite there are minor offsets in the roll angle towards the end of the test sections. The off-axis results for the lateral doublets are somewhat adequate; however, there is certainly room for improvement in the u , w and θ responses. The pedal doublets again present decent on-axis results but the pedal to roll rate and roll angle relation shows deviations. The collective doublet to w responses are acceptable and yaw rate to collective doublets seem satisfactory. Overall the primary on-axis responses and the important cross coupling responses are suitable. There are still potential for enhancement for

Table 3.6: Identified Derivatives from Flight Test Data - Normalized

Param	Val.	CR-%	Param.	Val.	CR-%
X_u	-0.01	12.4	N_r	-0.52	8.64
Z_u	0 ^a	-	X_{lon}	-0.029	3.57
Z_w	-0.52	6.57	Z_{col}	-0.21	4.25
Z_q	44.05	3.76	Z_{lon}	-0.073	21.29
Z_r	0 ^a	-	Z_{ped}	-0.01	24.73
M_u	0.035	14.04	M_{col}	0.01	3.88
M_w	-0.024	15.78	M_{lon}	0.03	3.20
M_q	-1.075	5.06	M_{lat}	0 ^a	-
M_v	0.04	4.81	M_{ped}	0	6.59
M_p	-0.07	58.70	Y_{col}	0.038	11.79
M_r	0.08	52.60	Y_{lat}	-0.057	12.64
Y_v	0.06	20.25	Y_{ped}	0.077	12.40
Y_p	4.06	14.67	L_{col}	0.013	4.69
Y_r	-41.45	3.39	L_{lon}	-0.029	5.76
L_u	-0.035	13.69	L_{lat}	0.096	3.94
L_w	0.052	6.13	L_{ped}	0.013	5.86
L_q	1.08	10.79	N_{col}	0.012	3.55
L_v	-0.05	6.23	N_{lon}	-0.013	13.57
L_p	-1.77	4.62	N_{lat}	0.016	5.05
L_r	0.067	14.5	N_{ped}	-0.018	3.45
N_u	-0.013	12.05	τ_{col}	0.22	2.06
N_w	-0.0006	18.91	τ_{lon}	0.12	4.38
N_q	0 ^a	-	τ_{lat}	0.086	7.08
N_v	0.025	6.78	τ_{ped}	0.027	19.43
N_p	-0.41	6.47			

^a Eliminated from model structure

the remaining input output pairs.

As a final point, even though it was not the main focus of this work, it is convenient

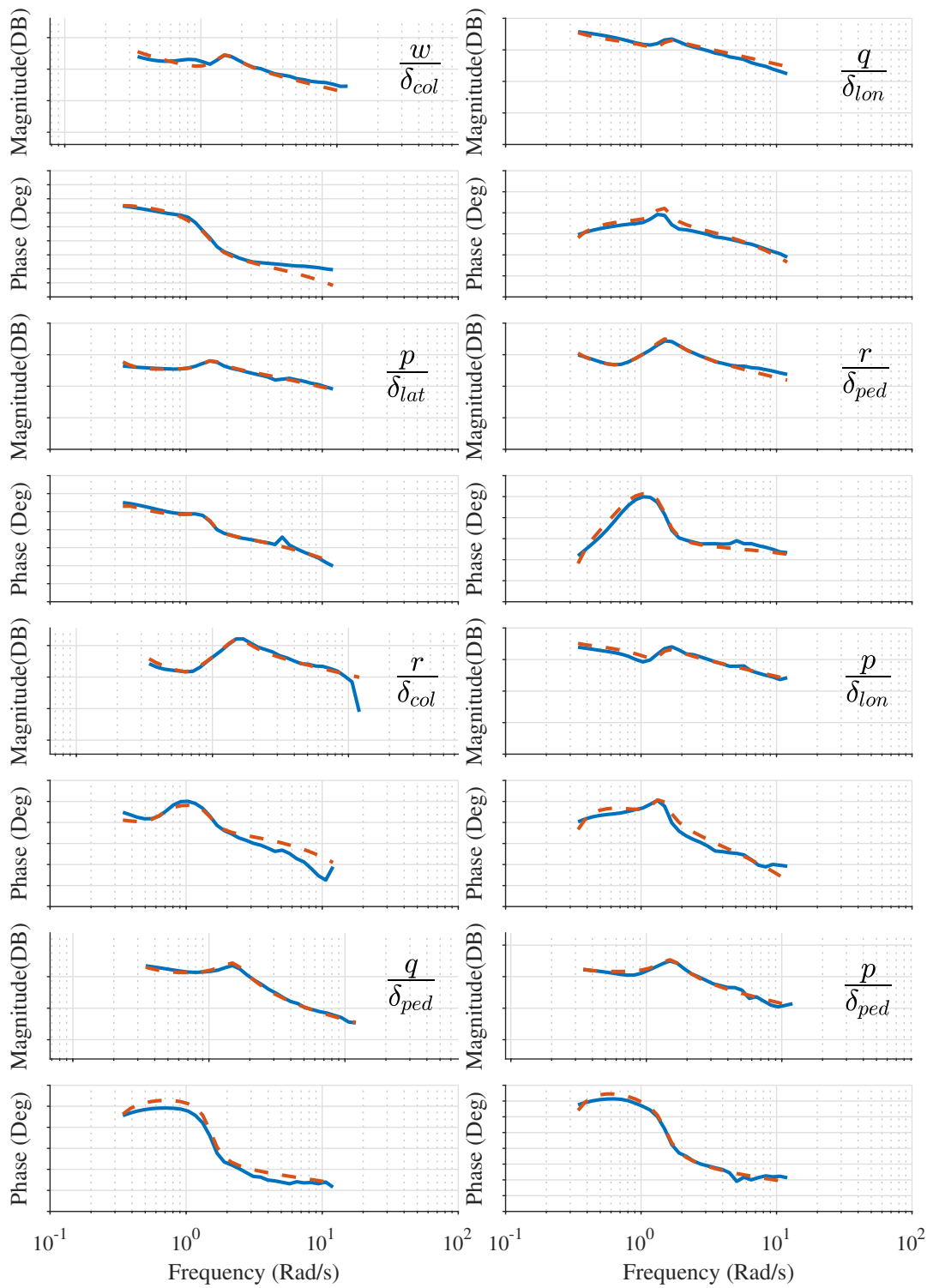


Figure 3.36: Flight Test versus System ID Model Bode Plots

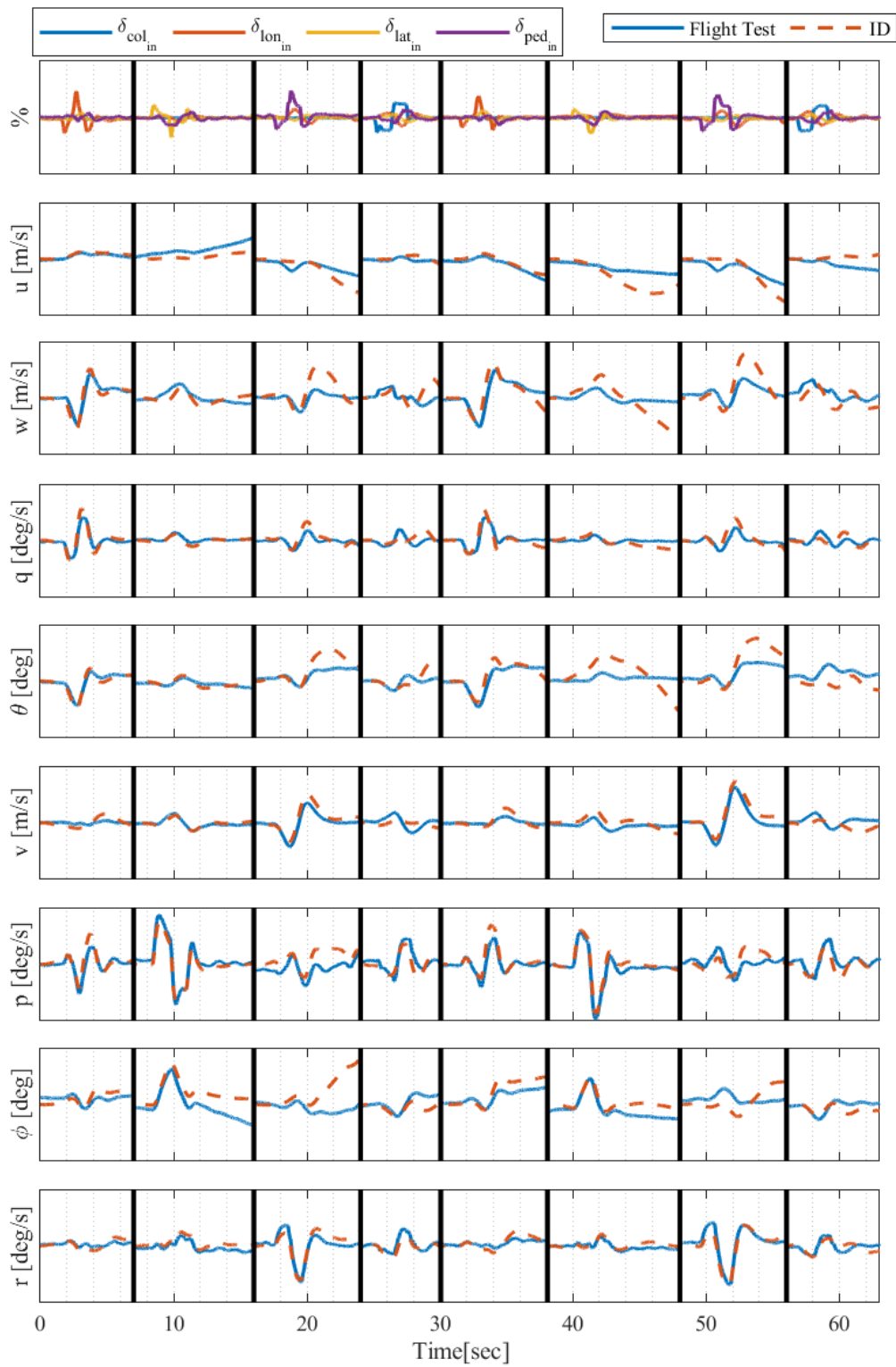


Figure 3.37: Flight Test Validation Time Domain Step Responses

to address the controller design. JIO approach makes it possible to identify unstable systems with the help of a controller.

If one wants to come up with a controller just to be able to collect system identification data for an unstable system, what should the controller specifications be? For the most part, JIO approach is able to work with any type of control architecture. The identification applications on sections 3.2 and 3.3 prove JIO is able to deal with different linear control architectures. Although not showcased in the scope of this work, JIO should also be able to perform with nonlinear control strategies as well from a theoretical standpoint. In this work the controller is used only to stabilize the system and stabilizing the system seems to be sufficient for performing a system identification for JIO approach; however, it is possible to define a set of controller specifications to ensure informative data sets for system identification experiments. This way if the aim is to generate system identification data by using a controller, one can design a controller for this specific case only.

Designing a controller for just system identification opens up a number of possibilities. There are several noteworthy studies in the literature about the informative conditions of system identification experiments for MIMO systems [97, 98, 99, 100]. By carefully designing the controller itself it is even possible to obtain identification data without any excitation. Overall there is a trade-off between the control effort versus experimental information. The more aggressive the controller, more information is necessary for identification [101]. There is an intricate balance between the two and having flexibility on the controller structure can mean more effective identification experiment design.

CHAPTER 4

CONCLUSION

4.1 Conclusion

In this thesis work an approach was found, validated and utilized to identify the rigid body dynamics of a 6 ton manned classical configuration helicopter with flight test data collected while the feedback regulation is active. By doing so, flight test safety of flight crew is increased, flight test costs reduced since no repeats were necessary, and the helicopter prototypes were kept away from their extremes in terms of load and attitude envelopes and same test data could be used both for identification and autopilot performance tests. To sum up, this work covers;

- Lateral model identification of a fixed wing from closed loop linear simulation data,
- Lateral model identification of a rotary wing from closed loop linear simulation data,
- Full rigid body dynamics identification of a rotary wing from both linear and nonlinear simulation data,
- Full rigid body dynamics model parameterization,
- Parameter optimization to identify model parameters with respect to linear and nonlinear simulation frequency responses,
- Time domain validation for parameterized models,
- Flight Tests for MIMO Closed Loop system ID of full rigid body dynamics of T-625 helicopter.

4.2 Future Work

During the progression of this work, numerous opportunities for additional research and development emerged. However, limited time and effort prevented the pursuit of all these opportunities. The following list is a subset of those opportunities which the author feels that are worth to explore. The identification approach and constructed model in this work can provide an solid ground for more progressive breakthroughs in the coming years, especially in the helicopter flight mechanics, flight control and simulation area.

- Study the effects of different input types (Phase optimized multi-sine inputs, 3-2-1-1 inputs, step inputs, etc.),
- Reduced cost identification by using a single input channel or by using switching feedback algorithm,
- Identification of sub component models with JIO approach like engine dynamics or inflow dynamics,
- Study the applicability of JIO approach for linearizing non-linear simulation models,
- Study the applicability of JIO approach with test data with random excitations not specific to system identification,
- Compare the identified model with TOROS to perform a dynamic response validation of TOROS.

Different input types for system identification may present unique advantages over the frequency sweep technique used in this work. One major disadvantage of the frequency sweeps are the long duration necessary to capture the low frequency dynamics. The situation becomes more time consuming when identifying a multi-input system since each input channel is excited individually. While shorter duration excitation signals like the 3-2-1-1 input types can be used to extend the higher frequency range, phase optimized multi-sine inputs offer a way to shorten the total testing time necessary by overlapping the excitation of different input channels.

For the specific helicopter with SAS regulation case, identification using only collective as an excitation input may be possible. Being able to identify a MIMO system by exciting just only one input within a closed loop framework is a documented possibility [102, 103, 104]. The excitation signal should be carefully designed considering the feedback mechanism to produce informative data content for such a case. The possibility of applying this method to helicopter dynamics can be investigated. It would be possible to identify the helicopter dynamics with a quarter of the flight testing time required if such a method was available. Switching between different feedback algorithms can also produce informative data content for identification.

JIO approach can be used to identify sub component models that have an explicit input output relationship with the remaining model. Engine dynamics is a good example, main rotor, inflow, tail rotor dynamics are other good examples. Figure 4.1 shows how JIO can be implemented to identify engine dynamics, given helicopter input output data.

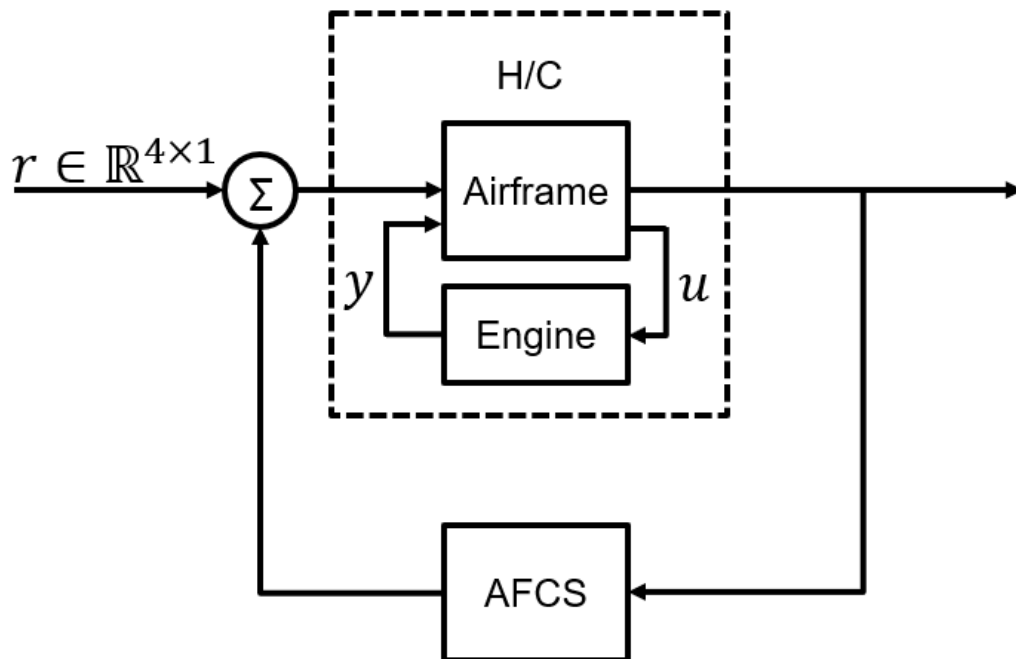


Figure 4.1: Engine Model Identification Framework Block Diagram

Frequency sweep linearization models are more accurate than their perturbation based counterparts as can be seen from T-625 non-linear simulation identification results

obtained in this study. What is more, in order to collect simulation model data for an unstable system one needs to use an active controller or the system diverges during data gathering. Thus, JIO approach becomes a natural tool for the overall linearization process.

REFERENCES

- [1] F. D. Harris, “Introduction to autogyros, helicopters, and other v/stol aircraft volume II: Helicopters,” *National Aeronautics and Space Administration*, 2012.
- [2] R. D. Leoni, *Black hawk: The story of a world class helicopter*. American Institute of Aeronautics and Astronautics, 2007.
- [3] A. W. Linden and C. Team, *The RAH-66 Comanche Helicopter: Technical Accomplishment, Program Frustration*. American Institute of Aeronautics and Astronautics, Inc., 2022.
- [4] F. A. Administration and U. S. F. S. Service, *Helicopter flying handbook*. Skyhorse Publishing Inc., 2013.
- [5] M. J. Lopez, C. S. Duffy, M. B. Tischler, and P. Ruckel, “Bell v-280 hover flight dynamics model validation and update with flight test data,” in *Vertical Flight Society 77th Annual Forum*, 2021.
- [6] C. Fegely, O. Juhasz, H. Xin, and M. B. Tischler, “Flight dynamics and control modeling with system identification validation of the sikorsky x2 technology demonstrator,” in *American Helicopter Society 72nd Annual Forum, West Palm Beach, FL*, 2016.
- [7] J. Gertler, *V-22 Osprey Tilt-Rotor Aircraft*. CreateSpace Independent Publishing, 2009.
- [8] K. Grina, “Helicopter development at boeing vertol company,” *The Aeronautical Journal*, vol. 79, no. 777, pp. 401–416, 1975.
- [9] M. H. Mansur, M. B. Tischler, M. D. Bielefield, J. W. Bacon, K. K. Cheung, M. G. Berrios, and K. E. Rothman, “Full flight envelope inner-loop control law development for the unmanned k-max,” in *Proceedings of the 67th Annual Forum of the AHS International, Virginia Beach, Virginia*, 2011.

- [10] B. Etkin and L. D. Reid, *Dynamics of flight*. Wiley & Sons, 1959.
- [11] T. Berger, E. L. Tobias, M. B. Tischler, and O. Juhasz, “Advances and modern applications of frequency-domain aircraft and rotorcraft system identification,” *Journal of Aircraft*, pp. 1–23, 2023.
- [12] E. A. Morelli and J. A. Grauer, “Advances in aircraft system identification at nasa langley research center,” *Journal of Aircraft*, pp. 1–17, 2023.
- [13] C. Deiler, W. Mönnich, S. Seher-Weiß, and J. Wartmann, “Retrospective and recent examples of aircraft and rotorcraft system identification at dlr,” *Journal of Aircraft*, pp. 1–27, 2023.
- [14] B. Hosseini, A. Steinert, R. Hofmann, X. Fang, R. Steffensen, F. Holzapfel, and C. Göttlicher, “Advancements in the theory and practice of flight vehicle system identification,” *Journal of Aircraft*, vol. 60, no. 5, pp. 1419–1436, 2023.
- [15] C. C. de Visser and D. M. Pool, “Stalls and splines: Current trends in flight testing and aerodynamic model identification,” *Journal of Aircraft*, vol. 60, no. 5, pp. 1480–1502, 2023.
- [16] C. Leshikar, J. Valasek, and C.-K. McQuinn, “System identification of unmanned air systems at texas a&m university,” *Journal of Aircraft*, vol. 60, no. 5, pp. 1437–1460, 2023.
- [17] J. N. Dias and B. G. O. Silva, “Recent applications of system identification techniques at ipev,” *Journal of Aircraft*, pp. 1–21, 2023.
- [18] B. M. Simmons, J. L. Gresham, and C. A. Woolsey, “Flight-test system identification techniques and applications for small, low-cost, fixed-wing aircraft,” *Journal of Aircraft*, pp. 1–19, 2023.
- [19] V. Klein and E. A. Morelli, *Aircraft System Identification Theory and Practice*. American Institute of Aeronautics and Astronautics, Inc., 2006.
- [20] M. B. Tischler and R. K. Remple, *Aircraft and rotorcraft system identification*. American Institute of Aeronautics and Astronautics, 2006.
- [21] R. V. Jategaonkar, *Flight Vehicle System Identification: A Time Domain Methodology*. American Institute of Aeronautics and Astronautics, Inc., 2006.

- [22] L. Ljung, *System Identification: Theory for the User*. Prentice Hall PTR, 1999.
- [23] J. W. Fletcher, “A Model Structure for Identification of Linear Models of the UH-60 Helicopter in Hover and Forward Flight,” NASA, Tech. Rep. August, 1995.
- [24] M. Gennaretti, R. Gori, J. Serafini, F. Cardito, and G. Bernardini, “Identification of rotor wake inflow finite-state models for flight dynamics simulations,” *CEAS Aeronautical Journal*, vol. 8, no. 1, pp. 209–230, 2017.
- [25] U. Forssell and L. Ljung, “Closed-loop identification Revisited,” *Automatica*, vol. 35, pp. 1215–1241, 1999.
- [26] T. Berger, M. B. Tischler, M. E. Knapp, and M. J. Lopez, “Identification of multi-input systems in the presence of highly correlated inputs,” *Journal of Guidance, Control, and Dynamics*, vol. 41, no. 10, pp. 2247–2257, 2018.
- [27] E. A. Morelli, “Practical aspects of the equation-error method for aircraft parameter estimation,” *Collection of Technical Papers - 2006 Atmospheric Flight Mechanics Conference*, vol. 1, no. August, pp. 345–362, 2006.
- [28] D. R. Vieira, D. Silva, and A. Bravo, “Electric vtol aircraft: the future of urban air mobility (background, advantages and challenges),” *International Journal of Sustainable Aviation*, vol. 5, no. 2, pp. 101–118, 2019.
- [29] N. V. Hoffer, C. Coopmans, A. M. Jensen, and Y. Chen, “A survey and categorization of small low-cost unmanned aerial vehicle system identification,” *Journal of Intelligent and Robotic Systems: Theory and Applications*, vol. 74, no. 1-2, pp. 129–145, 2014.
- [30] W. Johnson, C. Silva, and E. Solis, “Concept vehicles for vtol air taxi operations,” in *AHS Technical Conference on Aeromechanics Design for Transformative Vertical Flight*, 2018.
- [31] G. D. Padfield, *Helicopter Flight Dynamics*. John Wiley & Sons, 2018.
- [32] W. Johnson, *Rotorcraft Aeromechanics*. Cambridge University Press, 2006.

- [33] R. A. Ormiston, “Revitalizing advanced rotorcraft research—and the compound helicopter: 35th ahs alexander a. nikolsky honorary lecture,” *Journal of the American Helicopter Society*, vol. 61, no. 1, pp. 1–23, 2016.
- [34] B. Mettler, *Identification Modeling and Characteristics of Miniature Rotorcraft*. Kluwer Academic Publishers, 2003.
- [35] M. B. Tischler and M. G. Cauffman, “Frequency-Response Method for Rotorcraft System Identification: Flight Applications to BO 105 Coupled Rotor/Fuselage Dynamics,” *American Helicopter Society*, vol. 37, 1992.
- [36] S. Seher-Weiß, “ACT/FHS system identification including rotor and engine dynamics,” *Journal of the American Helicopter Society*, vol. 64, no. 2, pp. 1–13, 2019.
- [37] R. W. Prouty, *Helicopter Performance, Stability and Control*. Krieger Publishing Company, 2002.
- [38] J. L. Crassidis and J. L. Junkins, *Optimal Estimation of Dynamic Systems*. Taylor & Francis, 2012.
- [39] M. Verhaegen and V. Verdult, *Filtering and System Identification: A Least Squares Approach*. Cambridge University Press, 2007.
- [40] S. Thrun, W. Burgard, and D. Fox, *Probabilistic Robotics*. The MIT Press, 2005.
- [41] J. W. Fletcher, “Obtaining consistent models of helicopter flight-data measurement errors using kinematic-compatibility and state-reconstruction methods,” in *American Helicopter Society*, 1990.
- [42] M. B. Tischler and E. L. Tobias, “A model stitching architecture for continuous full flight-envelope simulation of fixed-wing aircraft and rotorcraft from discrete point linear models,” *US Army Aviation and Missile Research Development and Engineering Center*, 2016.
- [43] S. Seher-Weiss, “Fitlabgui A versatile tool for data analysis, system identification and helicopter handling qualities analysis.” in *42nd European Rotorcraft Forum*, 2016.

- [44] İ. Uyanık, U. Saranlı, M. M. Ankaralı, N. J. Cowan, and Ö. Morgül, “Frequency-domain subspace identification of linear time-periodic (ltp) systems,” *IEEE Transactions on Automatic Control*, vol. 64, no. 6, pp. 2529–2536, 2018.
- [45] S. Avcioğlu, “Physical Subspace Identification For Helicopters,” Ph.D. dissertation, Middle East Technical University, 2019.
- [46] S. Seher-Weiß and J. Wartmann, “Initial investigation into the complementary use of black box and physics-based techniques in rotorcraft system identification,” *CEAS Aeronautical Journal*, no. 0123456789, 2019. [Online]. Available: <https://doi.org/10.1007/s13272-019-00431-z>
- [47] J. Wartmann, “Closed-loop rotorcraft system identification using generalized binary noise,” *Annual Forum Proceedings - AHS International*, pp. 1892–1903, 2017.
- [48] M. Bergamasco, “Continuous-time model identification with applications to rotorcraft dynamics,” Ph.D. dissertation, Politecnico Di Milano, 2013.
- [49] S. Avcioğlu, A. T. Kutay, and K. Leblebicioğlu, “Identification of physical helicopter models using subspace identification,” *Journal of the American Helicopter Society*, vol. 65, no. 2, pp. 1–14, 2020.
- [50] AGARD, “Rotorcraft system identification,” NATO - AGARD, Tech. Rep., 1991.
- [51] E. A. Morelli and V. Klein, “Application of system identification to aircraft at nasa langley research center,” *Journal of Aircraft*, vol. 42, no. 1, pp. 12–25, 2005.
- [52] H. Akaike, “Some problems in the application of the cross-spectral method,” *Spectral analysis of time series*, 1967.
- [53] S. Hersey, R. Celi, O. Juhasz, M. B. Tischler, O. Rand, and V. Khromov, “State-Space Inflow Model Identification and Flight Dynamics Coupling for an Advanced Coaxial Rotorcraft Configuration,” in *AHS International 73rd Annual Forum*, 2017.

- [54] M. E. Knapp, T. Berger, M. Tischler, and M. C. Cotting, “Development of a Full Envelope Flight Identified F-16 Simulation Model from Closed-loop Flight Data,” in *AIAA Atmospheric Flight Mechanics Conference*, 2018.
- [55] P. Lichota, J. Szulczyk, M. B. Tischler, and T. Berger, “Frequency responses identification from multi-axis multisine manoeuvre,” *AIAA Scitech 2019 Forum*, pp. 1–17, 2019.
- [56] J. A. Grauer and M. J. Boucher, “Identification of Bare-Airframe Dynamics from Closed-Loop Data Using Multisine Inputs and Frequency Responses,” in *AIAA Scitech 2019 Forum*, 2019.
- [57] ———, “Real-time estimation of bare-airframe frequency responses from closed-loop data and multisine inputs,” *Journal of Guidance, Control, and Dynamics*, vol. 43, no. 2, pp. 288–298, 2020.
- [58] J. A. Grauer, “Frequency response estimation for multiple aircraft control loops using orthogonal phase-optimized multisine inputs,” *Processes*, vol. 10, no. 4, p. 619, 2022.
- [59] C. S. Berrigan, M. J. Lopez, P. Ruckel, and J. V. Prasad, “Bell V-280 System Identification: Application of joint input-output methodology for hover model identification,” *2020 Rotorcraft Handling Qualities Technical Meeting*, pp. 1–9, 2020.
- [60] S. J. Nadell, T. Berger, C. DiMarco, and M. J. Lopez, “System Identification and Stitched Modeling of the ADAPT™ Winged Compound Helicopter Scaled Demonstrator,” *78th Vertical Flight Society Annual Forum*, 2022.
- [61] J. Wartmann, S. Seher-Weiß, P. Petit, A. Dikarew, A. Voigt, and K. K. Fetting, “System Identification of a Compound Intermeshing Rotor UAV,” *Vertical Flight Society 79th Annual Forum and Technology Display*, 2023.
- [62] E. A. Morelli and V. Klein, “Application of system identification to aircraft at NASA Langley research center,” *Journal of Aircraft*, vol. 42, no. 1, pp. 12–25, 2023.

- [63] K. Sansal, V. Kargın, and U. Zengin, “A generic ground dynamics model for slope landing analysis,” in *72nd Annual Forum of the American Helicopter Society*, 2016.
- [64] B. L. Stevens and F. L. Lewis, *Aircraft control and simulation*. John Wiley & Sons, 2003.
- [65] K. H. Fu and J. Kaletka, “Frequency-domain identification of BO 105 derivative models with rotor degrees of freedom,” *Journal of the American Helicopter Society*, vol. 38, no. 1, pp. 73–83, 1993.
- [66] R. K. Heffley, S. M. Bourne, H. C. J. Curtiss, W. S. Hindson, and R. A. Hess, “Study of helicopter roll control effectiveness criteria,” NASA, Tech. Rep., 1968.
- [67] R. T. N. Chen, “Effects of Primary Rotor Parameters on Flapping Dynamics,” NASA, Tech. Rep. January, 1980.
- [68] ———, “A Simplified Rotor System Mathematical Model for Piloted Flight Dynamics Simulation,” NASA, Tech. Rep. May 1979, 1979.
- [69] R. K. Heffley, W. F. Jewell, J. M. Lehman, and R. A. V. Winkle, “A Compilation and Analysis of Helicopter Handling Qualities Data,” NASA, Tech. Rep., 1979.
- [70] K. Şansal, G. Koçak, and V. Kargın, “Multi-objective horizontal stabilizer optimization using genetic algorithm,” in *AHS International 74th Annual Forum & Technology Display*, 2018.
- [71] K. Sansal, A. Caliskan, and V. Kargın, “Investigation of the effects of slung load coupled dynamics on helicopter controllability and handling quality,” in *AIAA Scitech 2021 Forum*, 2021.
- [72] I. Okcu, K. Sansal, I. Uysal, and G. Virlan, “Dual-engine failure emergency procedure development using an engineering simulator,” in *78th AHS Annual Forum*, 2022.
- [73] G. Koçak, K. Şansal, S. Sağıroğlu, and V. Kargın, “A generic ground dynamics model for ground handling evaluations,” in *European Rotorcraft Forum*, 2018.

- [74] A. Çalışkan, D. Yıldız, and V. Kargin, “Extensive analysis of hardover and trim-runaway failures on tluh mathematical model based on cs-29 requirements,” in *European Rotorcraft Forum*, 2018.
- [75] U. Türe, S. B. Sarsılmaz, I. Sahin, and U. Zengin, “Optimization of flight control system and handling quality evaluation of a limited authority helicopter,” in *71st Annual Forum of the American Helicopter Society*, 2015.
- [76] U. Türe and I. Okcu, “HQ based optimization and piloted evaluation of model following control architectures for ACAH response types,” in *7th Asian/Australian Rotorcraft Forum*, 2018.
- [77] U. Türe and I. Okcu, “A summary of rotary-wing sil activities: Flight mechanics & control perspective,” in *Asian/Australian Rotorcraft Forum*, 2019.
- [78] I. Okcu and U. Türe, “Evaluation of optimal model following controllers in terms of handling qualities,” in *European Rotorcraft Forum*, 2017.
- [79] —, “Higher augmented control of a utility helicopter using model following controllers,” in *European Rotorcraft Forum*, 2019.
- [80] U. Durak, T. Gerlach, A. Ozturk, V. Kargin, H. Aydemir, and U. Zengin, “Flight simulator model integration for supporting pilot-in-the-loop testing in model-based rotorcraft design,” in *AIAA Modeling and Simulation Technologies Conference*, 2016.
- [81] C. Onur, S. Sarsılmaz, U. Türe, I. Sahin, and U. Zengin, “Development of a computational model of pilot manual control and its application on mission-task-element evaluation of a limited authority helicopter,” in *72th AHS Annual Forum*, 2016.
- [82] C. Onur, U. Türe, and U. Zengin, “Pilot perception and control behavior models as a tool to assess motion-cueing algorithms,” in *AIAA Modeling and Simulation Technologies Conference*, 2017.
- [83] C. Onur, U. Türe, O. Akın, and U. Zengin, “Pilot control behavior model and its model-matching procedure via mission-task-element flight tests,” in *73rd Annual Forum of the American Helicopter Society*, 2017.

- [84] J. J. Corrigan and J. J. Schillings, “Empirical model for stall delay due to rotation,” in *American Helicopter Society Aeromechanics Specialists Conference, San Francisco, CA*, vol. 21, 1994.
- [85] D. A. Peters and C. J. He, “Finite state induced flow models. ii-three-dimensional rotor disk,” *Journal of Aircraft*, vol. 32, no. 2, pp. 323–333, 1995.
- [86] J. G. Leishman, *Principles of Helicopter Aerodynamics*. Cambridge University Press, 2006.
- [87] M. E. Dreier, *Introduction to helicopter and tiltrotor flight simulation*. American Institute of Aeronautics and Astronautics, 2007.
- [88] H. Khalil, “Nonlinear systems,” *3rd edition*, 2002.
- [89] J. S. Bendat and A. G. Piersol, *Engineering applications of correlation and spectral analysis*, 2nd ed. Wiley & Sons, 1993.
- [90] M. S. Bazaraa, *Nonlinear Programming: Theory and Algorithms*. John Wiley & Sons, 2016.
- [91] D. P. Bertsekas, “Dynamic programming and Optimal Control,” Massachusetts, 1995.
- [92] E. A. Morelli and J. A. Grauer, “Practical aspects of frequency-domain approaches for aircraft system identification,” *Journal of Aircraft*, vol. 57, no. 2, pp. 268–291, 2020.
- [93] R. E. Maine and K. W. Iliff, “The theory and practice of estimating the accuracy of dynamic flight-determined coefficients,” NASA, Tech. Rep., 1981.
- [94] T. Berger, M. B. Tischler, S. G. Hagerott, M. Christopher Cotting, and W. R. Gray, “Identification of a full-envelope learjet-25 simulation model using a stitching architecture,” *Journal of Guidance, Control, and Dynamics*, vol. 43, no. 11, pp. 2091–2111, 2020.
- [95] R. Pintelon and J. Schoukens, *System identification: a frequency domain approach*. John Wiley & Sons, 2012.

- [96] A. Cooke and E. Fitzpatrick, *Helicopter test and evaluation*. John Wiley & Sons, 2009.
- [97] W. Yan and Y. Zhu, “Informative conditions for identification of miso armax model in closed-loop systems,” *IFAC-PapersOnLine*, vol. 51, no. 15, pp. 455–460, 2018.
- [98] Y. Zhu, W. Yan, and Y. Zhu, “Mpc closed-loop identification without excitation,” *Journal of Process Control*, vol. 106, pp. 122–129, 2021.
- [99] K. Colin, L. Bako, and X. Bombois, “Data informativity for the closed-loop identification of miso arx systems,” *IFAC-PapersOnLine*, vol. 54, no. 7, pp. 779–784, 2021.
- [100] A. S. Bazanella, M. Gevers, and L. Miškovic, “Closed-loop identification of mimo systems: a new look at identifiability and experiment design,” *European Journal of Control*, vol. 16, no. 3, pp. 228–239, 2010.
- [101] H. Hjalmarsson, “From experiment design to closed-loop control,” *Automatica*, vol. 41, no. 3, pp. 393–438, 2005.
- [102] K. Colin, L. Bako, and X. Bombois, “Data informativity for the closed-loop identification of MISO ARX systems,” *IFAC-PapersOnLine*, vol. 54, no. 7, pp. 779–784, 2021. [Online]. Available: <https://doi.org/10.1016/j.ifacol.2021.08.456>
- [103] K. Colin, X. Bombois, L. Bako, and F. Morelli, “Closed-loop identification of MIMO systems in the Prediction Error framework: Data informativity analysis,” *Automatica*, vol. 121, p. 109171, 2020. [Online]. Available: <https://doi.org/10.1016/j.automatica.2020.109171>
- [104] W. Yan and Y. Zhu, “Informative Conditions for Identification of MISO ARMAX Model in Closed-loop Systems*,” *IFAC-PapersOnLine*, vol. 51, no. 15, pp. 455–460, 2018. [Online]. Available: <https://doi.org/10.1016/j.ifacol.2018.09.187>

APPENDIX A

SIMULATION RESULTS

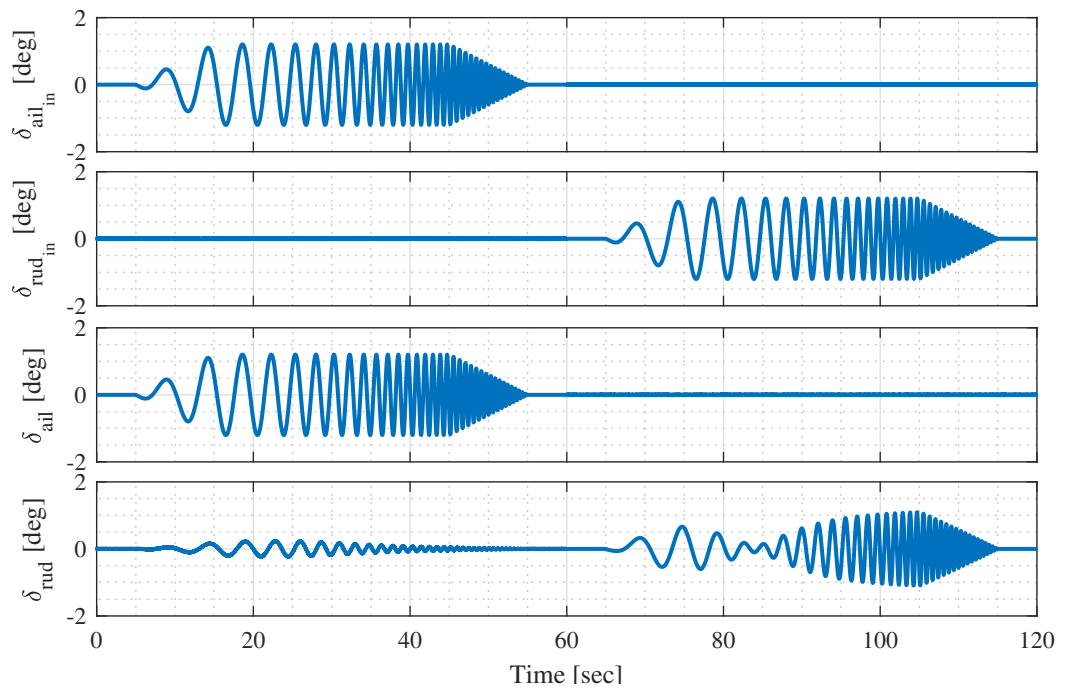


Figure A.1: LJ-25 Simulation Inputs

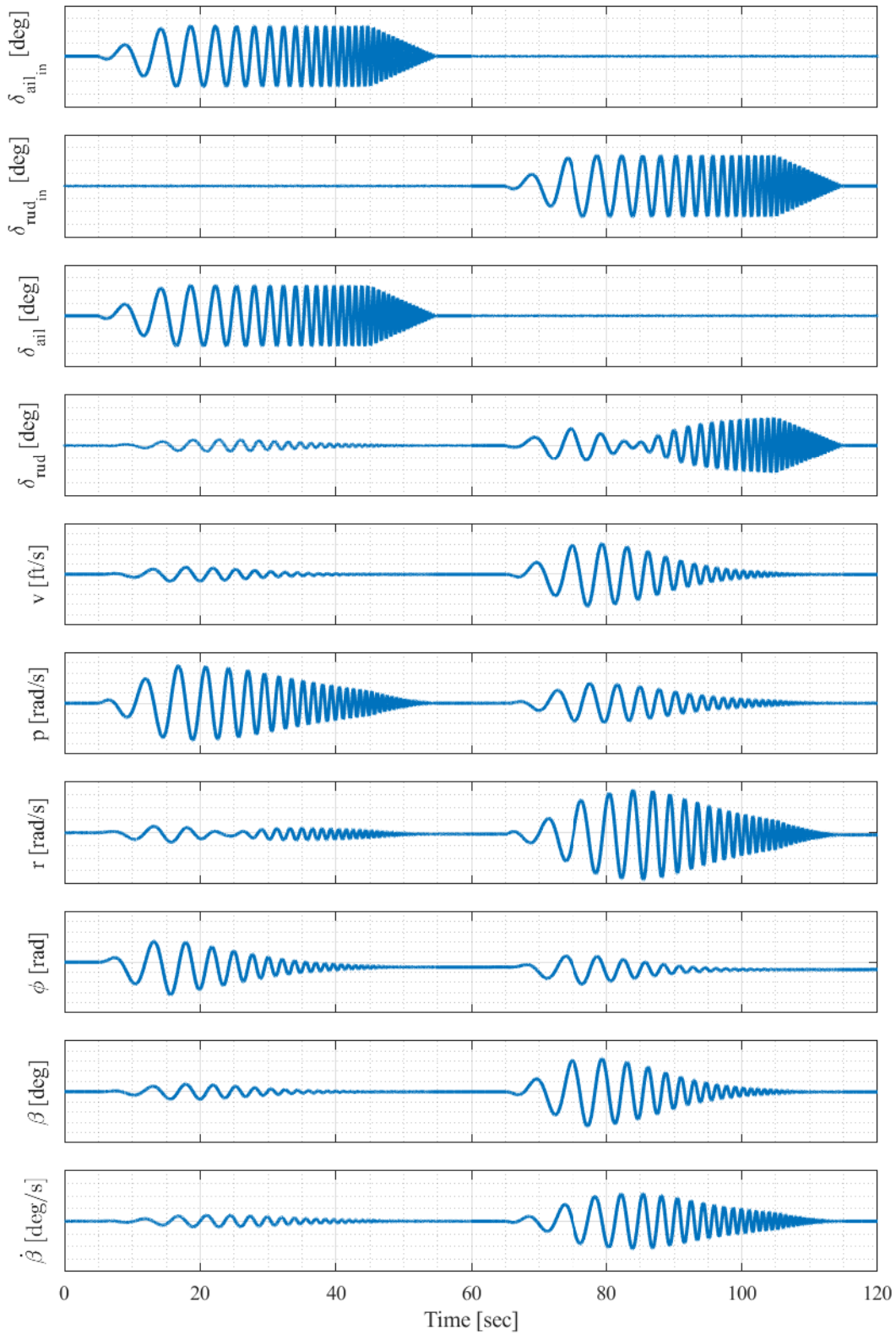


Figure A.2: LJ-25 Simulation Results

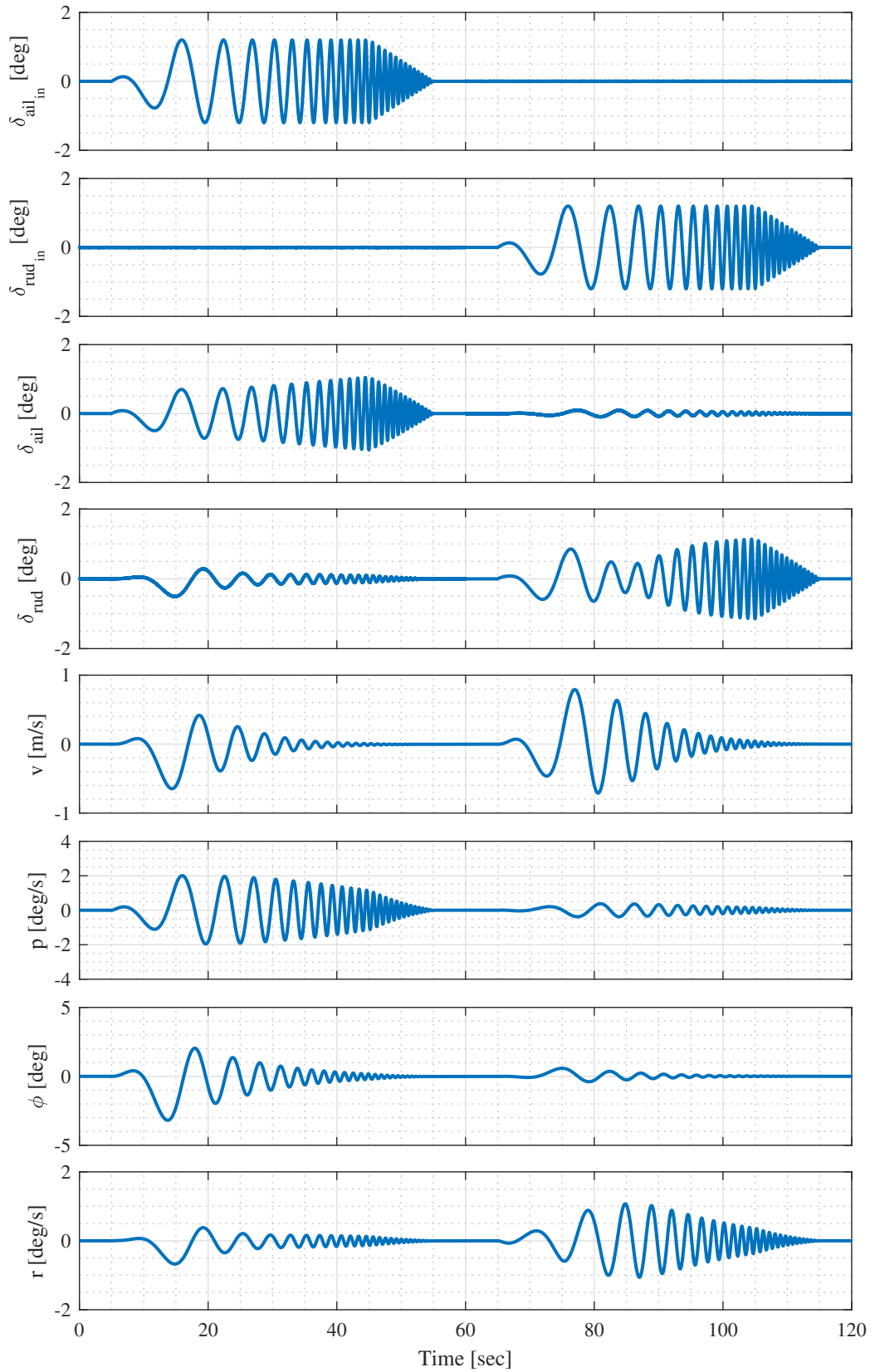


Figure A.3: T-625 Lateral Dynamics Linear Simulation Results

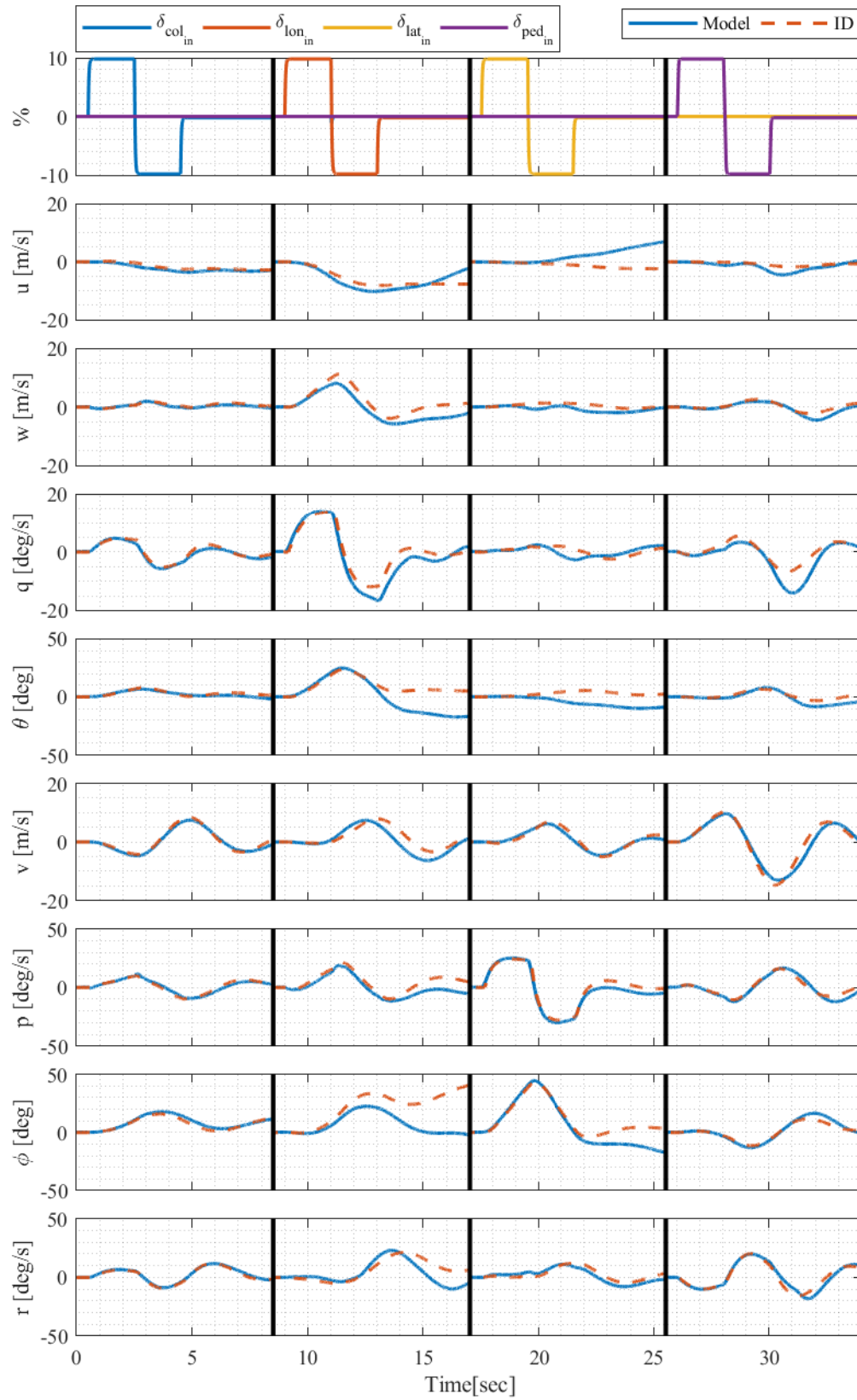


Figure A.4: T-625 Nonlinear Simulation Identification Results - SAS OFF

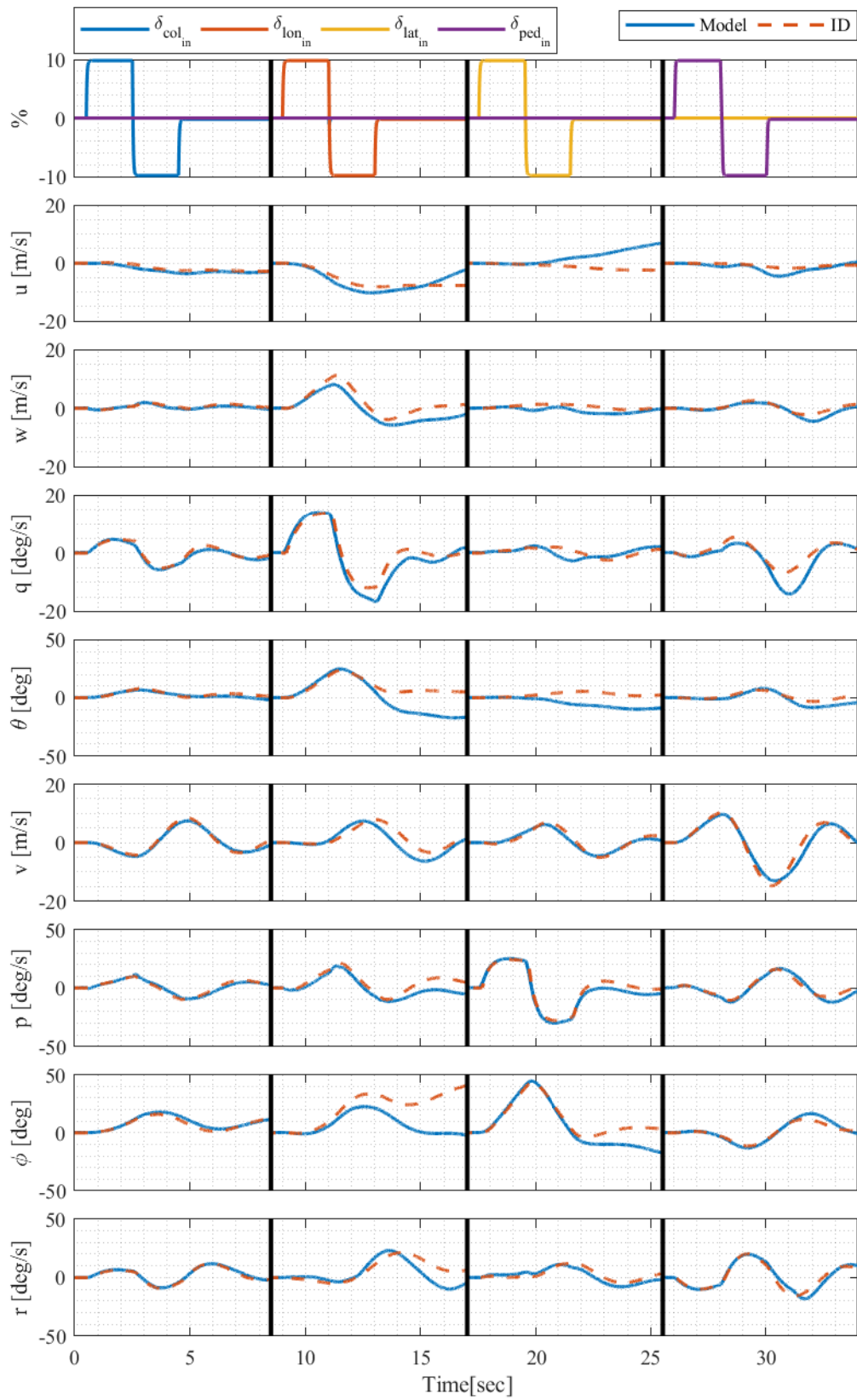


Figure A.5: T-625 Nonlinear Simulation Identification Results - SAS OFF

APPENDIX B

ADDITIONAL FREQUENCY RESPONSE COMPARISONS

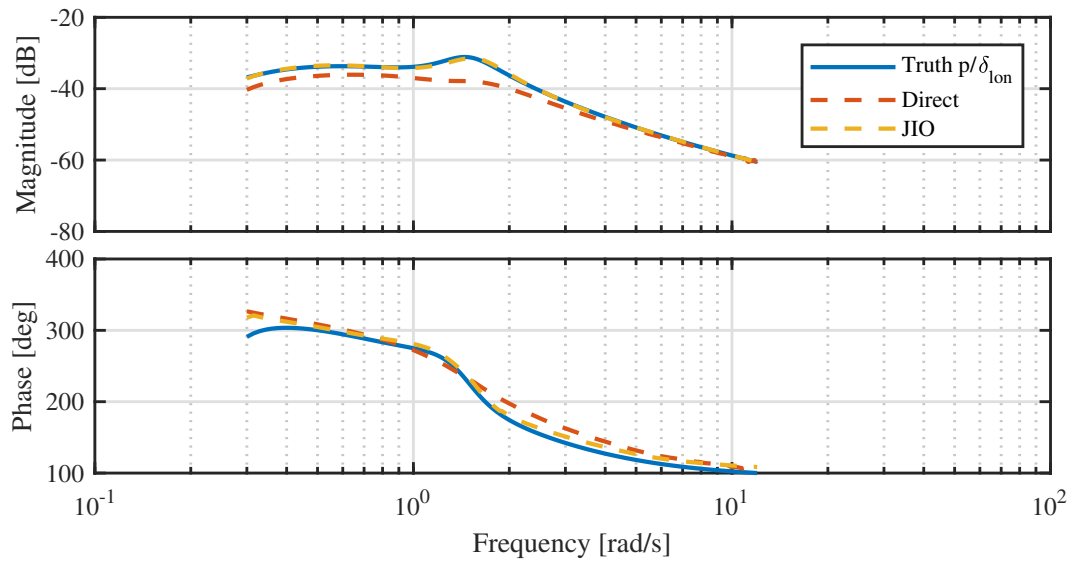


Figure B.1: T-625 Rigid Body Dynamics Linear Off Axis Lon. Cyc. Response Comparison

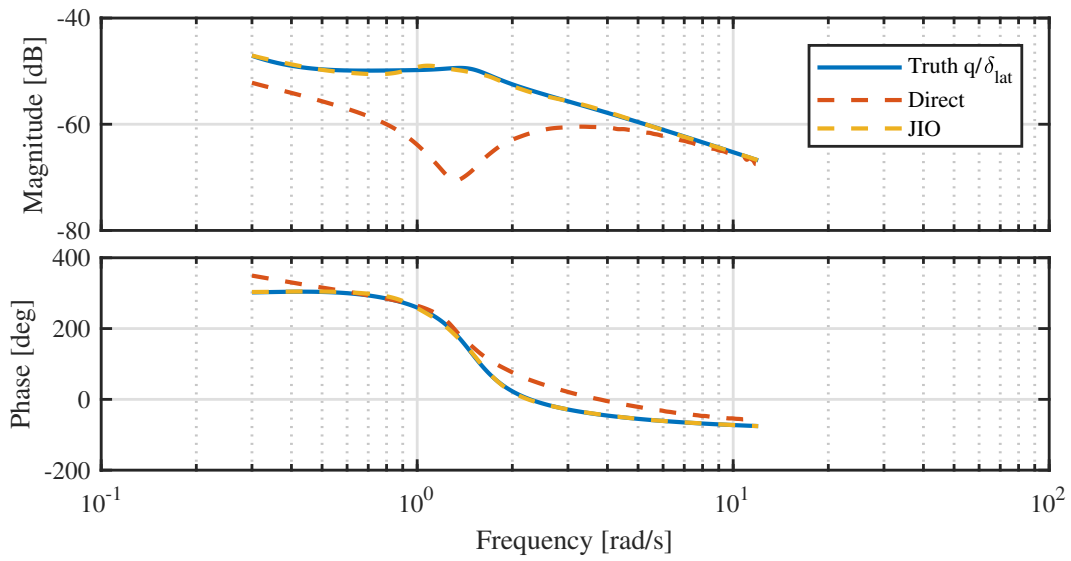


Figure B.2: T-625 Rigid Body Dynamics Linear Off Axis Lat. Cyc. Response Comparison

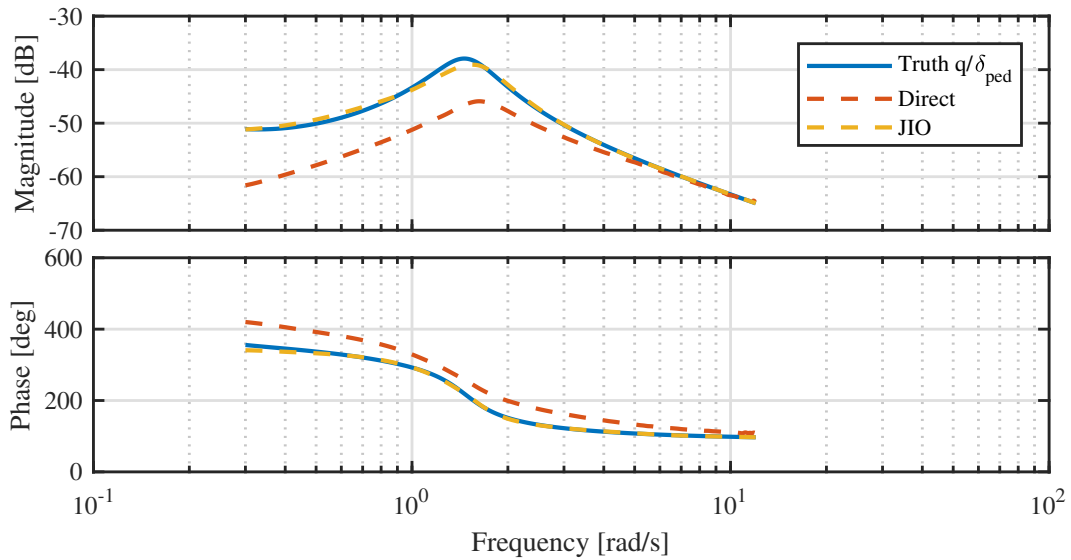


Figure B.3: T-625 Rigid Body Dynamics Linear Off Axis Pedal Response Comparison

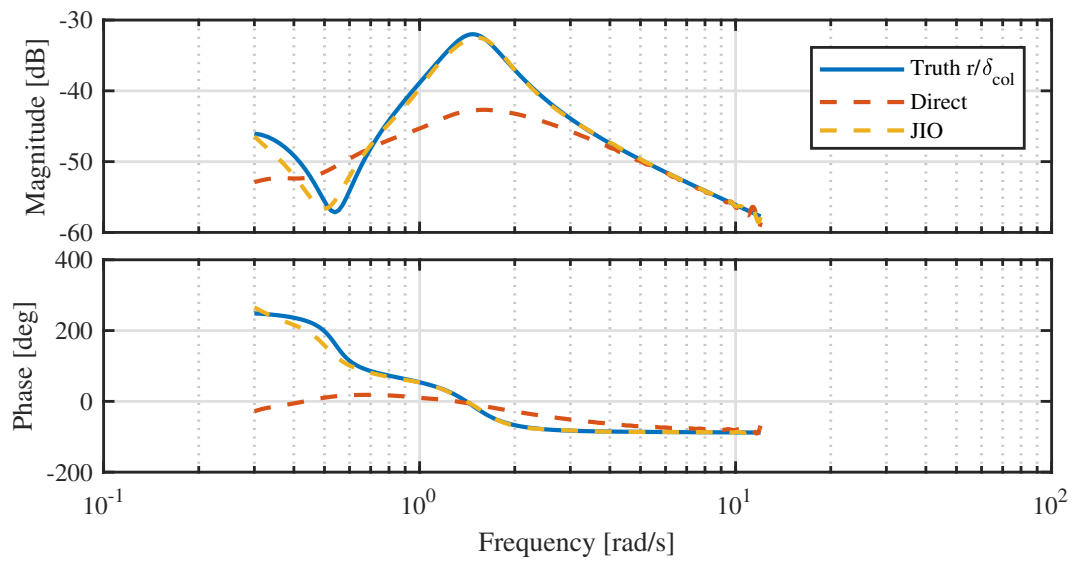


Figure B.4: T-625 Rigid Body Dynamics Linear Off Axis Collective Response Comparison

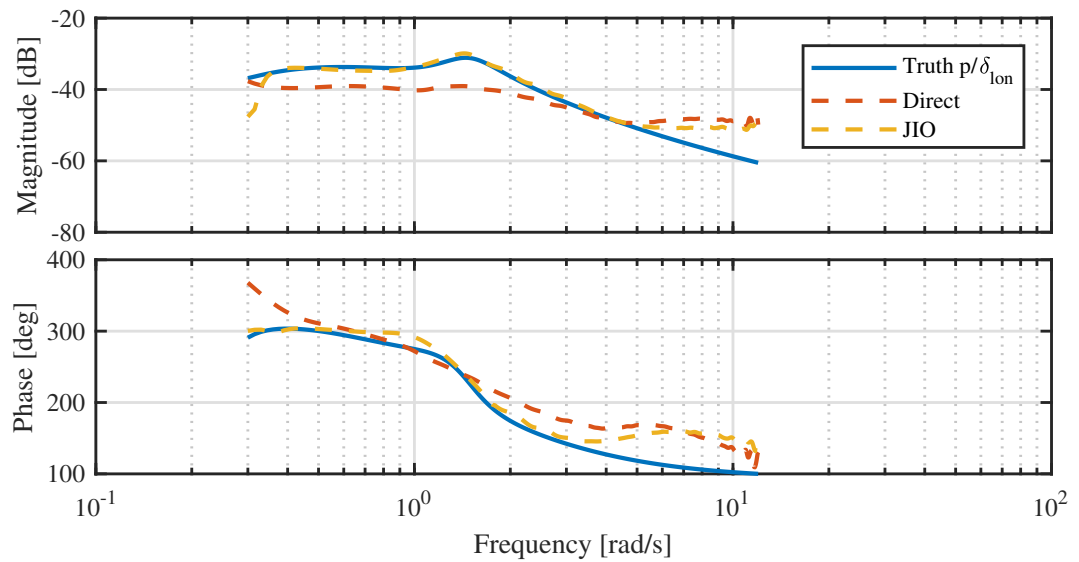


Figure B.5: T-625 Rigid Body Dynamics Non-Linear Off Axis Lon. Cyc. Response Comparison

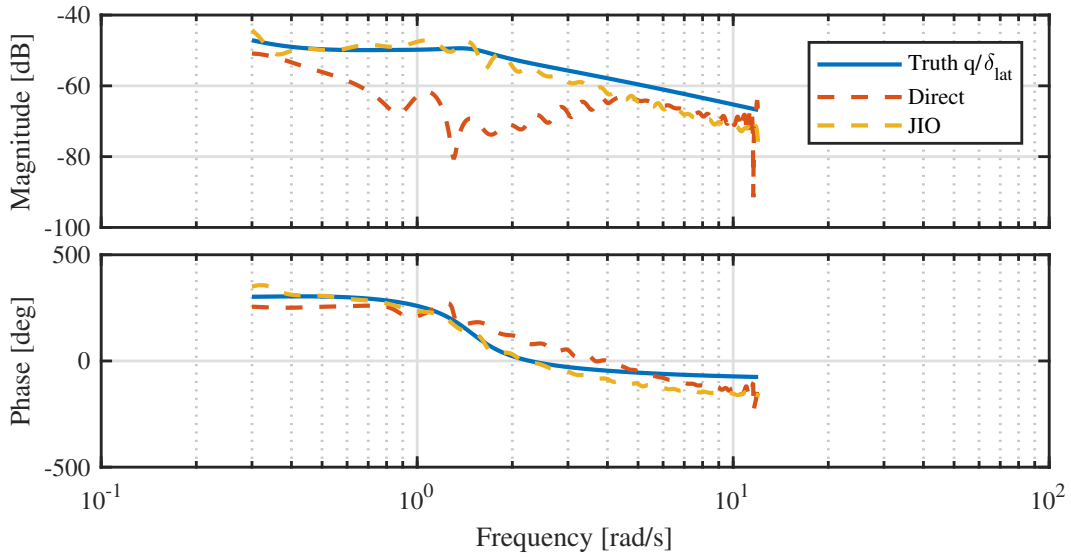


Figure B.6: T-625 Rigid Body Dynamics Non-Linear Off Axis Lat. Cyc. Response Comparison

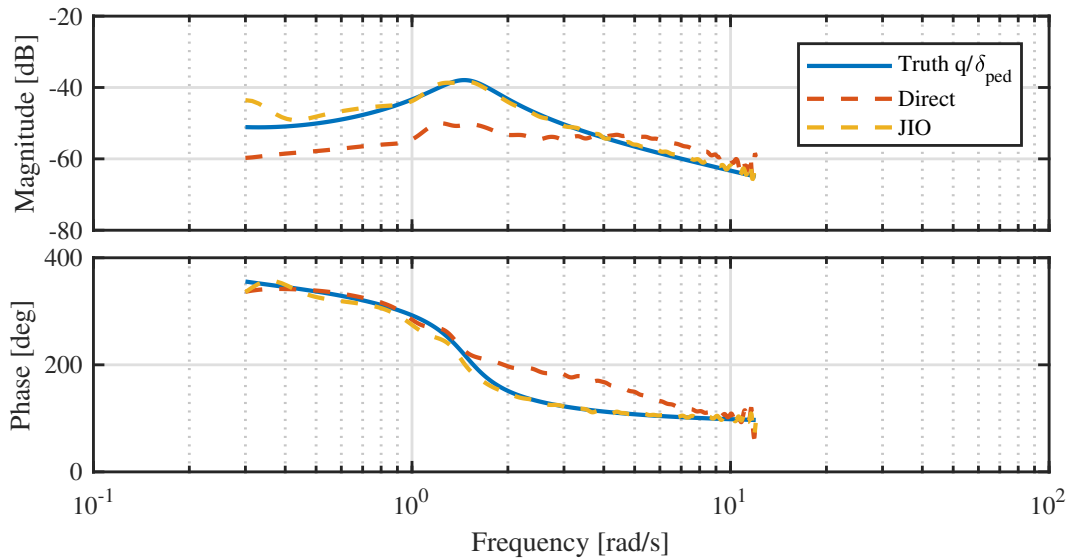


Figure B.7: T-625 Rigid Body Dynamics Non-Linear Off Axis Pedal Response Comparison

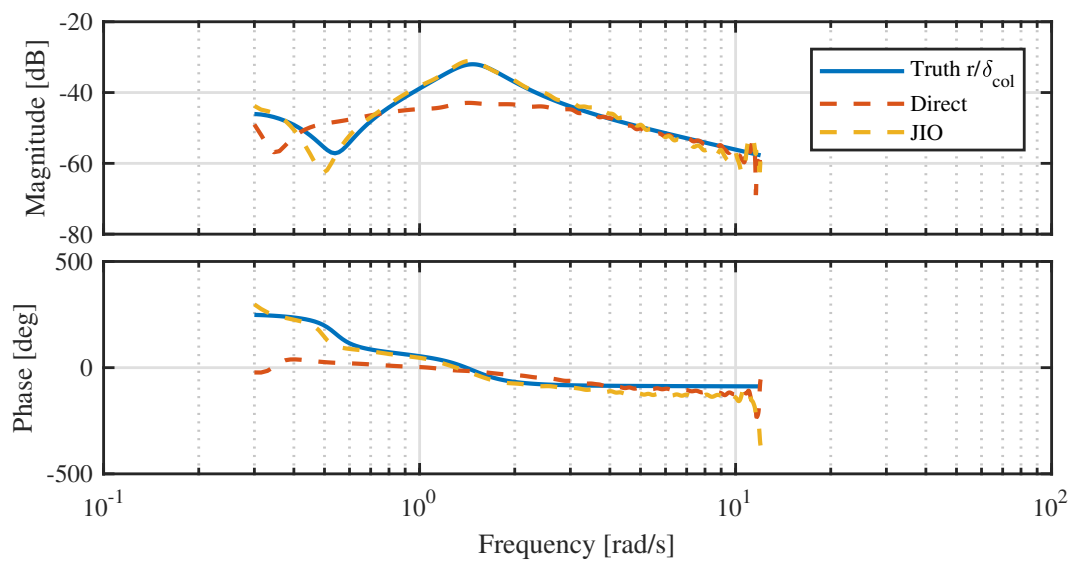


Figure B.8: T-625 Rigid Body Dynamics Non-Linear Off Axis Collective Response Comparison

CURRICULUM VITAE

Surname, Name: Okcu, Ilgaz Doğa

EDUCATION

Degree	Institution	Year of Graduation
MS	METU Aerospace Engineering	2015
BS	METU Aerospace Engineering	2012
High School	Bornova Anadolu Lisesi	2007

EXPERIENCE

Duration	Company	Title
2022-present	Turkish Aerospace	Flight Mechanic Chief Engineer
2017-2022	Turkish Aerospace	Design Specialist
2014-2017	Turkish Aerospace	Design Engineer
2012-2014	Turkish Aerospace	Assistant Design Engineer

PUBLICATIONS

- 2024** K. Sansal and I.D. Okcu, *Utilizing Machine Learning for Improving Rotorcraft Flight Simulation Model Fidelity of T-625 Helicopter*, Vertical Flight Society Forum 80, Montreal, Canada
- 2023** Y. Bayrak, A. Dağalp, M. Boynukalın, C.C. Esmek, I.D. Okcu and N. S. Uzol, *Development and Validation of a Blade Element Model in Simulink for Rotary Wing Flight Mechanic Applications*, 12th Ankara International Aerospace Conference, Ankara, Turkey

- 2023** M. Şenipek, I.D. Okcu, O. Tekinalp and K. Leblebicioğlu, *System Identification of E-Vtol Rotor in Vortex Ring State by Viscous Vortex Particle Method*, 49th European Rotorcraft Forum, Bückeburg, Germany
- 2023** Y.O. Arslan and I.D. Okcu, *Flight Trajectory Tracking for a Helicopter in Tail Rotor Failure*, 49th European Rotorcraft Forum, Bückeburg, Germany
- 2022** I.D. Okcu and M.K. Leblebicioğlu, *Kapalı Döngü Test Verisis Kullanarak Helikopter Dinamik Sistem Tanımlaması*, Fırat Üniversitesi Uzay ve Savunma Teknolojileri Dergisi, 1(1), 422-429, 2022
- 2022** Y.O. Arslan, I.D. Okcu and I. Yavrucuk, *Kuyruk Rotoru Arızalı Olan Bir Helikopterin Uçuş Yörüngesi Hesaplaması*, 9. Ulusal Havacılık ve Uzay Konferansı, İzmir, Turkey
- 2022** I.D. Okcu and K. Leblebicioğlu, *Helicopter Dynamic System Identification using Closed-Loop Test Data*, Otomatik Kontrol Ulusal Kongresi 2022, Elazığ, Turkey
- 2022** Y.O. Arslan, I.D. Okcu and I. Yavrucuk, *Flight Path Generation for a Helicopter in Tail Rotor Failure Condition*, 48th European Rotorcraft Forum, Winterthur, Switzerland
- 2022** K. Sansal, I.D. Okcu, I. Uysal and G. Virlan, *Dual-Engine Failure Emergency Procedure Development Using an Engineering Simulator*, Vertical Flight Society Forum 78, Fort Worth, Texas, USA
- 2021** Y.O. Arslan and I.D. Okcu, *Initial Data Compatibility Check Effort for T625 Flight Data*, 11th Ankara International Aerospace Conference, Ankara, Turkey
- 2019** U. Türe and I.D. Okcu, *Summary of Rotary-Wing SIL Activities: Flight Mechanics & Control Perspective*, 8th Asian/Australian Rotorcraft Forum, Ankara, Turkey
- 2019** I.D. Okcu and U. Türe, *Higher Augmented Control of a Utility Helicopter Using Model Following Controllers*, 45th European Rotorcraft Forum, Warsaw, Poland

- 2018** U. Türe and I.D. Okcu, *HQ Based Optimization and Piloted Evaluation of Model Following Architectures for ACAH Response Types*, 7th Asian/Australian Rotorcraft Forum, Jeju Island, Korea
- 2017** I.D. Okcu and U. Türe, *Evaluation of Optimal Model Following Controllers in Terms of Handling Qualities*, 43rd European Rotorcraft Forum, Milan, Italy
- 2014** A. Yücekayalı and I.D. Okcu, *İnsansız Bir Helikopter için Kontrol Edilebilirlik, Statik ve Dinamik Kararlılık Değerlendirmesi*, Ulusal Havacılık ve Uzay Konferansı, Kayseri, Türkiye